TRANSPORTATION RESEARCH RECORD 676

Bridge Design, Evaluation, and Repair

TRANSPORTATION RESEARCH BOARD

COMMISSION ON SOCIOTECHNICAL SYSTEMS
NATIONAL RESEARCH COUNCIL

NATIONAL ACADEMY OF SCIENCES
WASHINGTON, D.C. 1978

Transportation Research Record 676
Price $3.00

modes
1 highway transportation
3 rail transportation

subject areas
25 structures design and performance
40 maintenance

Transportation Research Board publications are available by ordering directly from the board. They may also be obtained on a regular basis through organizational or individual supporting membership in the board; members or library subscribers are eligible for substantial discounts. For further information, write to the Transportation Research Board, National Academy of Sciences, 2101 Constitution Avenue, N.W., Washington, DC 20418.

Notice
The papers in this Record have been reviewed by and accepted for publication by knowledgeable persons other than the authors according to procedures approved by a Report Review Committee consisting of members of the National Academy of Sciences, the National Academy of Engineering, and the Institute of Medicine.

The views expressed in these papers are those of the authors and do not necessarily reflect those of the sponsoring committee, the Transportation Research Board, the National Academy of Sciences or the sponsors of TRB activities.

To eliminate a backlog of publications and to make possible earlier, more timely publication of reports given at its meetings, the Transportation Research Board has, for a trial period, adopted less stringent editorial standards for certain classes of published material. The new standards apply only to papers and reports that are clearly attributed to specific authors and that have been accepted for publication after committee review for technical content. Within broad limits, the syntax and style of the published version of these reports are those of the author(s).

The papers in this Record were treated according to the new standards.

Library of Congress Cataloging in Publication Data
National Research Council. Transportation Research Board.
Bridge design, evaluation, and repair.

(Transportation research record; 676)
1. Bridges–Design–Congresses. 2. Bridges–Maintenance and repair–Congresses. I. Title. II. Series.
TE7.H5 no. 676 [TG300] 380.5'08s [624'.2]
ISBN 0-309-02819-1 79-10376

Sponsorship of the Papers in This Transportation Research Record

GROUP 2–DESIGN AND CONSTRUCTION OF TRANSPORTATION FACILITIES
Eldon J. Yoder, Purdue University, chairman

Structures Section
Ivan M. Viest, Bethlehem Steel Corporation, chairman

Committee on General Structures
Heinz P. Koretzky, Pennsylvania Department of Transportation, chairman
Kenneth L. Heilman, Pennsylvania Department of Transportation, secretary
Dan S. Bechly, Neal H. Bettigole, William E. Brakensiek, Martin P. Burke, Jr., Daniel E. Czernik, Arthur L. Elliott, Jack H. Emanuel, Donald J. Flemming, Donald C. Frederickson, G. G. Goble, William A. Kline, Celal N. Kostem, Clellon Lewis Loveall, Gordon R. Pennington, Charles G. Schilling, Frank D. Sears, Wendell M. Smith, Marcello H. Soto

Committee on Steel Bridges
John W. Fisher, Lehigh University, chairman
J. Hartley Daniels, Lehigh University, secretary
Dan S. Bechly, Russell L. Chapman, Jr., Paul F. Csagoly, Arthur L. Elliott, Gerard F. Fox, Karl H. Frank, T. V. Galambos, Wayne Henneberger, William A. Kline, Andrew Lally, Joseph M. McCabe, Jr., Roy L. Mion, Robert H. Scanlan, Frank D. Sears, Michael M. Sprinkel, Carl E. Thunman, Jr., Ivan M. Viest, Charles H. Wilson, A. I. Zuckerman

Committee on Dynamics and Field Testing of Bridges
Conrad P. Heins, Jr., University of Maryland, chairman
Charles F. Galambos, Federal Highway Administration, secretary
James W. Baldwin, Jr., William G. Byers, Paul F. Csagoly, David William Goodpasture, Hans K. Hagemann, Cornie L. Hulsbos, Henry L. Kinnier, Celal N. Kostem, Robert H. Lee, Fred Moses, M. Noyszewski, Leroy T. Oehler, Frederick H. Ray, W. W. Sanders, Jr., Robert F. Varney, William J. Venuti, William H. Walker

Construction Section
David S. Gedney, Federal Highway Administration, chairman

Committee on Construction of Bridges and Structures
Marvin H. Hilton, Virginia Highway and Transportation Research Council, chairman
Robert M. Barnoff, D. Stephen Brown, Harry E. Brown, Dale F. Downing, Howard L. Furr, George A. Harper, Richard Heinen, Wayne Henneberger, Andrew Lally, J. C. McGrew, G. I. Sawyer, W. H. Shaw, Sydney W. Smith, Man-Chung Tang, James T. Triplett, J. R. Wilder, Thomas G. Williamson, Kenneth C. Wilson

GROUP 3–OPERATION AND MAINTENANCE OF TRANSPORTATION FACILITIES
Adolf D. May, University of California, Berkeley, chairman

Committee on Structures Maintenance
Roland H. Berger, Byrd, Tallamy, McDonald and Lewis, chairman
Jimmy D. Lee, North Carolina Department of Transportation, secretary
Myron G. Brown, William G. Byers, Robert C. Donnaruma, Al J. Dunn, Ian J. Dussek, Karl H. Frank, Stanley Gordon, Gayle E. Lane, Jack L. Percival, James D. Rose, Alden L. West

Lawrence F. Spaine, Adrian G. Clary, and William G. Gunderman, Transportation Research Board staff

Sponsorship is indicated by a footnote at the end of each report. The organizational units and officers and members are as of December 31, 1977.

Contents

Tests and Analysis for Composite Action in Glulam Bridges

R. M. Gutkowski and J. R. Goodman, Department of Civil Engineering, Colorado State University
J. D. Pault, Hensel Phelps Construction Company

Studies are described that assess the feasibility and value of including the effects of composite behavior in the design of glulam bridges. Analytical and experimental work is presented for the verification of a mathematical model developed for this modern timber bridge system. Six (three southern pine and three Douglas fir) different reduced-scale double T-beams, which modeled glulam-bridge cross sections, were structurally tested in the working-load range and to failure. The specimens were constructed of glulam stringers that ranged in size from 7.6 x 53.3 cm (3 x 21 in) to 12.7 x 76.2 cm (5 1/8 x 30 in) and had a nominal span of 12.2 m (40 ft). Glulam deck panels 1.2 m (4 ft) wide provided a 7.9- x 209-cm (3 1/8- x 82-in) flange. The mechanical fasteners consisted of steel dowels between panels and lag bolts to provide vertical anchorage into the stringers. Finite-element techniques were used in the verification of the theory and in the analytical evaluation of the test results. The major parameters affecting composite action were (a) discontinuities or gaps in the deck layer, (b) slip moduli or connector properties, and (c) the modulus of elasticity of the deck. Composite-action curves were generated to illustrate the effects of these parameters. These curves were further used to extrapolate the test results to full-size components, which leads to greater understanding of the incomplete composite behavior of the glulam bridge system.

The recent development of glulam has markedly expanded the use of timber as a basic building material for large buildings and bridges. And as the sources of large, sawn timber members decrease and the costs of other materials increase, laminated timber will experience still wider use. Because of this anticipated growth, a new timber bridge configuration (1, 2), built of preservative-treated glulam stringers and novel glulam deck panels, has been developed and achieves a modern, practical, timber bridge system.

Because it is a multilayer system, the glulam bridge can be expected to, and indeed does, exhibit a degree of composite action. Composite action offers the advantages of added strength and stiffness under working loads. Layered systems perform at maximum structural capability when the individual components interact as a single unit. If the mechanical fasteners provide complete strain compatibility and force transfer at points of physical discontinuity, the system is rendered functionally monolithic. However, most fasteners do not fully achieve this behavior, and the resulting composite action is incomplete.

Theoretical solutions for the behavior of layered systems have been given by earlier workers. Clark (3) has developed solutions for layered beams rigidly connected at discrete intervals; Granholm (4) and Pleshkov (5) have independently presented theories that account for interlayer slip. Newmark, Siess, and Viest (6, 7) have studied incomplete composite action in steel-concrete T-beams. Norris, Erickson, and Kommers (8) have developed a theory based on sandwich construction, and Kuenzi and Wilkinson (9) have extended the theory to include the effects of elastomeric glues and of fasteners that have finite rigidity. Goodman (10, 11, 12) has presented comprehensive closed-form solutions for layered wood systems, including plates and shells.

Unfortunately, the equations developed in these earlier studies are strictly correct only if the material properties of the individual layers are constant along the entire span. For wood, which has properties that are affected by the presence of knots, the orientation of the grain, its moisture content, and its natural variability, this is not true. Consequently, the solutions obtained by using these earlier methods give the designer only an analysis based on average values for the necessary material properties.

This paper uses a finite-element procedure for the prediction of the incomplete composite behavior of glulam-stringer bridge systems. Gaps between individual deck panels and interlayer slip at the deck-stringer interface reduce the degree of composite action; these effects are included in the model. The results of structural tests of reduced-scale specimens are given to provide verification of the theoretical work. Composite-action curves are used to illustrate the effects of parameters and to extrapolate the test results and permit understanding of the behavior of full-scale bridge systems.

DESCRIPTION OF THE GLULAM-STRINGER BRIDGE

Glulam bridges are increasing in popularity because of their low material cost, ease of erection, and natural beauty. The most common type is the longitudinal stringer bridge. Normally simply supported, stringer bridges provide economic spans of 6.1 to 24.4 m (20 to 80 ft) and are particularly suitable for rural roadways where the site requires such a short-to-medium span structure. The stringers used generally range in width from 13.0 to 31.1 cm (5.125 to 12.25 in) and have varying depths. The deck panels are made of nominal 5-cm (2-in) materials vertically laminated to form a flat slab. Individual panels are generally 1.22 m (4 ft) in width and have lengths equal to the full width of the bridge. Deck thickness is usually 13.0 or 17.2 cm (5.125 or 6.75 in) but conditions can necessitate thicker panels. Weatherproofing is accomplished by using an asphalt wearing surface and, consequently, a service life of 50 years (2) can be expected under normal conditions.

The connection devices are the critical features in the glulam bridge system. Commonly, steel dowels are provided to develop shear and moment transfer between adjacent deck panels, and interconnection of the deck panels and the supporting stringers is by lag bolts.

THEORETICAL ANALYSIS

In analyzing the glulam bridge system, both the effects of the two layers of different orthotropic properties and of the interlayer slip associated with the mechanical fasteners that connect them must be considered. In addition, the partial gaps between deck panels affect the transfer of axial force within this layer. These factors necessitate a sophisticated (e.g., the finite difference or the finite-element) method of analysis for a proper prediction of behavior. A finite-element approach formulated by Thompson and others (13) has been successfully used for a number of layered sys-

tems [see Kuo (14), Tremblay (15), Vanderbilt and others (16)] and was adopted for use in this study.

Thompson's finite element is based on the principle of minimum potential energy. The potential energy functional is

$$\pi_p = \sum_{i=1}^{n_L} \int_0^{\ell} [(1/2)E_i I_i (d^2y/dx^2)^2]\,dx + \sum_{i=1}^{n_L} \int_0^{\ell} [(1/2)E_i A_i (du_i/dx)^2]\,dx + \sum_{i=1}^{n_L-1} \int_0^{\ell} (1/2)(k_i n_i/s_i)[(u_{i+1} - u_i) - (1/2)(h_{i+1} + h_i)(dy/dx)]^2\,dx - \int_0^{\ell} w(y)\,dx \quad (1)$$

where

n_L = number of layers,
E_i = modulus of elasticity of layer i,
I_i = moment of inertia of layer i,
k_i = slip modulus of connector between layers i and i + 1,
n_i = number of rows of connectors between layers i and i + 1,
s_i = spacing of connectors between layers i and i + 1,
h_i = depth of layer i,
w = beam loading,
x = length along beam,
y = vertical displacement of beam,
ℓ = beam length, and
u_i = axial displacement of layer i.

The first and second terms in Equation 1 are the flexural and axial strain energies respectively and the last term is the work due to w. Energy losses due to interlayer slip are accounted for in the third term. In formulating the first and fourth terms, it is necessary to assume that the individual layers have identical curvature.

Two techniques for modeling gaps in the layers of the beam have been suggested. Either a special element or a soft element can be used. The special element consists of releasing the continuity of axial force at the gapped location by making the axial force of the two elements adjacent to the gap independent of each other and is similar to releasing the moment at an internal hinge of a framed structure. A soft element (used in this study) is an element of finite, but small, length that has a low modulus of elasticity and is placed at the gap location.

EXPERIMENTAL STUDIES

Description of Specimens

Six twin T-beams, all having the configuration shown in Figure 1, were built and tested. A double T-beam cross section was used for the test specimens, primarily to eliminate lateral instability. Three specimens were made entirely (deck and stringer) of southern pine, and three were made entirely of Douglas fir. The specific types and sizes of stringer are listed below (1 cm = 0.39 in).

Specimen No.	Species	Width (cm)	Depth (cm)
SP-21	Southern pine	7.6	53.3
SP-25.5	Southern pine	12.7	64.8
SP-30	Southern pine	12.7	76.2
DF-25.5	Douglas fir	7.9	64.8
DF-20.75	Douglas fir	13.0	52.7
DF-30	Douglas fir	13.0	76.2

Deck panels were the generally standard field width of 10.4 m (4 ft) but had a reduced thickness of 7.94 cm (3.125 in). Holes for the 25.4-cm (10-in) lag bolts, 10.1 mm (0.75 in) in diameter (drilled during erection), were placed at the recommended locations of 20.3 cm (8 in) in from the longtitudinal edge of the deck panels and 50.8 cm (20 in) from the transverse edge to align with the stringers. The lead-hole diameters were 14.3 mm (9.16 in) for the threaded portion. A clear span of 12.1 m (39.5 ft) was used for all specimens.

Test Setup and Instrumentation

The test framework, especially constructed for the project, is shown in Figure 2. The system is a closed frame consisting of a concrete pad tied to the existing floor slab and a pair of overhead steel frames. Each movable test frame is equipped with a single Material Testing System 445-kN (100 000 lbf) hydraulic actuator. The Material Testing System closed-loop system consists of three basic components: the central power-supply unit, the dual-actuator control console, and the two actuators and their associated load cells. The closed-loop control of load automatically compensates for changing conditions in the test specimens caused by such effects as creep, localized failures, and sudden jumps in deflection caused by interlayer slip and intralayer gap movements.

Transmission of the load from each actuator to the actual test specimen was provided by the assemblage illustrated in Figure 3. This type of loading ensured the direct and equal transmission of loads to each stringer, thus eliminating load-distribution considerations, which were not a part of this study. The two actuators were symmetrically positioned 0.61 m (2 ft) each side of the midspan. Thus, each bridge specimen was tested with four equally applied forces, representative of a static vehicular load. This configuration was used for both the working-load range (WLR) tests and the tests to failure.

The data were recorded by an automatic logger system that consisted of 100 channels of recording and signal conditioning and appropriate transducers to measure the deflections and interlayer slip of the test specimens. The deflections were recorded by using 14 linear variable differential transformers (LVDTs) placed at intervals along both stringers. The slip data were obtained by horizontally mounting six LVDTs within the uppermost lamination of the stringers as shown in Figure 4. Data were recorded at various load increments and locations for each of a series of WLR tests. During the subsequent tests to failure, the instruments were removed to avoid possible damage. However, midspan displacements were monitored by mounting scales at the midspan of each stringer and tracing the motion of the girders.

Testing of Materials and Mechanical Fasteners

The longitudinal modulus of elasticity (MOE) for each test girder was obtained by a simple beam flexural test of the individual stringers. Preliminary analytical studies indicated that deck MOE values would have little

influence on the performance of the particular test specimens used and that accurate measurement of these values was unnecessary. Thus, the average values reported by Bodig and Goodman (17) [specifically, MOE (transverse to grain) values of 966 MPa (140 000 lbf/in^2) and 938 MPa (136 000 lbf/in^2) for Douglas fir and southern pine respectively] were used in the computer programs.

Moisture-content readings taken as close to the time of testing as possible had a range of values between 7.0 and 17.5 percent for southern pine and between 7.4 and 12.3 percent for Douglas fir. The average values were 9.6 and 10.6 percent for southern pine and Douglas fir respectively.

The magnitude of the interlayer slip is a function of the interlayer connection. The stiffness of this connection, i.e., the slip modulus, was evaluated by using the special laboratory device shown in Figure 5, which was similar to one used by McLain (18). By the use of this device, specimens comprised of a small piece of deck panel and bridge stringer fastened together by a single lag bolt were tested in a single shear configuration. The result of each test is a slip curve, such as that shown in Figure 6. As an approximation to the nonlinear slip curve, a secant at the 0.25-mm (0.010-in) slip level was adopted for use in the analytical work. Because the actual slip recorded during WLR testing of the double T-beam specimens ranged up to 0.13 mm (0.005 in), this secant is a conservative choice. Two slip specimens were made for each stringer; the average values of slip modulus obtained were 8.23 MN/m (47 000 lbf/in) and 8.060 MN/m (46 000 lbf/in) for southern pine and Douglas fir respectively. The overall average for both species combined was 8.200 MN/m (46 800 lbf/in).

Quantification of the axial stiffness of the dowel connection used between adjacent deck panels is necessary for proper modeling of the joint in the finite-element analysis. To accomplish this, the load frame used in the T-beam tests was adapted as shown in Figure 7 to permit axial tests of the deck material. Test panels were cut to 0.61-m widths to facilitate handling and satisfy the clearance constraint of the framework. Dowel holes were oversize by 0.79 mm ($\frac{1}{32}$ in) and lubricated before assembly (as done in the structural tests). A W8 × 15 steel beam was grouted on top of the specimen to distribute the applied loads. Six LVDTs recorded the deformations across the dowel joint to provide the data needed for plotting load versus deflection curves. Conversion to stress versus deflection data permits computation of the axial stiffness according to

Figure 1. Typical cross section of twin T-beam test specimen.

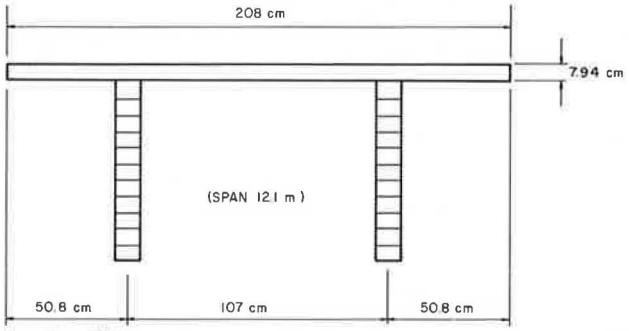

Note: 1 m = 39.4 in.

Figure 2. Test setup.

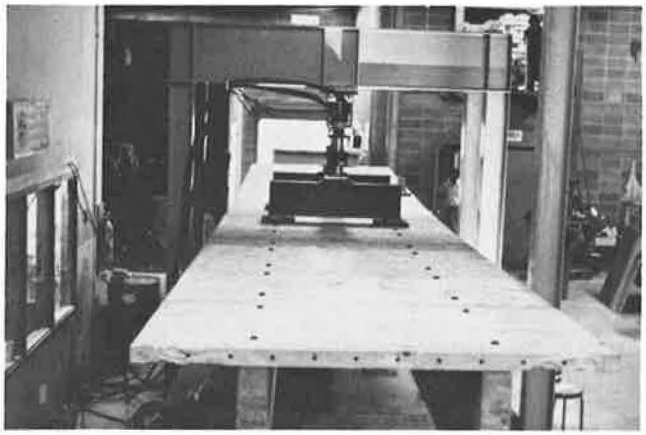

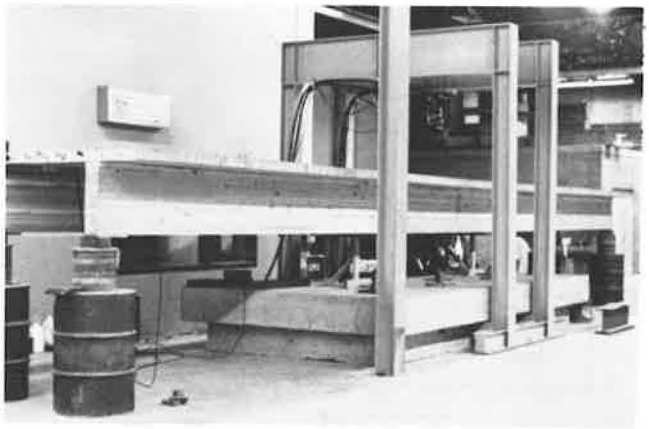

Figure 3. Loading apparatus.

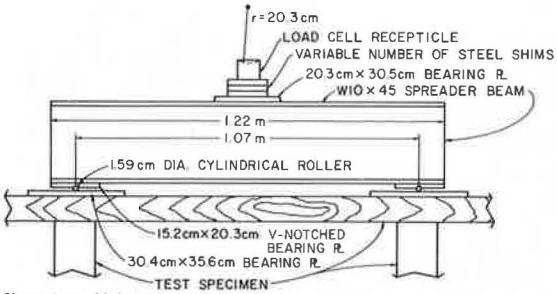

Note: 1 m = 39.4 in.

Figure 4. Slip instrumentation.

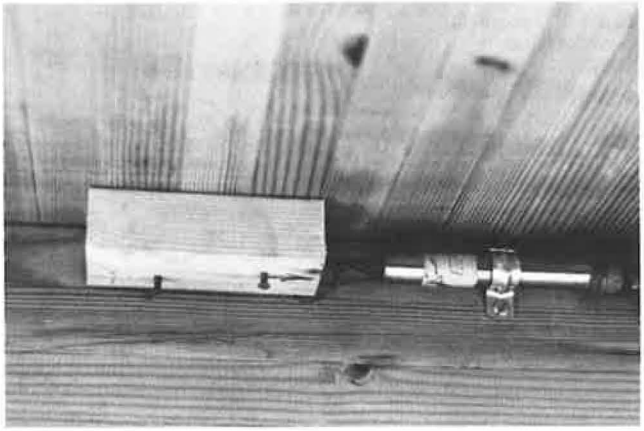

$$E/L = (P/A)/\Delta \quad (2)$$

where

P = applied load,
A = gross cross-sectional area of deck panel,
Δ = measured gap displacement, and
E/L = stiffness parameter used in the finite-element model. A typical stress versus deflection curve (for specimen DF-20.75) is shown in Figure 8.

The finite-element analysis indicated a flange stress ranging from 0.104 MPa (15 lbf/in^2) to 0.173 MPa (25 lbf/in^2). A tangent modulus at 0.138 MPa (20 lbf/in^2) was adopted for use in evaluating E/L from the gap test data. Tests on two southern pine and two Douglas fir specimens gave an average value of E/L of 283 000 kN/m^3 (1041 lbf/in^3).

Figure 5. Slip-testing setup.

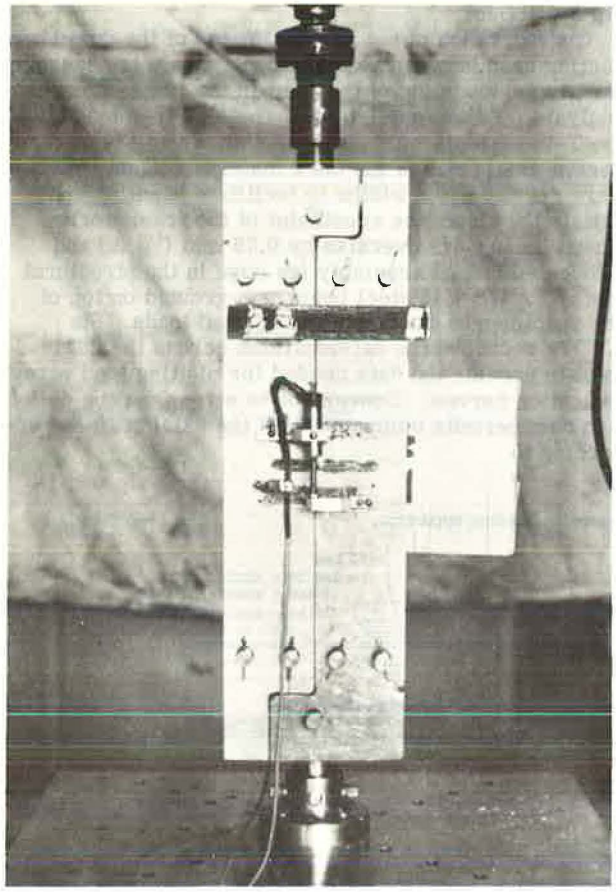

Figure 6. Typical slip curve for lag bolts.

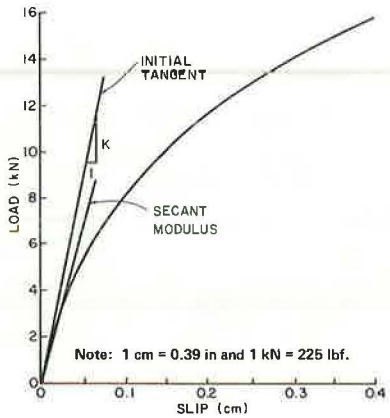

RESULTS OF VERIFICATION TESTS

Structural Testing

WLR testing was conducted to provide the deflection data needed to assess composite action in the double T-beam specimens. After completion of each WLR range test, the bridge specimens were loaded to failure. Load-deflection data were virtually linear throughout the entire range of each test. The modes of failure were typical tension failures at the extreme lower laminations at midspan of the weaker stringer, followed by widespread horizontal splitting throughout the span, with the exception of the SP-30 specimen in which the stringer initially failed at the one-third point. No significant damage to deck panels, dowels, or lag bolts was observed.

Composite-Action Curves

The finite-element program written to use the model of Thompson and others (13) permits generation of the

Figure 7. Dowel (gap) testing setup.

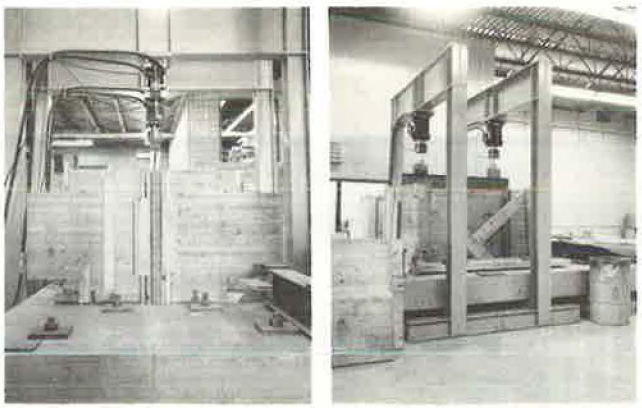

Figure 8. Typical stress versus deformation curve for dowel-connected deck panels.

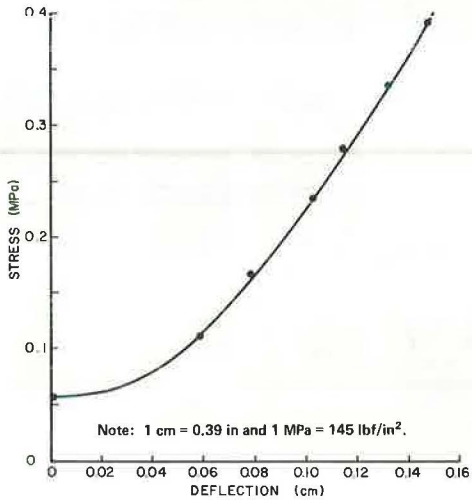

theoretical data needed for assessment of the observed behavior. The major output consists of numerical data needed to plot composite-action curves (CACs), which exhibit the significant parametric influences. CACs were prepared for all six test specimens and are given by Pault (19). The curves are derived for the specific loading condition used in the structural test. More important, the test specimens had reduced-scale dimensions and primarily provide verification of the mathematical model. The results presented for these specimens do not directly reflect the performance of larger members. However, the data base generated in the tests can be extrapolated to give a proper perspective of the composite behavior of full-sized systems.

Figure 9. Composite-action curve for specimen DF-20.75.

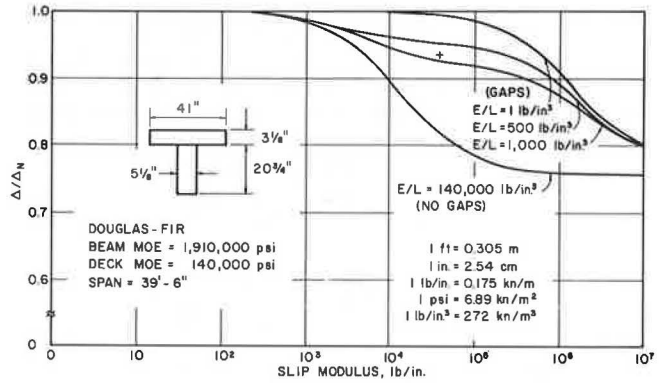

Figure 10. Composite-action curve for specimen SP-21.

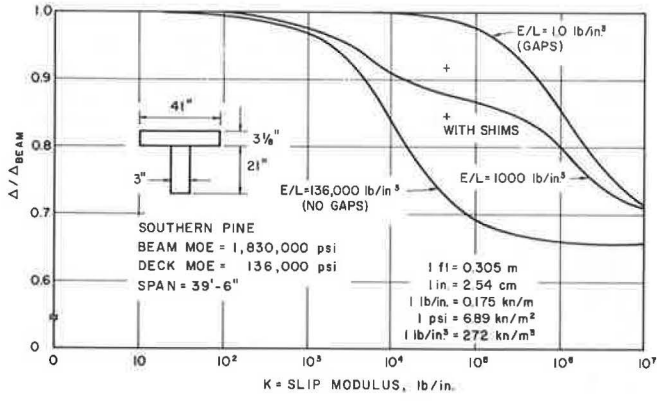

Figure 11. Effect of composite action on deflection behavior.

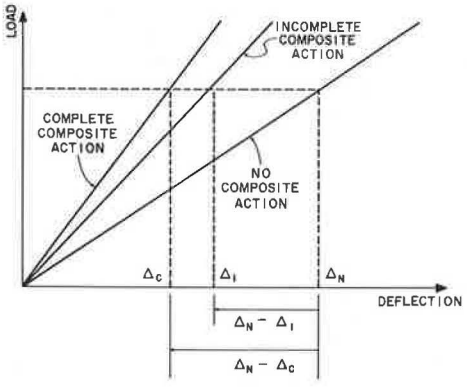

Because the CACs are generally alike in shape, only the results for specimens DF-20.75 and SP-21 are given (see Figures 9 and 10). (Because the use of the finite-element model developed here requires U.S. customary units, values in Figures 9, 10, 12, and 13 are not given in SI units.) Midspan deflections are plotted versus slip modulus values for various gap conditions. The abscissa is put in nondimensional form by normalizing the displacement values relative to Δ_N, the predicted noncomposite deflection. Each of the curves shown is indicative of a different interpanel gap condition, and each demonstrates the effect of slip modulus on the composite behavior. The lower curve represents a completely continuous deck system, i.e., no gaps in the decking, and the upper curve represents a completely discontinuous deck system, i.e., open gaps and no dowels between panels. The intermediate curves constitute gap conditions that are between the two extremes.

Figures 9 and 10 show that, at low k-values, there is essentially no composite action regardless of the gap conditions. At an infinite k-value, all three converge to the rigid system (fully composite) deflection value. The vertical distance between these two extreme levels constitutes the maximum possible percentage reduction in deflection (or the total amount of composite action) that is available. This total composite action can be realized only under ideal conditions, namely a monolithic system. For the particular test structures, DF-20.75 and SP-21, 24.5 and 34.3 percent reductions in deflection respectively are possible at the ideal limit.

The vertical distance above the NO GAPS CAC is a measure of the percentage reduction in deflection available for any given k-value. This represents the loss of stiffness that can be attributed to the use of a particular number and size of lag bolts for the deck-to-stringer connection.

Further loss of stiffness is caused by the presence of gaps in the deck. As E/L decreases, the CAC assumes a higher position. Thus, in effect, for a given k-value, the observed composite action decreases as E/L decreases (the nature of the gaps is worsened), reaching a limit at the GAPS CAC. The remaining vertical distance above the GAPS CAC indicates that, for large k-values, some composite behavior is guaranteed.

The CACs and test data are used in the following way: The mathematical model is used to establish the upper and lower bounds (NO GAPS and GAPS) on composite action for each test specimen. The experimental results are then used to establish data points that fall between these two limits, thus permitting assessment of the composite behavior of the test specimen. For specimen DF-20.75 (illustrated in Figure 9), the recorded midspan deflection (Δ_i) was 2.84 cm (1.12 in) and the corresponding theoretical value (Δ_N) was 3.05 cm (1.20 in), which gives $\Delta_i/\Delta_N = 0.933$. The average slip modulus for material specimens taken from this specimen was 7.180 MN/m (41 000 lbf/in). The plot of these values is shown as a "+" in Figure 9. The accuracy of the theoretical model is demonstrated by the intermediate curve shown for E/L = 272 000 kN/m^3 (1000 lbf/in^3). It is seen that this curve nearly passes through the data point observed for the actual test specimen. The theoretical curve for E/L = 136 000 kN/m^3 (500 lbf/in^3) is shown as an indicator of the sensitivity of the E/L parameter.

Figure 10 shows the CACs for the SP-21 system. For this system, $\Delta_i/\Delta_N = 0.919$, and k = 7.880 MN/m (45 000 lbf/in), which is shown as a "+" in Figure 10. A second test was performed on the SP-21 system with the exception that wooden material was inserted, when-

Figure 12. Composite-action curve for extrapolated specimen DF-20.75.

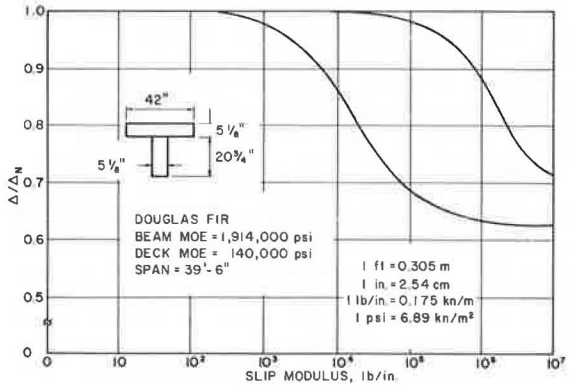

Figure 13. Composite-action curve for full-scale bridge that has a 12.2-m (40-ft) span.

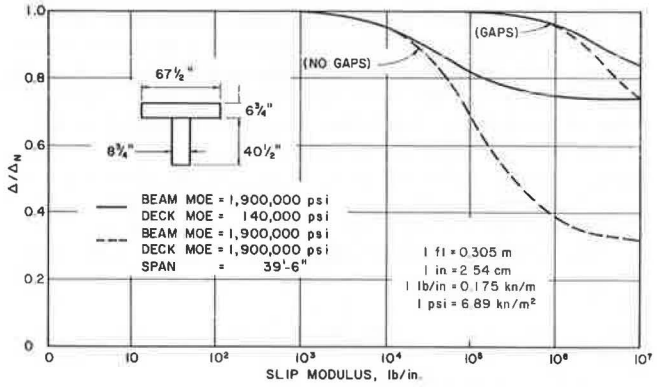

ever possible, in the gaps within the deck layer. This test gave a lower Δ_I-value and, consequently, lowered the abscissa (Δ_I/Δ_N) to a value of 0.849 (in Figure 10, this is the curve identified as "+ WITH SHIMS"). The decrease in deflection is emphasized by noting the position of the two data points relative to the gap-approximation curve, E/L = 272 000 kN/m^3 (1000 lbf/in^3). This procedure was repeated for the SP-30 system and led to similar results. The results are significant and serve to illustrate the variability and effect of the gap condition on overall performance.

Numerical Results

Figure 11 schematically illustrates the general load versus deflection curves for the two extremes of composite behavior and for the incomplete composite behavior that is typical of layered systems. The maximum percentage composite action available (CAA) is that realized by the monolithic system and is given by

$$CAA = (\Delta_N - \Delta_c)/\Delta_N \quad (3)$$

where

Δ_N = theoretical deflection of system if behavior is not composite and
Δ_c = theoretical deflection of system if behavior is completely composite.

The efficiency (EFF) exhibited by the actual layered system (the percentage of the CAA that is achieved) is given by

$$EFF = (\Delta_N - \Delta_I)/(\Delta_N - \Delta_c) \quad (4)$$

where Δ_I = the measured deflection. The percentage of the composite action observed (CAO) in the real system is given by

$$CAO = EFF \times CAA \quad (5)$$

For specimen SP-21, the values computed for Δ_N and Δ_c were 2.62 cm (1.03 in) and 1.72 cm (0.677 in) respectively. In the structural test, Δ_I was recorded as 2.41 cm (0.947 in). These values imply 34.3 percent CAA, 23.5 percent EFF, and 8.1 percent CAO for the specimen. In the second test, that with shimmed gaps, Δ_I was recorded as 2.22 cm (0.874 in). CAA, of course, is unchanged, but EFF is increased to 44.2 percent, thus increasing CAO to 15.2 percent.

The experimental results for the six test specimens are given below (1 MPa = 145 lbf/in^2); most of the MOE values listed are the average value for the two stringers.

		Working-Load Range		
Specimen	MOE (MPa)	CAA (%)	EFF (%)	CAO (%)
SP-21				
With shims	12 630	34.3	23.5	8.1
Without shims	12 630	34.3	44.2	15.2
SP-25.5	11 730	21.0	35.9	7.5
SP-30				
With shims	12 970	17.6	19.3	3.4
Without shims	12 970	17.6	37.6	6.6
DF-25.5 (west stringer only)	14 700	26.7	27.0	7.2
DF-20.75	13 180	24.5	27.2	6.7
DF-30	13 460	17.2	45.0	7.7

The theoretical and experimental results for the test specimens are given below (1 N = 0.225 lbf); the load values, P at failure, listed are the loads applied to the girder by the spreader beam reaction (as observed in the actual, laboratory, failure-load tests).

	Failure		Theoretical
Specimen	P (N)	MOR (MPa)	σ_m (MPa)
SP-21	25.1	37.7	34.5
SP-25.5	71.2	43.4	41.4
SP-30	110.0	47.6	47.4
DF-25.5	45.8	44.5	42.6
DF-20.75	42.3	38.0	36.1
DF-30	107.0	46.0	44.2

The CAAs ranged between 17.6 and 34.3 percent and between 17.2 and 26.7 percent for the southern pine and Douglas fir species respectively. The last two columns compare the observed modulus of rupture (MOR) based on the section modulus of the stringer alone with the theoretical outer-fiber tensile stress at the failure load as predicted by the mathematical model.

OBSERVATIONS FROM TEST PROGRAM RESULTS

The CACs show that four key variables have significant effects on the system performance. These are (a) the type and nature of the gaps (i.e., the gap effect) in the deck layer that is characterized by the axial stiffness E/L, (b) the interlayer connectivity achieved by the lag

bolts as characterized by the slip modulus, (c) the size of the deck panels, and (d) the deck panel MOE value.

The thinner deck used in the reduced-scale system is felt to be the primary cause of the large gap effect observed in the reduced-scale tests. The thickness of the deck gave rise to construction difficulties in panel alignment caused by warping (a problem not encountered in normal size deck panels). The gaps were not fully butted in most cases and, thus, the continuity was interrupted to a larger degree than expected in thicker decks.

The slip modulus is a function of the size and number of lag bolts provided for each deck panel. The degree of connection of the deck and girders can be improved by increasing the number of lag bolts or, as shown by Van Dyer (20), by changing the size of the connectors. Full-sized bridge systems generally have higher slip moduli than the reduced-scale system because of the larger bolts used and the effect of thicker deck panels.

IMPLICATIONS FOR FULL-SIZE SYSTEMS

The deficiencies of the reduced-scale test specimens were discussed above. By extrapolating the deck dimensions to full-sized cross sections and generating the CACs of these sections valuable comparisons are possible. This was done for all six test specimens; complete results are given by Pault (19). To illustrate this, the CAC for the extrapolated DF-20.75 section is given in Figure 12, in which the stringer size, span, and loads are identical to the test-specimen values, but the deck thickness and effective width have been increased to dimensions more practical for the stringer size (1). When compared with the test specimen, the CAA has increased from 24.5 to 37.3 percent. The average increase in the CAA for all six specimens, as reported by Pault (19), was 14 percent.

Perhaps the characteristic most detrimental to composite behavior in the glulam bridge system is the deck MOE. Figure 13 emphatically demonstrates this point. The solid curves show the limits of composite behavior possible for the existing system, i.e., a deck MOE of 966 MPa (140 000 lbf/in^2); the dashed curves are the limits corresponding to an identical system except that the deck MOE is 13 100 MPa (1 900 000 lbf/in^2), i.e., the longitudinal MOE value. At the ideal limits, a 68 percent reduction in deflection is possible. Even at practical k-values, conceptual innovations to better orient deck panels can result in greatly improved composite behavior.

CONCLUSION

An experimental and analytical investigation of the composite behavior in glulam bridge systems was successful. Composite action was predicted for a range of reduced-scale test specimens. Although this action was relatively low in the test specimens, the levels observed do not directly reflect the much greater degree of interaction available in actual bridges. A mathematical model was used to extrapolate the work and permit a study of full-sized systems. These extrapolations indicate that composite design can result in significant reduction in deflection as compared with current design procedures that neglect component interactions. Design improvements, particularly in the decking, could lead to even greater increases in stiffness.

ACKNOWLEDGMENTS

We gratefully acknowledge the support given this project by the Engineering Foundation, the principal sponsor. Material support and continuous input was given by the American Institute of Timber Construction. Several undergraduate students had significant involvement in the construction, testing, and data-reduction phases; we express appreciation for their energetic efforts.

REFERENCES

1. Glulam Bridge Systems. Plans and Details. American Institute of Timber Construction, Englewood, CO, 1974.
2. Modern Timber Highway Bridges. A State-of-the-Art Report. American Institute of Timber Construction, Englewood, CO., July 1973.
3. L. G. Clark. Deflections of Laminated Beams. Trans., ASCE, Vol. 119, 1954, pp. 721-736.
4. H. Granholm. Om Sammansatta Balkar Och Pelare Med Sarkilo Hansyn Till Sapikade Trakonstrakioner. Chalmers Tekniska Hogskoas Handlinger, No. 88, 1949.
5. P. F. Pleshkov. Teoria Rashceta Depeviannykh. Moscow, 1952.
6. N. M. Newmark, C. P. Seiss, and I. M. Viest. Tests and Analysis of Composite Beams With Incomplete Interaction. Proc., Society of Experimental Stress Analysis, Vol. 19, No. 1, 1951.
7. C. P. Seiss, I. M. Viest, and N. M. Newmark. Small-Scale Tests of Shear Connectors of Composite T-Beams. Univ. of Illinois Experimental Station, Bull. 396, Vol. 49, No. 45, Feb. 1952.
8. C. B. Norris, W. S. Erickson, and W. J. Kommers. Flexural Rigidity of a Rectangular Strip of Sandwich Construction—Comparison Between Mathematical Analysis and Results of Tests. Forest Products Laboratory, Madison, WI, Rept. 1505A, May 1952.
9. E. W. Kuenzi and T. L. Wilkinson. Composite Beams—Effect of Adhesive on Fastener Rigidity. Forest Service, U.S. Department of Agriculture, Res. Paper FPL 152, 1971.
10. J. R. Goodman. Layered Wood Systems With Interlayer Slip. Univ. of California, Berkeley, PhD thesis, 1967.
11. J. R. Goodman. Layered Wood Systems With Interlayer Slip. Wood Science, Vol. 1, No. 3, 1969.
12. J. R. Goodman and E. P. Popov. Layered Beam Systems With Interlayer Slip. Journal of the Structural Division, Proc., ASCE, Vol. 94, No. ST 11, Nov. 1968.
13. E. G. Thompson, J. R. Goodman, and M. C. Vanderbilt. Finite-Element Analysis of Layered Wood Systems. Journal of the Structural Division, Proc., ASCE, Vol. 101, No. ST 12, Dec. 1975, pp. 2659-2672.
14. M. L. Kuo. Verification of a Mathematical Model for Layered T-Beams. Colorado State Univ., Ft. Collins, MS thesis, 1974.
15. G. A. Tremblay. Nonlinear Analysis of Layered T-Beams With Interlayer Slip. Colorado State Univ., Ft. Collins, MS thesis, 1974.
16. M. D. Vanderbilt, J. R. Goodman, and M. E. Criswell. Service and Overload Behavior of Wood Joist Floor Systems. Journal of the Structural Division, Proc., ASCE, Vol. 100, No. ST 1, Jan. 1974, pp. 11-30.
17. J. Bodig and J. R. Goodman. Prediction of the Elastic Parameters for Wood. Wood Science, Vol. 5, No. 4, April 1973.
18. T. E. McLain. Curvilinear Load-Slip Relations in Laterally-Loaded Nailed Joints. Colorado State Univ., Ft. Collins, MS thesis, 1975.

19. J. D. Pault. Composite Action in Glulam Timber Bridge Systems. Colorado State Univ., Ft. Collins, MS thesis, 1977.
20. D. B. Van Dyer. Strength of Built-Up Timber Columns. Nova Scotia Technical College, Halifax, PhD thesis, 1976.

Publication of this paper sponsored by Committee on General Structures.

Some Examples of Detection and Repair of Fatigue Damage in Railway Bridge Members

R. A. P. Sweeney, CN Rail, Montreal

Examples of details that have caused fatigue damage in recently designed railway structures are given. Procedures for arresting crack growth and some repair details are described. Emphasis is placed on damage caused by secondary and out-of-plane effects often not considered by designers.

This paper is concerned with some details that have caused fatigue damage in recently designed railway structures and that may not be generally recognized as inadequate by the design profession.

Sufficient experience had been gained by World War I to determine the adequacy of various riveted details. In general, any fatigue problems on riveted structures experienced on our railroad are caused by extremely high cycle fatigue, overloading, or details that are well known to be inadequate. Detailing of riveted railway bridge construction has not changed appreciably during the last 40 years. This, together with the greater concern for the teaching of overall analysis brought about by the digital computer, has led to a generation of engineers unconcerned with details. In many cases, major details are left to the discretion of the draftsperson.

Unfortunately, welded structures tend to be less forgiving of small defects than are riveted structures because they normally contain less excess material and because the welds themselves are points of rigidity and residual stress. Details that had been proved over many years of experience to be adequate for riveted structures are proving to be inadequate for welded structures. In particular, much greater attention must be paid to out-of-plane stresses and secondary effects.

It is only within the last few years that, as a result of some failures (1), new research and the study of fracture mechanics (2, 3) have permitted including in the codes more detailed advice on the suitability and limitations of various welded details.

On our railway, the change from riveted to welded designs took place in the early 1960s. The first designs incorporated details patterned after existing riveted construction.

DETAILS

1. As an extreme example and to make a point, consider the multibeam structure shown in Figure 1. The cover plates are attached by intermittent welds. Each small length of weld is designed to replace a certain number of rivets. The current codes classify this as an E-detail because of the lack of adequate test data. Nevertheless, in this case, it is probable that higher strength exists because the intermittent welds are continuing so that the connected plates are about equally strained and because the welds are well made. This last point is crucial in evaluating details. Despite the fact that the structure has been in service since 1961, because of its redundancy, the actual average root-mean-square stress range is far below the limits of category E. Unfortunately, defective details take time to become evident and, because of redundancy, may never show up.

2. On our railway, the first group of problems to develop on welded structures were cracks at the bottoms of stiffeners on skewed structures. Figure 2 shows a typical example—a diaphragm or brace frame attached to a stiffener in which the stiffeners are not extended to the bottom flange. This was in blind obedience to the dictum of an early worker in welded construction that one should not weld to the tension flange. Because of the stresses introduced by the differential deflections of the connected girders and by small out-of-plane movements, cracks appeared in less than 5 years on heavily traveled lines. This type of crack begins at the bottom of the stiffener and then forms a "U" shape around it. If the original stiffener-web weld is of good quality, the crack turns out into the web and slows considerably. A temporary cure is to drill a round hole containing the crack tip. However, if the web-stiffener weld has a series of surface toe discontinuities (undercut or lack of penetration), the crack can run up the web, which causes the girder to split in half. Fortunately, our railway has not experienced such a failure. Figure 3 shows a crack following a weld upward. A circular hole was drilled to prevent any further propagation.

3. After cracks have occurred as described above, the next point of rigidity is that between the web and flange. If there is any motion out of the plane of the girder, it is only a matter of time before there will be cracks in the web-to-flange weld below the stiffener (Figure 4). Stopping these cracks is very important. Figure 5 summarizes the problems with this type of cracking.

4. Similar cracks have also occurred on a few non-skewed structures at the C-detail at the bottom of the stiffener simply because the stress range was too high.

These required about 10 years to develop a sufficient number of load cycles.

5. Another detail that has given unexpected trouble is the connection of brace frame angles to stiffeners (see Figure 6) that have the gusset groove welded to the stiffener. As shown in Figure 7, the critical detail has a zero radius (category E). The stress that causes crack growth is the lateral force from trains. Because the hunting (side-to-side snaking) of empty cars causes frequent maximum lateral impacts, it took less than 5

Figure 1. Multibeam structure that has cover plates attached by intermittant welds.

Figure 2. Crack at bottom of stiffeners on skewed structure.

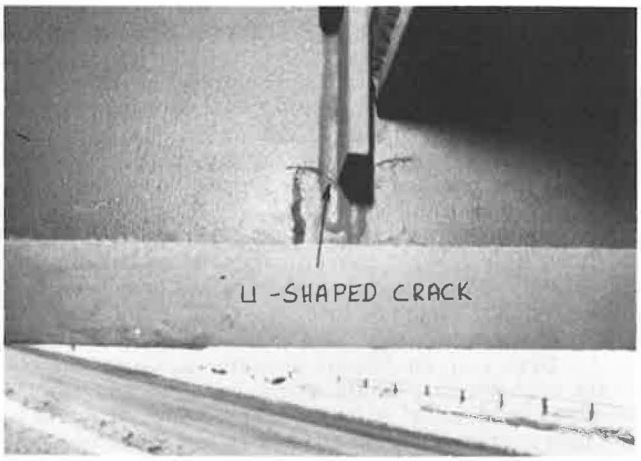

Figure 3. Crack following weld upward.

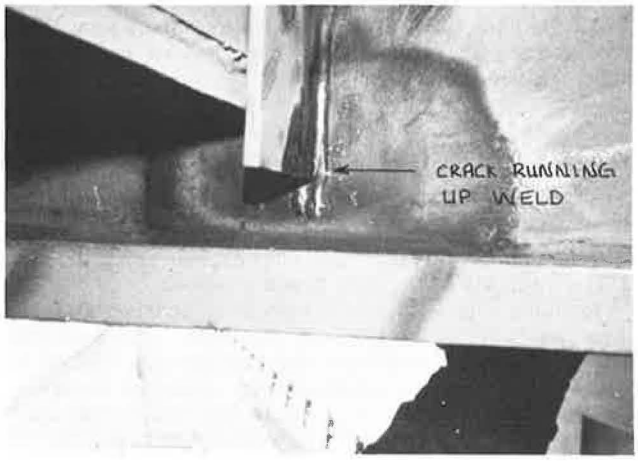

Figure 4. Crack in web-to-flange weld below stiffener.

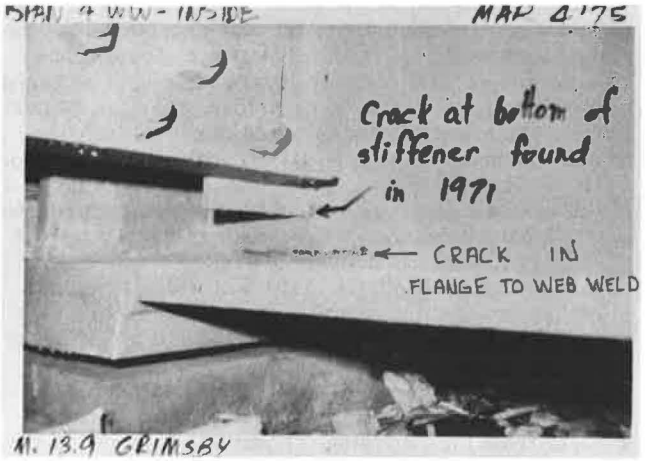

Figure 5. Summary of web-stiffener-flange cracking.

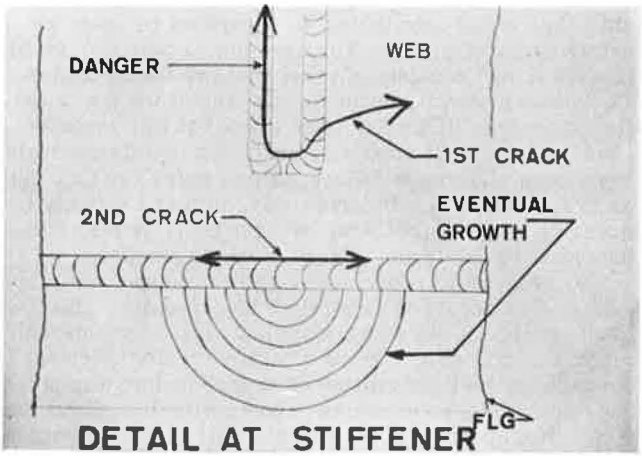

Figure 6. Connection of brace frame angle to stiffener that has gusset groove welded to stiffener.

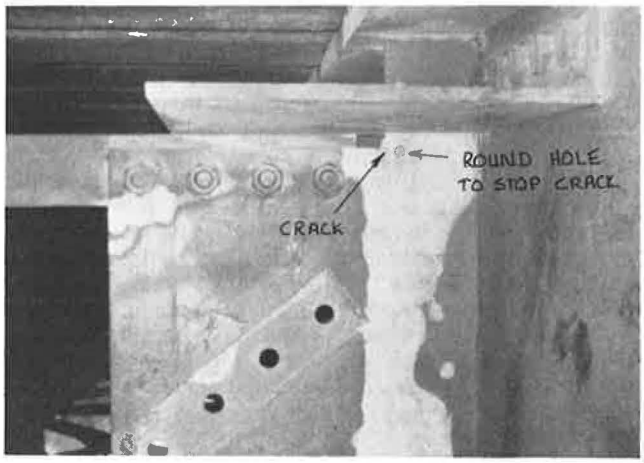

years for these cracks to develop. The time from the discovery of the first crack until the development of more than 400 on the same structure was less than 1 year. The danger is that, when the crack reaches the stiffener-to-web weld, if there are a few microdiscontinuities in that weld, the crack can run down the weld and split the web in half.

6. Longitudinal stiffeners are usually supplied in varying lengths and butt welded. Because they are usually in a compression area, not much concern has been given to inspection of them in the past. At least one railway and several highway departments have suffered failures from defects in these welds. Thus far, failures in this type of detail have initiated in overall tension areas. Although it is true that critical cracks occur only in tension areas, most welds are tension areas because of the residual stresses induced by the welding process. A crack can run along a weld until it reaches a tension area or until there is no material left. A crack (see Figure 8) can grow slowly in the butt weld, propagate along the longitudinal-stiffener-to-web weld, and then run down a vertical-stiffener-to-web weld and split the girder in half (4).

7. Intersecting welds pose serious problems. Fortunately, these have generally been prohibited on our railway from the beginning. There is, however, a very interesting case in the literature (5).

8. Patch plates and similar repairs (see Figure 9) always have an E-detail at the corners. There have not been significant failures on riveted structures at patches because (a) corrosion tends to erode the crack tip and slow the rate of growth and (b) redundant components act as crack stoppers. For example, a typical riveted tension flange consists of a web and two flange angles. Corrosion generally occurs in the web at the toe of the flange angles. If a patch plate placed at this location causes a crack, it must also crack the two flange angles to cause a significant failure. Rivet holes can also act as crack stoppers. Unfortunately, this is not likely to occur on welded structures because there is less component redundancy and almost no crack stoppers.

9. Figure 10 illustrates a rather unexpected fatigue failure that occurred as a result of corrosion. The I-beam stringers shown were subjected to a considerable amount of oil, grit, and such because trains often sat for quite some time waiting clearance and also engaged in frequent stops and starts during switching operations. The bottom portion of the web above the bearing corroded sufficiently so that the out-of-plane bending stresses reached a critical level. Lateral forces caused a crack to run along the fillet between the flange and web. Within a very short time, the bottom flange, which suddenly had to act as a beam, tore through. If bearing stiffeners had been placed as required by the code, the small lateral movements could not have occurred and the web could literally have rusted to nil before failure. The time to failure of these stocky web sections was about 15 years.

10. In many beam-and-deck-plate girder spans that have open timber decks, the inside part of the top flange must resist the bending of the ties (Figure 11). A larger than average tie will carry excess load. If there are insufficient stiffeners or if the stiffeners do not fit snugly to the flange, the flange will crack. If the crack is not arrested, it can turn down at the first vertical weld and split the web in half.

11. At stringer or floor beam connections, inadequate copes can approach an E-detail. Under normal traffic, these will not behave as pin connections but as nearly fixed. The resulting tension can cause a crack to propagate (see Figure 12). The beam is resting upside down.

12. Welds and notches that do not meet the design codes are a source of almost certain future cracking, as are notches caused by impacts from trucks (see Figure 13), loose shipments (see Figure 14), or even ships. The rapid rate of dynamic loading caused by a shipment collision usually causes immediate brittle fracture. An example of the damage that a loose shipment can cause is shown in Figure 15; the bridge truss collapsed when one of the tension members was severed by a load of culvert pipe.

On rarely used branch lines, restrictions can be relaxed considerably.

STOPPING CRACKS

The classic way to stop a crack is to drill a round hole (6). This converts a running crack that must be considerably worse than an E-detail to a B-detail if the hole is carefully reamed or at least to a D-detail (unless the workmanship is really sloppy). On our railway, a 1.27- to 22.7-cm (0.50- to 0.875-in) diameter hole is specified, depending on how easy it is to get at the crack tip. It is imperative that the hole contain the crack tip. If there is any doubt, it is better to lead the crack. Figure 16 shows a hole that did not contain the tip. The crack propagated from the hole edge where it was not visible when the hole was drilled to that shown in less than 4 weeks.

On flat surfaces, a Halec eddy-current crack detector is used to find the crack tip because this avoids removing the paint. On one bridge, this saved the cost of the machine. Note that the crack tip may not have broken the surface paint.

In other cases, the paint is removed and either a magnetic particle test or a good visual examination with is a magnifying glass are used. Dye penetrants do not offer a significant benefit over a magnifying glass in this type of work and, because of generally windy conditions, are messy to work with.

In some cases, such as cracks that penetrate the stiffener-to-web weld, a minimum of three holes must be drilled. The following procedure has been used successfully on at least two bridges:

1. Drill 1.11-cm ($\frac{7}{16}$-in) diameter holes on both sides at the stiffener through the web at an approximate angle of 30° away from the stiffener (Figure 17a), ensuring that the hole is truly circular and has as few rough edges as possible.
2. Ream the resulting hole in the web from the outside by using a reamer of the same diameter throughout until the hole reaches the stiffener and the surfaces are left smooth.
3. Be sure that all rough edges are made smooth even if a truly circular hole is not obtained and if hand filing is necessary.

Figure 17b shows the two holes drilled from the inside as shown in Figure 17a before the web was reamed to produce one smooth hole. Figure 17c shows the appearance after the two holes drilled from the inside had been reamed to one hole from the outside flush with the stiffener on the inside. (The white metal along the vertical centerline of the hole is the stiffener.)

In cases where the round hole is an unacceptable fatigue detail and it is physically possible, a high-strength bolt can be placed to ensure that the nonburr side of the washer is placed against the steel. This will ensure a B- detail or better and prevent further crack propagation because of the clamping force, should the crack tip have

Figure 7. Critical detail from Figure 6.

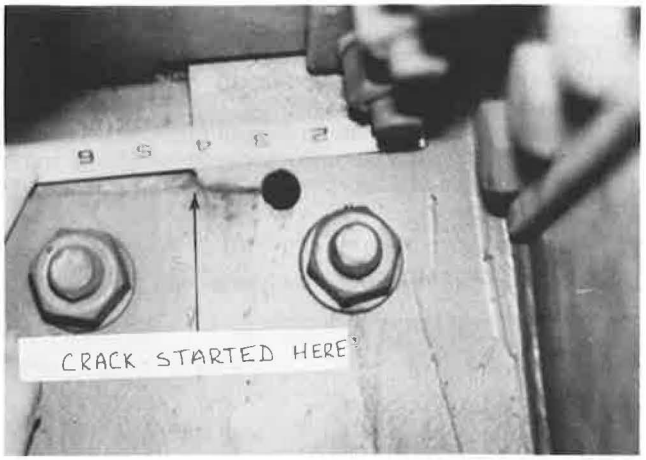

Figure 8. Crack growth from butt weld.

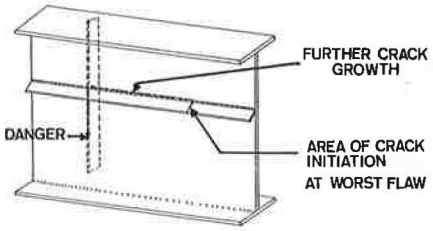

Figure 9. Typical repair section.

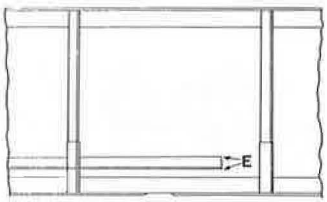

Figure 10. Corrosion-caused crack.

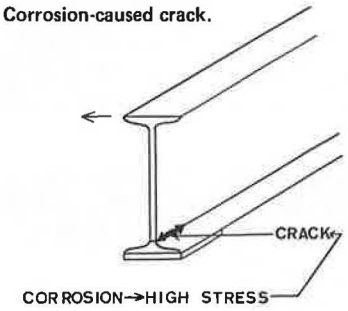

Figure 11. Crack caused by insufficient or badly fitting stiffeners.

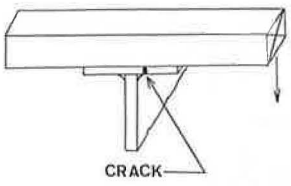

Figure 12. Crack caused by inadequate cope.

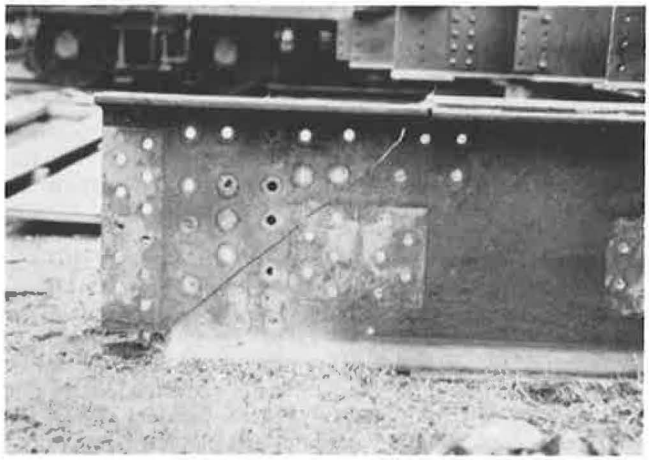

Figure 13. Notch caused by impact from truck.

Figure 14. Notch caused by impact from loose shipment.

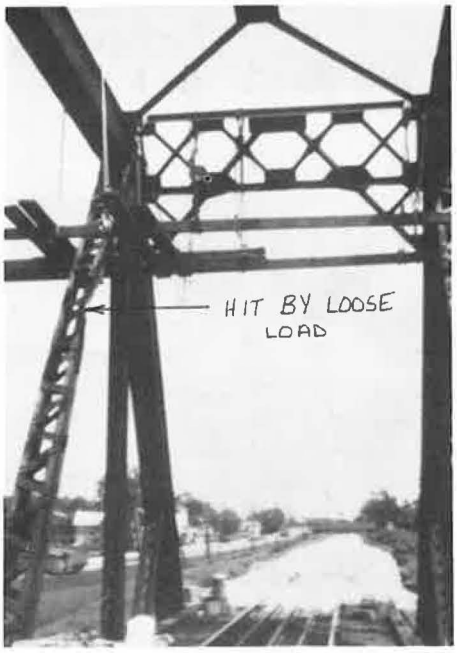

penetrated the far side of the hole. After stopping the crack, attention can then be focused on the repair.

REPAIRS

Unfortunately in many cases, the only adequate cure is not to use the detail in the first place. If the crack is not going to propagate and has not damaged the structure too severely, it is best left alone because the repair may make things worse. Cracks at the bottoms of stiffeners tend to be in this category.

If the structure cracked because it was restrained from movement and movement is essential to its function, as in the skewed-girder case, then a repair of the existing detail will be of no value. In fact, the next crack may be not in the same place but at a more serious location. A quick calculation of the stresses in a squared brace frame between skewed girders shows that these stresses will be very high and cannot be taken by the web alone (Figure 18). In addition to the obvious differences in vertical deflection of skewed girders, one should consider conceptually that the torsion in a girder will occur in the part most capable of rotating. The flange is generally much stiffer than the web, particularly in the space between the stiffener and the bottom flange, and any girder rotation (out-of-plane movement) will be forced to occur in this small space (Figure 4). Needless to say, the stresses will be enormous. To solve the problem, either the stiffeners must be run down to the bottom flange, or they must be cut back far enough to relieve the stresses, or the source of rotation must be removed. If the stiffeners are connected to the bottom flange in an area that has a high positive moment, this may entail a reduction in capacity. In some cases of composite deck slabs, a repair is not worth doing. The cracked detail will suffice for the one-shot accidental load.

Similar problems occur in curved girders.

Repairing cracks that occur between the flange and the web is extremely important. The general procedure for any crack is to

Figure 15. Truss collapse caused by impact from loose load.

Figure 16. Hole that did not contain crack tip.

Figure 17. Procedure for stopping crack propagation.

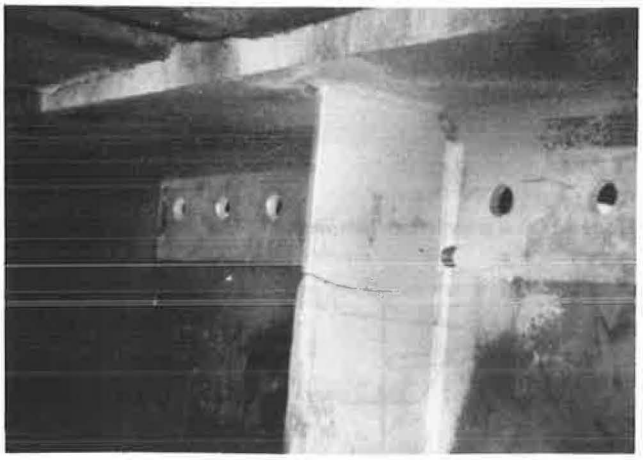

(a)

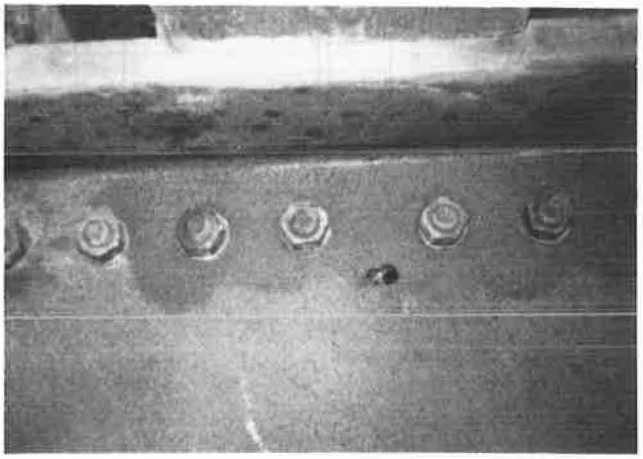

(b)

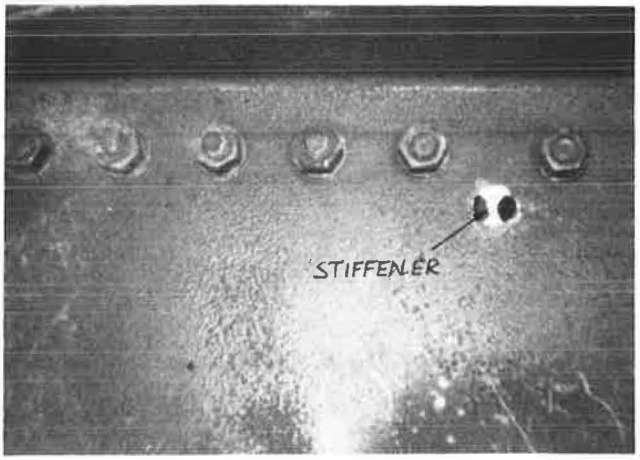

(c)

Figure 18. Stresses in squared brace frame between skewed girders.

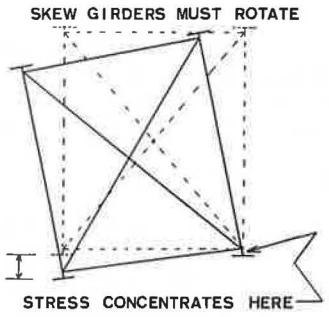

Figure 19. Procedure for repairing crack in gusset groove welded to stiffener.

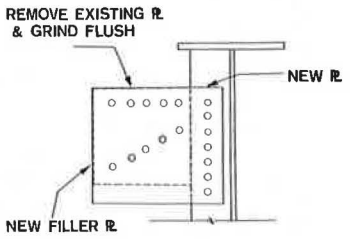

Figure 20. Illustration of procedure shown in Figure 19.

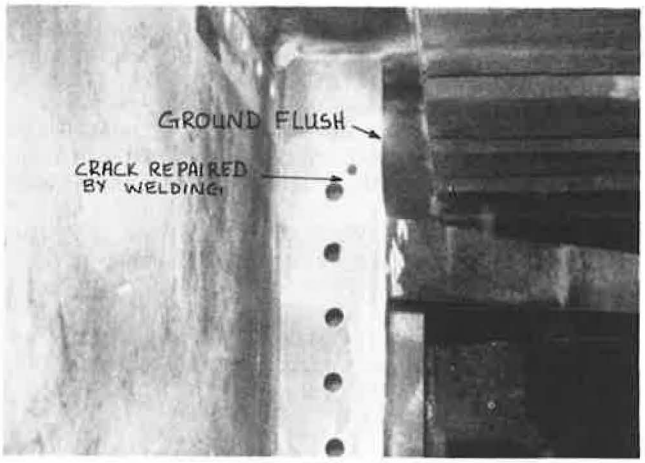

1. Use a chisel to vee out the crack,
2. Fill the resulting groove by using 7018 electrodes, and
3. Grind flush.

At this stage, an economic evaluation must be made as to the desirability of altering the detail that caused the crack, or of being prepared to accept that similar cracks will reoccur or, worse still, of accepting that eventually the structure may have to be replaced. In any organization where capital is in short supply, demanding high rates of return (15 percent or more), the usual decision is to leave the detail as is.

For the railway's rates of return, it is more economical to leave the detail alone if the repair will last at least 10 years.

New technologies, in particular the gas-tungsten arc remelt (7), may make future repairs easier and more reliable.

The detail of the gusset groove welded to the stiffener developed problems in less than 5 years; thus, problems with these details can be expected to reoccur in the same time frame if they are repaired. Therefore, it was decided to replace the butt-welded detail with a bolted detail for the brace frames (Figure 19). Before doing this, all cracks were repaired by welding (Figure 20) and the top and bottom 7.6 cm (3 in) of the stiffener, where the gusset was removed, were ground smooth to remove any incipient cracks.

In the case of longitudinal stiffeners, if the crack is caught before it propagates, it is usually left alone.

When patching girders, it is a simple matter to run patch plates far enough so that the girder stress will be small enough to permit an E-detail.

Figure 21. Procedure for repair of cope that has small cracks.

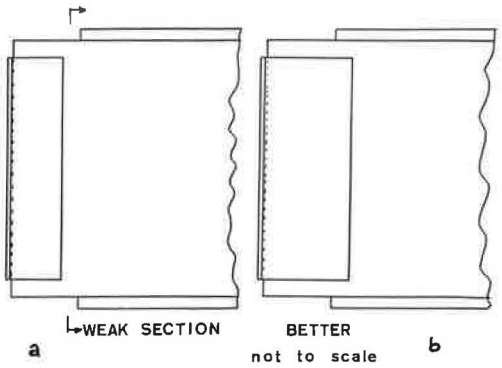

Figure 22. Sharp notch in member.

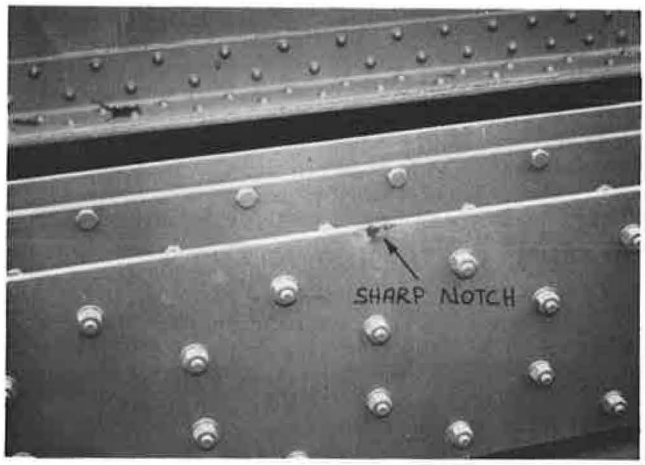

Figure 23. Truss repaired by welding and peening.

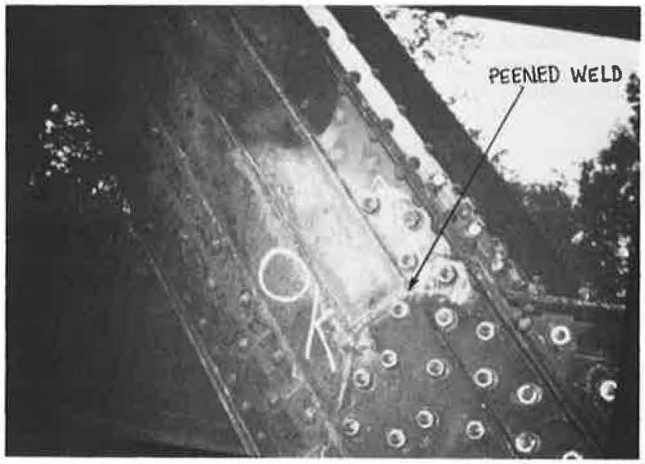

The corroded web was repaired by welding the flange to the web and adding a bearing stiffener. Those in which the flange had cracked through were replaced.

Failures in top flanges caused by transverse tie loading are rewelded. In some cases, stiffeners are added. These are welded to the top flange and not simply ground to fit because there is evidence (8) that fitting stiffeners is not adequate.

In the case of copes, those that have small cracks or none at all are ground to a smooth radius, which eliminates the problem. Others are handled in a variety of ways, taking care to use details that are adequate for the negative bending that designers do not calculate, but that actually occurs. The detail shown in Figure 21a is poor because there is a relatively highly stressed E-detail. A better solution is to use an oversized connection and not stiffen the joint in a prying sense (Figure 21b). This reduces the stress considerably at the notch.

Whenever a sharp notch is noticed in a member (Figure 22), if it is in a highly stressed area and if it is not on an almost abandoned branch line, it should be ground out at the first opportunity. The same should be done for tack welds, which seriously increase stress.

Several years ago, some strengthening was done to a truss (Figure 23). The welding was quite poor, and several cracks were detected on the surface. Some of the rough spots were removed and rewelded, and the entire weld was peened with a ball peen hammer. Sufficient peening was done to flatten any surface cracks and perhaps introduce a certain amount of residual surface compression. In theory, this should prevent surface crack growth. The structure has been in service since 1972 on a lightly traveled branch line in northern Vermont; it is too early to tell whether the desired effect was achieved. However, hand peening is extremely time consuming and unreliable if more than a short length of weld is involved.

For riveted connections, the expedient of replacing rivets that may be as bad as a D-detail by high-strength bolts (9), a B-detail, has been used after repairing the crack. As mentioned above, if the crack is still within the area of the washer, the residual compression induced by the bolt will prevent it from growing.

A note of caution is in order. There was one case in which a connection was badly underdesigned, and rough calculations that were inconclusive as to the number of cycles indicated that only a B-detail could have lasted so long. But after two rivets popped, it was quite clear that those rivets were functioning as high-strength bolts. Obviously, replacement with bolts would offer no advantage. The structure was replaced.

REFERENCES

1. J. W. Fisher and I. M. Viest. Fatigue Life of Bridge Beams Subjected to Controlled Truck Traffic. Proc., Seventh Congress, International Association of Bridge Structural Engineers, 1964.
2. J. W. Fisher, K. H. Fank, M. A. Hirt, and B. M. McNamee. Effect of Weldments on the Fatigue Strength of Steel Beams. NCHRP, Rept. 102, 1970.
3. J. W. Fisher, P. A. Albrecht, B. T. Yen, D. J. Klingerman, and B. M. McNamee. Fatigue Strength of Steel Beams With Transverse Stiffeners and Attachments. NCHRP, Rept. 147, 1974.
4. J. W. Fisher, M. D. Sullivan, and A. W. Pense. Improving Fatigue Strength and Repairing Fatigue Damage (Appendix F: Analysis of Crack Growth in the Quinnipiac River Bridge). Lehigh Univ., Bethlehem, PA; NCHRP, Final Rept. of Project 12-15(1), Dec. 1974.
5. J. W. Fisher, A. W. Pense, and R. Roberts. Evaluation of Fracture of Lafayette Street Bridge. Journal of the Structural Division, Proc., ASCE, Vol. 103, No. ST7, July 1977, pp. 1339-1358.
6. S. Timoshenko and J. N. Goodier. Theory of Elasticity. McGraw-Hill, New York, 2nd Ed., Chap. 4, 1951.
7. J. W. Fisher, A. W. Pense, and R. E. Slockbower. Retrofitting Fatigue-Damaged Cover-Plated Bridge Members. Paper presented at the 57th Annual Meeting, TRB, 1978.
8. D. A. Demo and J. W. Fisher. Analysis of Fatigue of Welded Crane Runway Girders. Journal of the Structural Division, Proc., ASCE, Vol. 102, No. ST5, May 1976, pp. 919-934.
9. H. S. Reemsnyder. Fatigue-Life Extension of Riveted Connections. Journal of the Structural Division, Proc., ASCE, Vol. 101, No. ST12, Dec. 1975, pp. 2591-2608.

Publication of this paper sponsored by Committee on Steel Bridges.

Stiffening the Manhattan Bridge

A. I. Zuckerman, Steinman, Boynton, Gronquist, and Birdsall, New York

The Manhattan Bridge is a suspension bridge located in New York City. Its lower level carries three lanes of traffic at the center of the bridge and two transit tracks on either side. Its upper level carries two lanes of traffic over each set of tracks. The loads are supported by four cables suspended over four stiffening trusses. After the bridge was opened to traffic in 1909, breaks appeared in the upper laterals. Substituted larger members also broke. The broken pieces were hazardous to the trains, which required the removal of the entire top lateral system. The breaks were attributed to torsional stresses induced by eccentric transit loads. Because it has no top laterals, the bridge has little torsional stiffness and large vertical and lateral motions occur between adjacent trusses during passage of trains, which causes many maintenance problems. Load tests for stresses and deflections were performed on the bridge, and a single-plane 50-scale model, 18 m (59 ft) long was constructed to duplicate the motions and stresses of the prototype. Schemes for stiffening the bridge—stays radiating from the tower tops to the stiffening trusses, tie cables that had small sags from anchorage to anchorage, diagonal ties between the cables and the stiffening truss, and side-span supports—were tested on the model. The side-span supports are efficient and economical in reducing deflections at the main-span center and almost eliminate deflections of the side spans. The tower stays and diagonal ties at the center of the main span are effective in reducing deflections of the main-span quarter points.

BACKGROUND

The Manhattan Bridge is the middle one of the three suspension bridges that connect lower Manhattan to

Figure 1. Typical cross section of bridge.

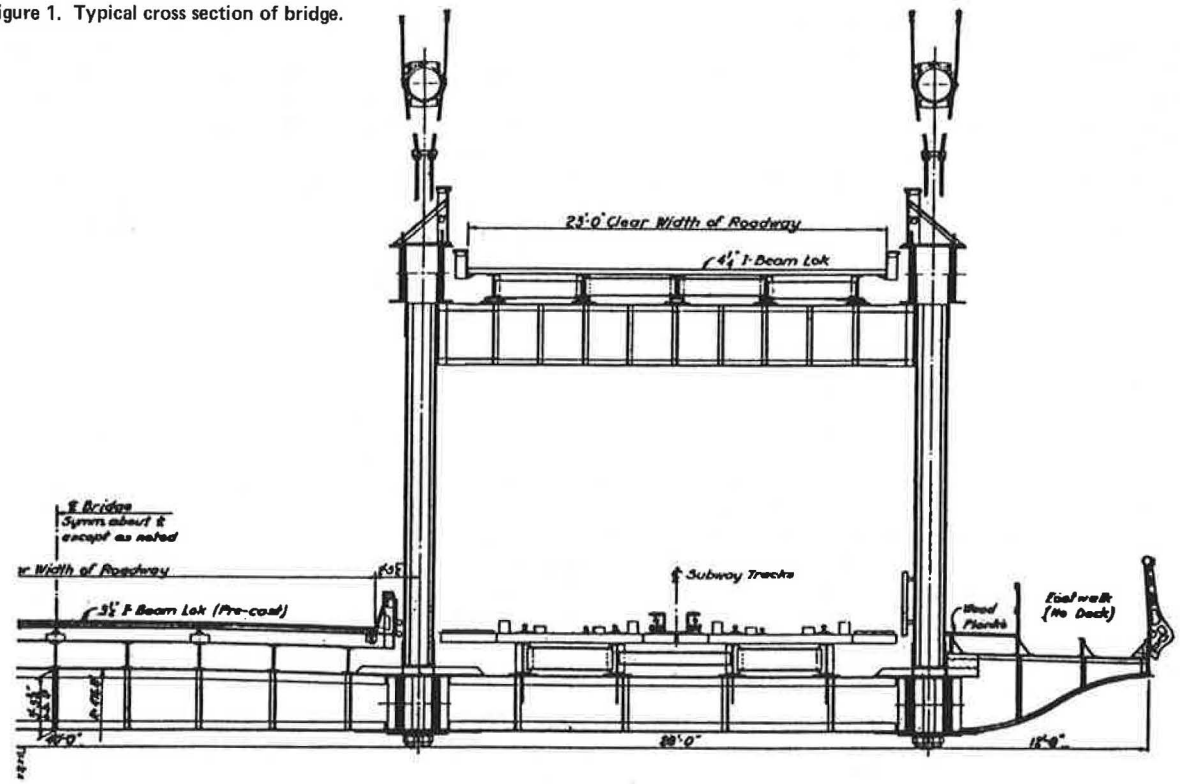

Brooklyn. It was completed in 1909 at a cost of $14 100 000, which is about the cost of painting it today.

The main span is 448 m (1470 ft) long—not large by present day standards—but it was a major undertaking at the time of construction.

The bridge has a number of unique features. It is one of the few suspension bridges that carry railroad loading and was the first suspension bridge in the United States designed according to the deflection theory.

This bridge, over the years, has generated more engineering studies and has had higher maintenance costs than many other bridges of its size. The basic reasons arise from two directions: (a) based on present day knowledge and criteria, the design and construction of the bridge incorporated certain imperfections, and (b) the vehicular roadways are filled with the heaviest type of metropolitan freight traffic, and the rail traffic (two subway tracks at each outer extremity of the bridge) creates even heavier loading.

Every time a subway train passes or, as frequently happens, two trains pass simultaneously, the bridge is wrenched, twisted, and wracked, and this has caused much distress and damage to the structural details. Fortunately, this represents no present danger to the safety of the structure. As long as the primary members (the cables, foundations, and main towers) remain in good condition, the effect of the damage is in the field of maintenance expense rather than of overall safety.

Structure of Bridge

On the cross section shown in Figure 1, some of the deficiencies and some of the corrective measures already taken can be pointed out. The cross section originally consisted of four cables supporting four trusses that are tied together only by the main floor beams at the level of their lower chords. The cables and suspenders were detailed and erected without regard to the amount of dead load pertaining to each plane of cable and truss. Thus, the floor beams were required to distribute the dead load equally to all cable systems. As a result, all floor beams have a measureable dish, or concave profile under dead load. The suspenders passed through the upper chord with no centering devices and were anchored below the bottom chord. Each time the bridge tipped with the passage of a train or of two trains on the same side, the suspenders moved toward and made contact with the members of the upper chords. This condition was most pronounced near the midspan. These suspenders have been replaced by using details that incorporate a single-part suspender in place of each two-part suspender, which has improved the clearance between suspenders and top chords.

There is full-width lateral bracing in the plane of the lower chords. In the plane of the upper chords, the original design included two independent sets of lateral bracing between each pair of trusses but none over the central lower roadway.

Problems and Corrective Measures

The upper lateral systems began to break up soon after the bridge was opened to traffic in 1909. The members were repaired and strengthened but continued to fail, and the pieces falling on the tracks below created a dangerous condition. Therefore, the top lateral systems were removed.

A complete top and bottom lateral system together with vertical trusses forms a rigid box that resists torsional deformations and attempts to equalize the loads transmitted to each cable. Because the top laterals have been removed from the Manhattan Bridge, the cables are now loaded quite unequally by eccentric loading. Under certain conditions of loading, the difference in elevation between the outer trusses can be as much as 2.4 m (8 ft).

The difference in loads taken by the cables also makes them move longitudinally with respect to one another as

a load passes across the bridge. This motion has caused a great deal of the wear of the steel between the stringers and the floor beams on the lower roadways and also resulted in the cracking of the floor beams under the upper roadways. These upper roadway floor beams were replaced in 1958 by a floating structure connected by elastic hinges to the stiffening trusses.

Another problem that has plagued the bridge was that of the cable bands slipping along the steeper portions of the cable. The original bands were designed as two sections of a hoop and tightened on the cable by using short bolts. These have been replaced by a modern type that uses heavy bolt housings to stiffen the hoop so that, as the bolts are tightened, the halves of the cable band are drawn against the cable, rather than just pinching the ends. Also, longer bolts are now used to achieve a greater elongation for a given stress and to minimize creep and relaxation of tension in the bolts.

However there still remains a need to reduce the torsional deflections of the bridge if it can be done at a reasonable cost. One of the previous ideas was to remove the trains from the bridge or at least move them to the center, but the New York City Transit Authority would not consider this. Another idea was to put in a full-width upper lateral system. This would be the perfect solution if we were building a new bridge. In this case, however, incorporating a heavy lateral system and reinforcing the cross section to maintain the shape of the box would be very expensive.

Thus, the following plan was developed for attacking the problem:

1. By a field survey, measure the deflections and stresses on the bridge structure under controlled loads to determine the effective moment of inertia of the trusses, the magnitude of the deflections, and the stresses and distribution of live load to each of the four truss-cable systems.
2. Design and construct a structural model of the bridge and calibrate it by comparison with comparable readings on the prototype.
3. Use the model to evaluate various schemes for reducing deflections under various loading conditions.
4. Make preliminary designs and estimates for the implementation of the best schemes.

The field survey was done at night. All traffic was diverted from the bridge. The controlled loading consisted of two empty 10-car subway trains approximately 183 m (600 ft) long side by side on the easterly (uptown) tracks. Complete sets of readings of deflection and stresses for all four trusses were made with the trains at the center and quarter points of the main span and the center point of the side span. The tower movements were also measured.

The deflections of each truss were measured by rod readings from a fixed line of sight, from a transit at one tower sighting a painted target at the other tower, and from the anchorages. The tower movements were measured by plumb line, and the stresses were measured by electric strain gauges.

The calculated stress agreed quite closely with the field measurements when the distribution of live loads was 50 percent to the outer cable, 35 percent to the next, 15 percent to the third, and 0 percent to that farthest from the load and the distribution of dead load was assumed to be equal to all cables.

The results of the survey were very gratifying in their consistency and similarity to the computed values.

Figure 2 shows the relationship of the stresses for the four trusses at the center of the main span. Even on this exaggerated vertical scale, the observed deflections appear as a straight line.

To compare the relative magnitudes of the survey stresses, the original design stresses, and the actual live-load stresses on the bridge, the truss stresses were measured during a typical 24-h period on the outer truss by using a recording strain meter. Figure 3 shows the repetitions versus the stress level at the centerline of the main span. The observed stresses are less than 8.3 MPa (12 000 lbf/in^2), which is the stress for the normal regular design load of 39.4 kN/m (2700 lbf/ft) of truss. On a suspension bridge, the theoretical loading pattern for maximum stress rarely occurs in practice.

Model

The model is a single-plane model that uses music wire for the cable and suspenders and steel bars to duplicate the properties of the stiffening truss. There are electric strain gauges attached to measure the stresses in the cables, suspenders, trusses, and any proposed stiffening devices. Ames dials were used to measure deflections.

After the model was completed, we were anxious to check whether it truly represented the Manhattan Bridge. The stresses and deflections were read for

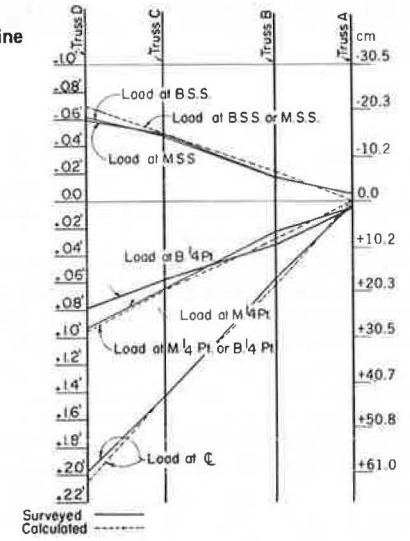

Figure 2. Torsional deflections at centerline of main span.

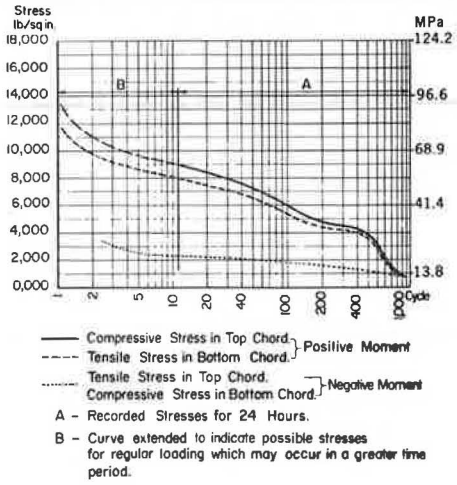

Figure 3. Stresses in top and bottom chords at main-span center.

live-load conditions that duplicated the field survey. These results were compared with the field survey and with the mathematical analysis. For comparable conditions of loading, the deflections and stresses were within 5 percent of each other. In some cases, the model compared more favorably with the field survey than with the mathematical analysis shown in Figure 4. (Because the mathematical analysis of the model was carried out in U.S. customary units, SI units are not given in Figure 4.) The model is illustrated in Figure 5.

SCHEMES

The live-load deflection of a suspended span results from three main sources: (a) elongation of the cables; (b) deflection of the tower tops [a 2.54-cm (1-in) deflection of each of the towers toward the other causes a 10.2-cm (4-in) deflection of the center of the main span], and (c) distortion of the cable.

To reduce deflections by significantly decreasing the elongation of the cable would require another cable equal to the size of the original, which is an impractical solution. Therefore, the schemes are oriented toward reducing the deflections of the tower tops and reducing the distortion of the cable.

The four basic iedeas for stiffening the model are illustrated in Figure 6 and include the following:

1. To use a tie cable (i.e., to connect an auxiliary cable from the anchorages to the towers and between the tower tops and so reduce the deflections of the towers,
2. To use diagonal cables to form a truss system between the main cables and the stiffening truss and so minimize the distortion of the cable.
3. To use diagonals and stays (i.e., cables originating at the tops of the towers and connected to the stiffening trusses near the quarter point of the main span and center of the side span) and so reduce the tower deflections somewhat and also the distortions of the cable, and
4. To support the side spans by using two tie columns under each side span and so reduce the deflections of the towers and, of course, almost eliminate the deflections in the side spans and their effects on the main spans (a downward deflection in the side span causes an upward deflection in the main span, and a downward deflection in the main span causes an upward deflection in the side span).

Tie Cables

The tie cables used were equivalent to 129-cm^2 (20-in^2) cable on the prototype. To obtain the most efficiency from the tie cables they should be stressed as highly as possible. We used 690 MPa (100 000 lbf/in^2) for a condition of maximum live load at all spans loaded and minimum temperature. We used the model to determine the proper initial tension so as not to exceed the 690-MPa limit by working backwards.

Diagonals and Stays

For the diagonals and stays, we first used wires equivalent to two 5.87-cm ($2^5/_{16}$-in) diameter ropes. Diagonals and stays are most effective when the fewest number go slack under any loading condition.

For the first test, the initial tension applied to each diagonal and stay was the amount computed by setting the vertical component equal to 25 percent of the dead load and keeping all of the horizontal components balanced. The working stress in the diagonal was checked for the various conditions of loading, and no overstress was apparent during any of the setups.

Seeking greater efficiency, we then substituted different size diagonals for the original. The diagonals near the centers of the spans that had low stresses were reduced, and those near the towers were increased to 3.5 times the area of the original. The idea was to reduce the elongation of those diagonals thought to contribute the most to the deflection. This increase in area showed only slight improvement over the original—about 15 percent in the overall deflection.

A number of other trials were made varying the vertical component of the prestressing force in the diagonals from 50 to 100 percent of the dead load. But the use of more than a 30 percent dead-load prestressing force caused some of the suspenders to go slack under certain live-load conditions.

The prestressing of the diagonals and stays presented an interesting problem because when one is tightened, another is loosened. We found the easiest way was to run through a cycle, starting the prestressing at both ends of the span and working toward the center. After a few cycles, the change in prestressing required to bring it to the theoretical value becomes very small.

Figure 4. Deflection curves.

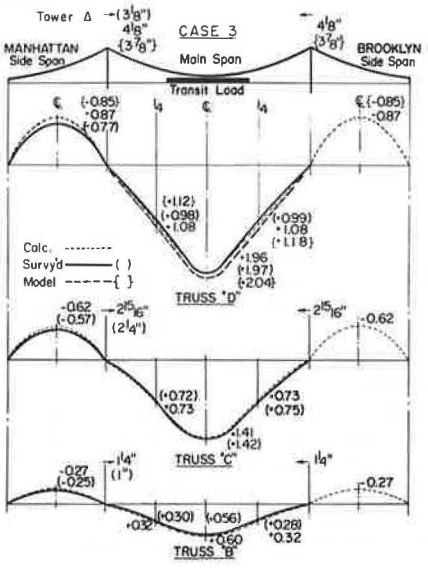

Figure 5. Basic structure of bridge.

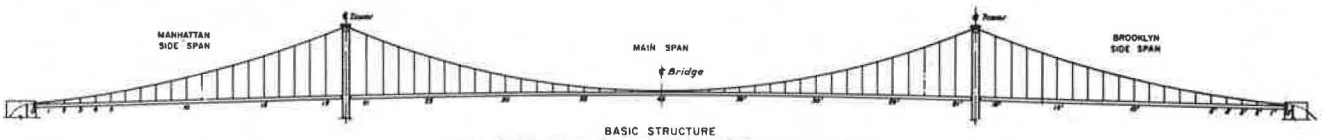

1. Test for Simulated Live Load in Transit Loadings used in Survey Case 1 to Case 5
2. Test for Deflections and Stresses. Regular Load and Congested Load.

Figure 6. Schemes tested.

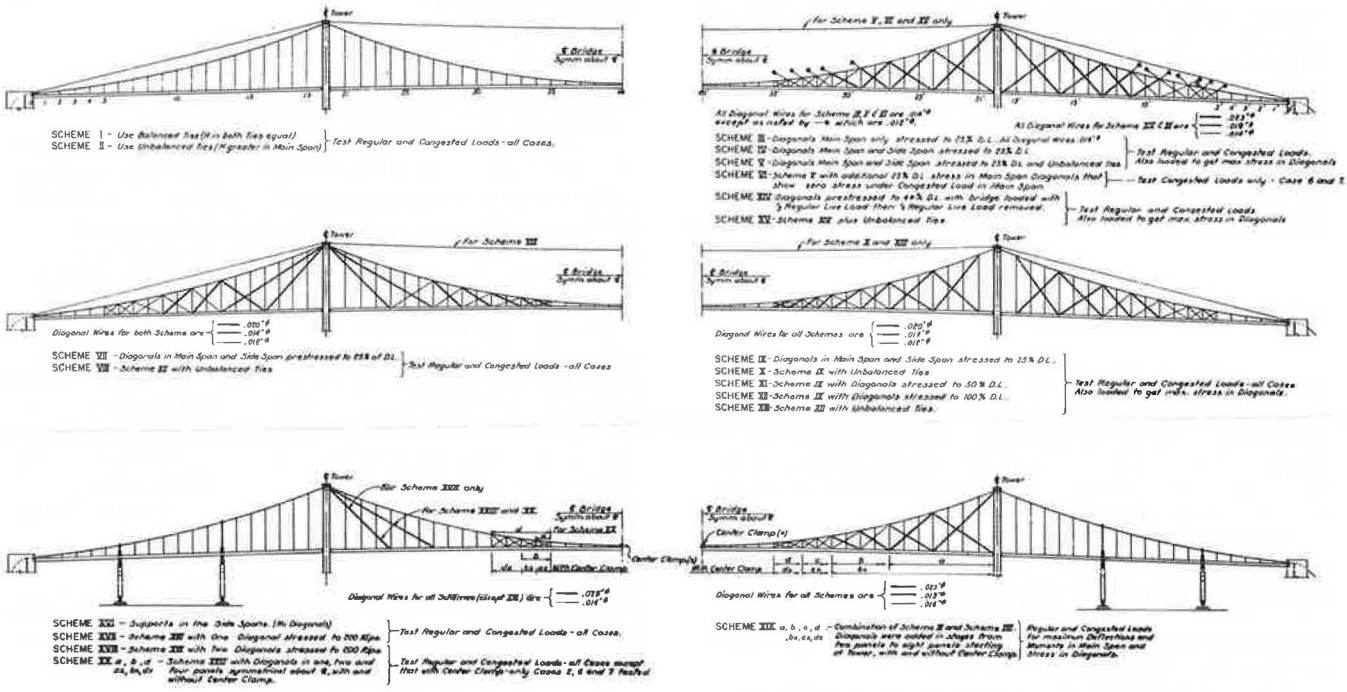

Figure 7. Torsional deflections.

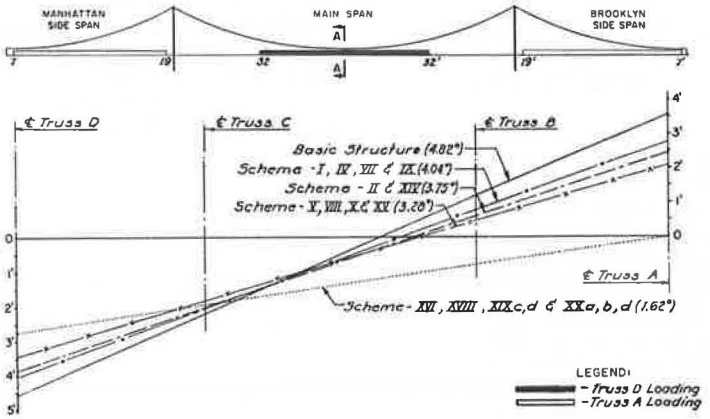

Tie Columns

For the tie columns, struts pinned at the top and bottom were placed as supports at the third points of the side spans. Ring transducers were placed at the bottom of the struts to measure tension or compression.

The tie columns were installed at zero dead-load stress by adjusting the height of each column to read zero stress in the transducers. The zero dead-load stress is important because it keeps the shearing stresses in the stiffening truss low. A suspension bridge has low live-load shear at the center of the side span when there are only minimum-sized diagonals at that location.

To obtain the maximum compression in the tie columns, the side span was loaded and the temperature increased. There were no slack suspenders.

The maximum tension in the tie columns was found by loading the main span and decreasing the temperature. During this trial, we found that all the suspenders in the side span participate in pulling on the stiffening truss, each in proportion to the vertical component of the live-load tension in the cable at its point.

Results of Tests

1. The tie cables reduce the vertical deflection 15 percent in the side span and 21 percent in the center of the main span, but only 12 percent at the quarter points of the main span (see Figure 7).
2. The diagonals and stays reduce the deflections in the side spans up to 40 percent and those at the quarter points of the main span up to 28 percent, but that in the center of the main span only 17 percent, which is disappointing.
3. The tie columns reduce the vertical deflections at the main-span quarter point by 32 percent and at the center by 48 percent.

Naturally, combinations of the various schemes—e.g., tie cables and diagonals, diagonals and side-span supports, and stays and side-span supports—were also tested. The combinations are more efficient than the individual basic schemes, but the reductions are not additive. For example, diagonals reduce the vertical deflection at the quarter point of the main span by 28 percent and side-span supports reduce this deflection

by 32 percent, but the combination of the two reduces the deflection by only 45 percent.

The moments in the stiffening truss are reduced at the quarter points of the main span and the center of the side span in all schemes. At the center of the main span, the moments increase up to 15 percent when diagonals are used, but less when other schemes are used.

The costs of the various schemes are given below.

Scheme	Cost ($)
Tie cables	4 000 000
Diagonals and stays	10 250 000
Side-span supports	4 750 000

COMMENTS

The question that many may ask is, Why use a model when a computer can do the work more easily? The computer can do the job more economically than a model for a specific condition or problem. In this case, however, we had some general ideas of what we wanted to try and thought that simply working with the model would generate additional ones.

Again you may ask, Why use a single-plane model to study ways to reduce torsional deflections? A three-dimensional model would have cost at least four times as much, because of the problems of duplicating the details and behavior of the floor beams and the bottom lateral system in the transverse and vertical planes. Also, we felt at the time that we could reduce the torsion by some means of resisting the change in the cable curve.

ACKNOWLEDGMENT

The model tests were made at Columbia University. I thank J. M. Garrelts, who made a space large enough to accommodate the model available to us.

Publication of this paper sponsored by Committee on Steel Bridges.

Stress Analysis of Haunch Region in a Rigid-Frame Bridge

S. D. Leftwich and F. W. Barton, University of Virginia and Virginia Highway and Transportation Research Council, Charlottesville

The primary purpose of this study was to develop an analytical model of the haunch region of a rigid-frame bridge, including the associated methodology for stress analysis, and to determine the magnitude and distribution of the stresses in a typical haunch configuration. A finite-element model was adopted for the haunch configuration, and loadings were determined from an analysis of the entire frame. Stresses and displacements throughout the haunch region were calculated for various live-load locations. The stresses in the web and flanges were compared with experimentally measured stresses available from a field test of the actual structure on which the analytical model was based. The comparison tended to validate the reliability of the model and method of analysis. Subsequent stress analyses were conducted to study the effect of including stiffeners in the haunch. The effects of web and flange thicknesses on the stress distribution in the haunch were also examined. Although only one bridge configuration and haunch geometry was considered, it is believed that the results of this study can be readily extrapolated to other haunch configurations in other rigid-frame bridges.

The use of rigid-frame structures for highway bridges is becoming increasingly popular. Bridges of this type generally have multispan, welded rigid frames and are so called because the supporting legs are integrally framed with the welded haunched girders that support the deck. In the analysis and design of such structures, it is necessary to make certain idealizing assumptions so that a reasonably uncomplicated solution may be achieved. These assumptions include (a) selecting effective lengths and stiffnesses for nonprismatic members, (b) idealizing the support conditions, and (c) making rather substantial simplifications that will permit the analysis of stresses in the haunch regions of the frame. Although certain of these assumptions can be made on a rational basis and have been shown to give reliable results, others are less reliable and the resulting solution is subject to question.

In the design of the haunch, accurate predictions of the stresses in the web under the design load are essential to ensure that AASHO specifications against buckling are satisfied and to determine the need and location for stiffeners. The application of traditional analysis and design procedures to this complex problem leads to results whose reliability and accuracy are uncertain. Thus, it seems desirable to develop a more accurate methodology for the prediction of haunch stresses by using contemporary analysis tools such as the finite-element method.

OBJECTIVE

The broad objective of this study was the development of a realistic model of the haunch region of a rigid-frame bridge element that would permit an accurate and reliable determination of the stresses within the haunch. The development of such a model would make possible subsequent parametric stress-analysis studies for the evaluation of the effects of geometry, stiffener location, and flange and web thicknesses on stress levels and locations of peak stresses within the haunch. The results of experimental stress measurements in the haunch region of a rigid-frame bridge, determined in earlier tests, were used as a basis of comparison for verifying the model.

Within the broad objective of the investigation, the following specific tasks were established:

1. The development of a realistic analytical model of the haunch region of a rigid-frame highway bridge that would permit accurate determination of stresses;
2. The determination of loadings on the haunch, corresponding to actual vehicle loads, by using standard modeling techniques for the entire bridge;
3. The calculation of the stress levels throughout the haunch for various vehicle locations;
4. The comparison of these analytical values of stress with those determined experimentally to provide some measure of verification of the haunch model; and
5. The evaluation of the effects of haunch parameters, such as stiffeners and thicknesses of the webs and flanges, on stress levels and peak stress locations.

The investigation was limited to the study of one bridge configuration and haunch geometry; namely, that of the rigid-frame bridge on I-64 near Charlottesville, Virginia. This particular bridge was chosen because it had recently been the subject of an extensive field study, and the results of the experimental stress and deflection measurements were available. The haunch configuration in this bridge is similar to that found in other rigid-frame structures, and the results of this study could be readily extrapolated to other haunch configurations. Because all of the experimental stress and deflection measurements correspond to a single vehicle load, the same live load was used throughout the study. The haunch parameters included were the thicknesses of the web and flange and the presence and absence of stiffeners in the haunch.

DESCRIPTION OF BRIDGE

The bridge studied carries the westbound lane of I-64 over US-250 about 4.8 km (3 miles) east of Charlottesville.

The bridge [see Figure 1 (2)] is 65.8 m (216 ft) long and has five three-span welded rigid frames. The structure [see Figure 2 (2)] was designed for an HS 20-44 live load by using A-36 structural steel in accordance with the AASHO specifications (1). The construction of the bridge was completed in the latter part of 1969, and the experimental load testing used as the model for this study was conducted in September 1972. Measured strains and deflections were recorded for a variety of load locations. In particular, on frame 2 (see Figure 2), eight rosette gauges were placed on the web of the haunch, and 19 SR-4 strain gauges were placed on the flanges and stiffeners of the same haunch. A sketch of the haunch instrumentation is shown in Figure 3 (2); further details of the instrumentation can be found in the report describing the field study (2).

The test vehicle used for the experimental study was a 3-axle diesel semitrailer loaded to simulate an HS 20-44 loading. This same vehicle loading was also used in the analytical investigation. Although the field study included test runs at various speeds and various lane locations, only data from crawl (static) runs in which the vehicle was centered over the test frame (frame 2) were used in the analytical study.

In the design of a bridge girder, total vehicle loads are usually distributed to each girder according to the AASHO specifications. In this analytical study, however, the distribution factor used was based on experimental measurements; that for the vehicle centered over the test girder was 0.3887 based on moments determined from strains measured at midspan.

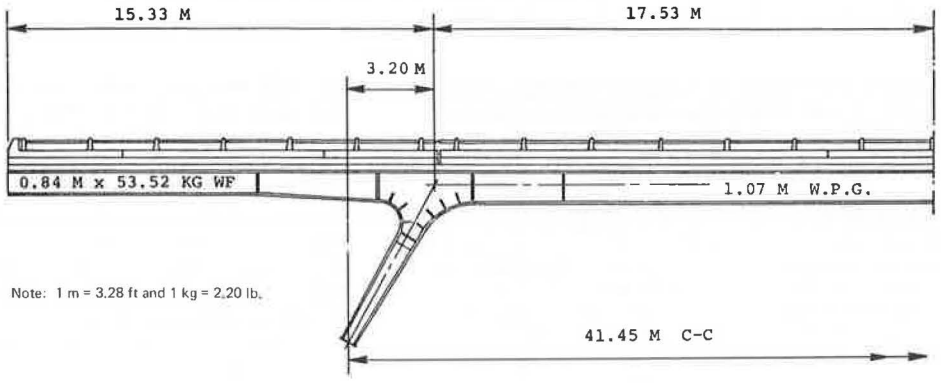

Figure 1. Partial elevation of test structure.

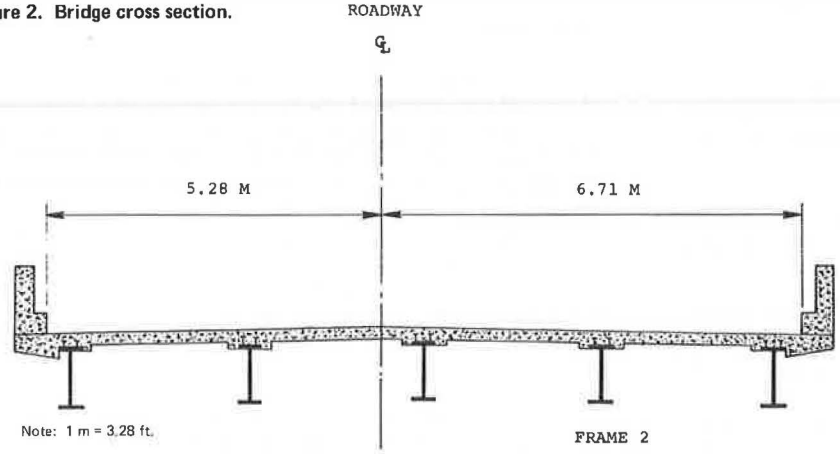

Figure 2. Bridge cross section.

Figure 3. Haunch gauge locations.

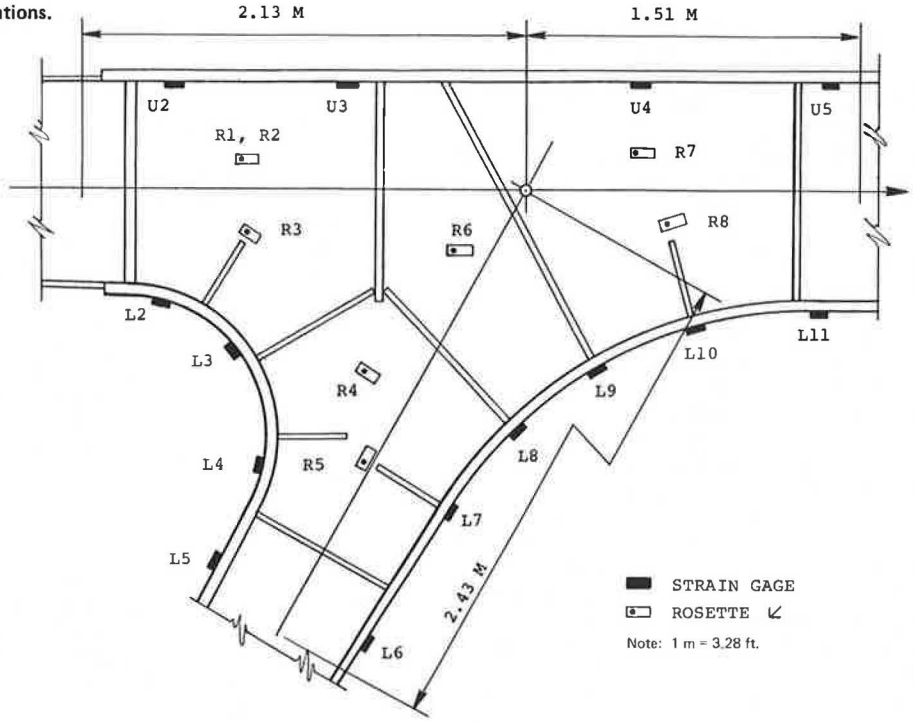

Figure 4. Finite-element model of haunch.

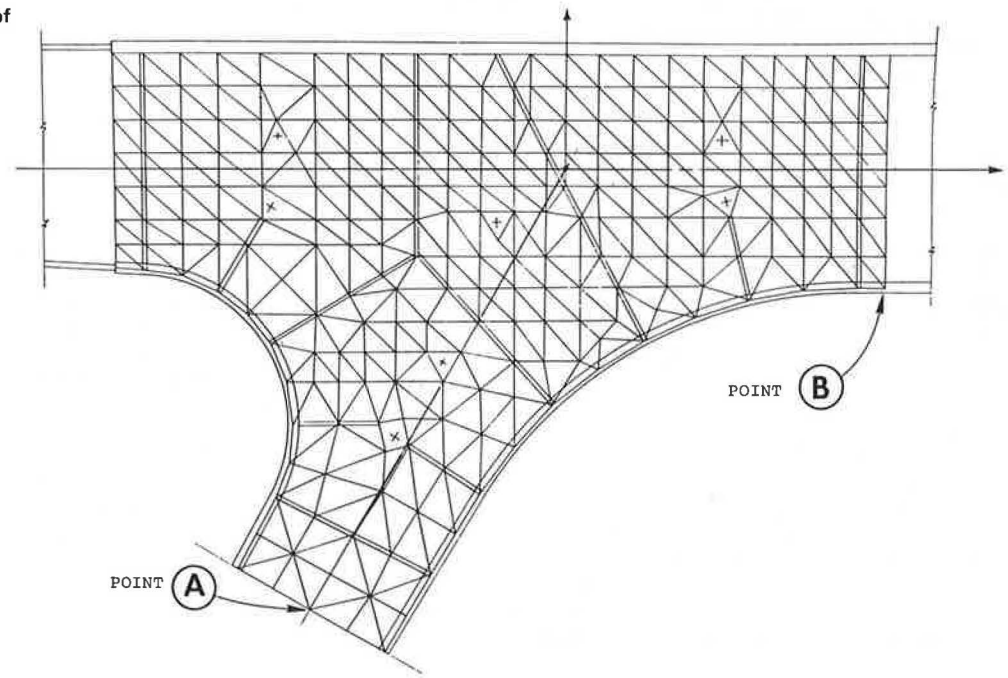

ANALYTICAL MODEL OF HAUNCH REGION

The upper portion of the haunch region of the rigid frame consists of a 0.203-m (8-in) concrete deck that overlays the top flange and is connected by studs to ensure composite action. A finite-element model was adopted as the analytical representation of the haunch. In the initial phase of the study, a number of mesh sizes and configurations were examined; the model finally adopted is depicted in Figure 4. The small crosses at the centroids of certain web elements indicate the locations of strain gauges on the actual bridge. Only four basic elements were used in the finite-element model of the haunch. Beam elements were used to represent the top steel flange and the concrete upper deck, bar elements were used to represent the stiffeners, the web region was modeled by using membrane elements, and the lower flanges of the haunch were represented by plate-membrane elements. Details of these elements can be found elsewhere (3).

Theoretically, the finite-element model of the haunch should require no support conditions for equilibrium, but, to prevent rigid body motion, the following support

conditions for the haunch region were imposed: (a) a pinned support at the middle node of the leg extremity (point A in Figure 4) and (b) a roller support at the lowest node of the haunch interior (point B in Figure 4). This method of supporting the haunch model seems rational because the legs were assumed to be pinned and the bearings at the abutments were taken as rollers in the bridge finite-element program.

DETERMINATION OF LOADS ON HAUNCH MODEL

The external loads applied to the haunch extremities correspond to internal forces at the haunch locations in the frame for a particular location of live load. These loadings on the haunch thus require an analysis of the entire frame, which was performed by using standard finite-element modeling in which the frame was represented as a series of prismatic beam elements.

This particular bridge model was also used in the earlier study of the bridge (2). In this model, the flexural characteristics of the structure were modeled as closely as possible. The concrete deck was transformed to an equivalent area of steel by using a value of n (ratio of E_c/E_s) equal to 6 and an effective slab width prescribed by AASHO specifications. The composite section was used in negative moment areas as well as in positive moment areas inasmuch as there was no apparent cracking in the deck slab. For support conditions, each of the inclined legs was assumed to be pinned at the base and the bearings at the abutments were treated as roller supports. The results of the analytical study compare favorably with the experimental results (2), thus indicating a reliable model. The results used in this comparison were based on the vehicle centered over the test frame and a transverse distribution factor of 0.3887, which was the experimentally measured distribution factor based on the midspan moments.

By using a live load corresponding to an AASHO HS 20-44 vehicle loading, the internal forces were calculated at frame locations corresponding to the haunch extremities for a variety of load locations; these forces were used as external loading on the haunch model. This same model was also used to define the loading at the haunch extremities caused by the dead load of the bridge.

After the external forces on the haunch were determined, they were transformed into nodal loads for use with the finite-element model. The shear and thrust forces were distributed evenly among the nodes at the haunch extremities. For the moments, an equivalent force at each node was determined by calculating the tributary area about the node in question multiplied by the average stress. The average stress about a node was obtained by evaluating the stress between adjacent nodes and taking the average of the two values.

RESULTS OF STRESS ANALYSIS OF HAUNCH

Stresses Caused by Live Loads

The haunch model was analyzed by using the large, general-purpose finite-element code called SPAR (3) to determine the nodal displacements and element stresses for all of the elements in the web and flanges of the haunch. Because the stress parameter of primary interest in the web of the haunch is the absolute maximum stress, the stress output from the SPAR program was transformed into principal stresses for the web elements. This value not only gives the best indication of critically stressed regions in the haunch, but also permits direct comparison with the experimentally determined stresses (which were available only in the form of principal stresses).

Two vehicle locations (where the vehicle location is defined as the location of the front axle of the vehicle given as a percentage of the distance between the air hoses used during the experimental testing of the bridge) were used for the live-load study. These were chosen on the basis of the influence lines and the experimental data and were those at 28 and 35 percent respectively, which were believed to be the ones that would produce the maximum stresses. Thus, 28 percent of the distance between air hoses is equivalent to the front axle of the vehicle's being a distance of 12.2 m (40.25 ft) from the left abutment (see Figures 5 and 6).

Contours of Minimum Principal Stress

The best method of representation of the stress levels within the haunch region appears to be in the form of stress contours. The minimum principal stresses are the largest in absolute value; thus, contours of these stresses were plotted for the two vehicle locations by extracting those calculated at the centroid of each element of the finite-element haunch model (see Figure 4) and then interpolating a smooth curve between values of equal stress to obtain a contour line. All contours shown are in intervals of 1.38 MPa (200 lbf/in^2) and for the minimum principal stress only. All stresses are in compression, and the direction of minimum stress is normal to the contour line. Stress contours were also generated for a haunch that did not have stiffeners to observe whether there were any significant changes in stress levels. To compare the contours, the stresses at three different locations within the haunch region are denoted to demonstrate the effect of the stiffeners. In all cases, the haunch loadings were calculated by assuming that the girders were on roller supports at the end abutments.

Figure 5. Vehicle at location 28 percent.

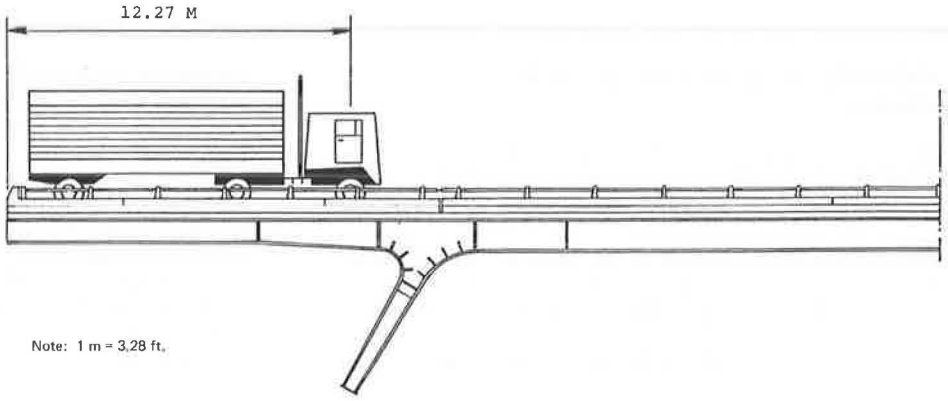

Figure 6. Vehicle at location 35 percent.

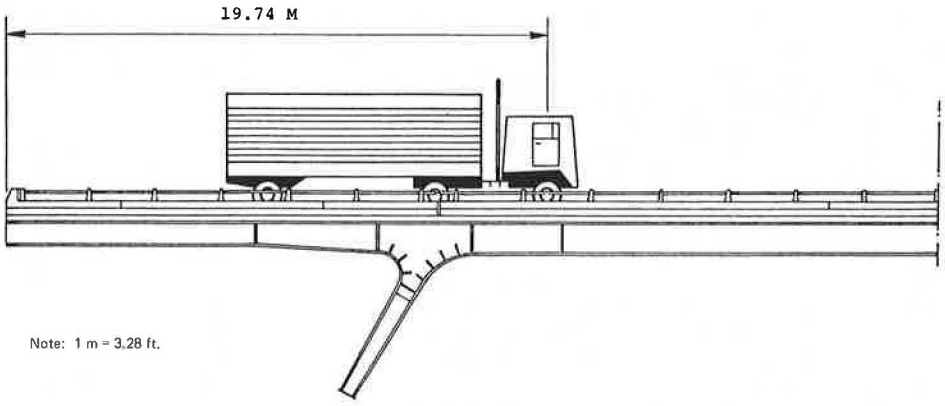

Figure 7. Stress contours in haunch that has stiffeners: vehicle at location 28 percent.

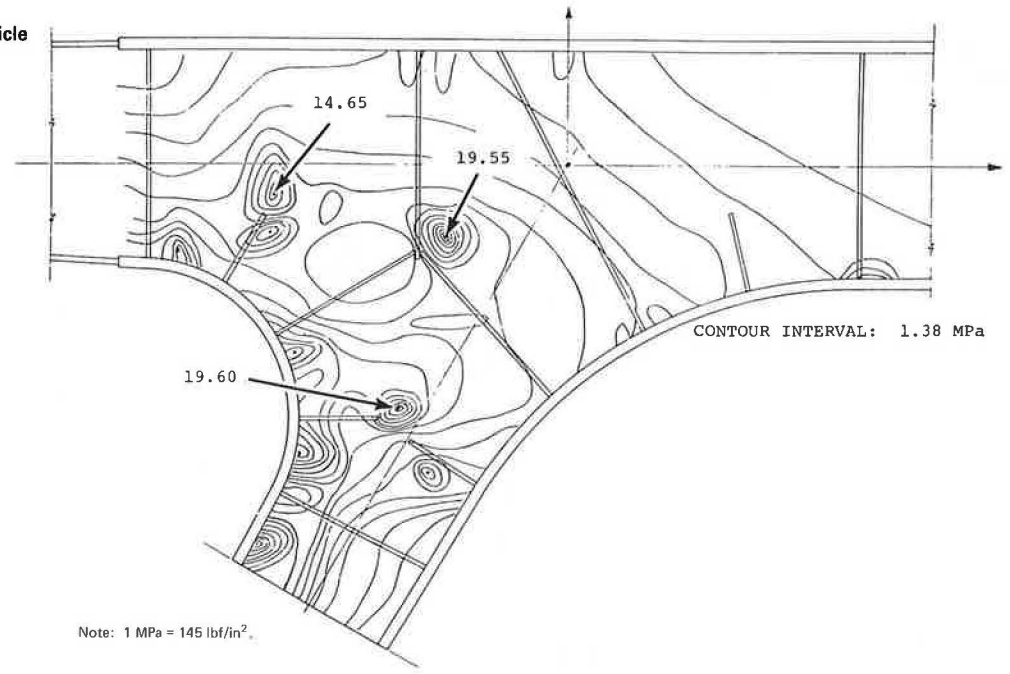

Figure 8. Stress contours in haunch that does not have stiffeners: vehicle at location 28 percent.

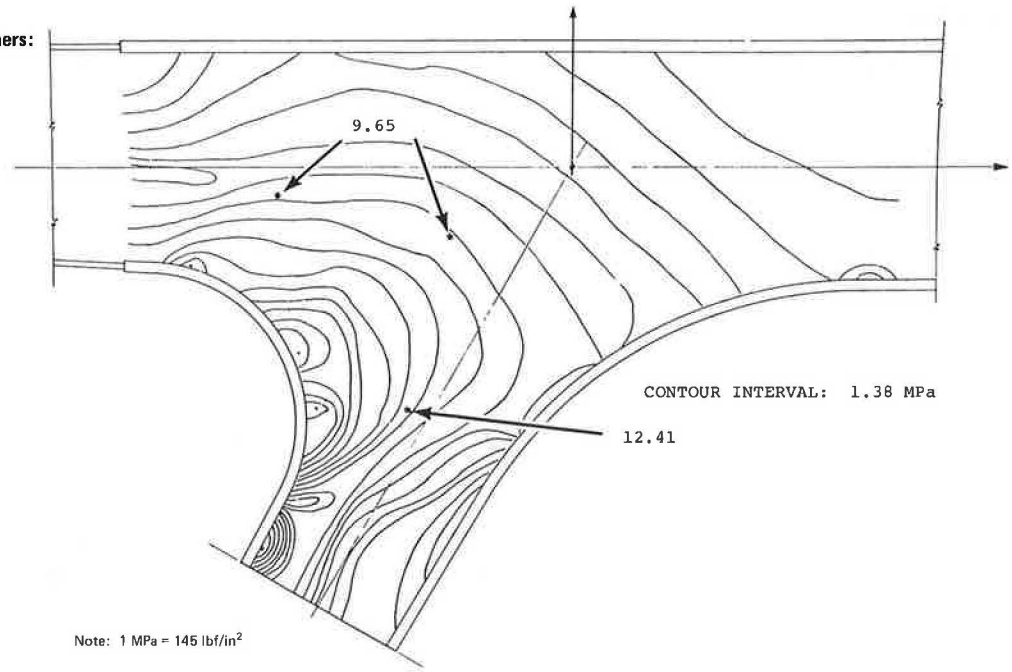

Figures 7 and 8 show the contours of the minimum principal stress for the vehicle at location 28 percent for the haunch region in the presence and absence of stiffeners respectively. Figure 7, that for the haunch that has stiffeners, shows a concentration of stresses at three locations corresponding to the end and junctions of stiffeners; Figure 8, that for the haunch that does not have stiffeners, has much smoother stress contours and only a few areas of stress concentration about the curved lower flange. Of particular interest is the fact that the stress levels at the three points identified in Figure 7 are significantly reduced. However, the largest compressive stress for the haunch that has stiffeners was 21.55 MPa (3126 lbf/in^2) and the largest for the haunch that does not have stiffeners was only 22.47 MPa (3259 lbf/in^2), which is an increase of only approximately 4 percent.

Figures 9 and 10 show the contours of the principal stress for the vehicle at location 35 percent for the haunch region in the presence and absence of stiffeners respectively. Again, there are stress concentrations at the end and junction of the stiffeners in Figure 9, but only a few areas of high stress concentration for the haunch region that does not have stiffeners (see Figure 10). The stress levels at two of the three designated locations within the haunch were reduced significantly by the deletion of the stiffeners. The largest compressive stress in the haunch that has stiffeners was 21.70 MPa (3147 lbf/in^2) and the largest for the haunch that does not have stiffeners was 24.24 MPa (3516 lbf/in^2), an increase of about 12 percent.

Figures 7 through 10 indicate that the inclusion of stiffeners in the haunch region of the bridge may lead to areas of high stress concentrations at the end and

Figure 9. Stress contours in haunch that has stiffeners: vehicle at location 35 percent.

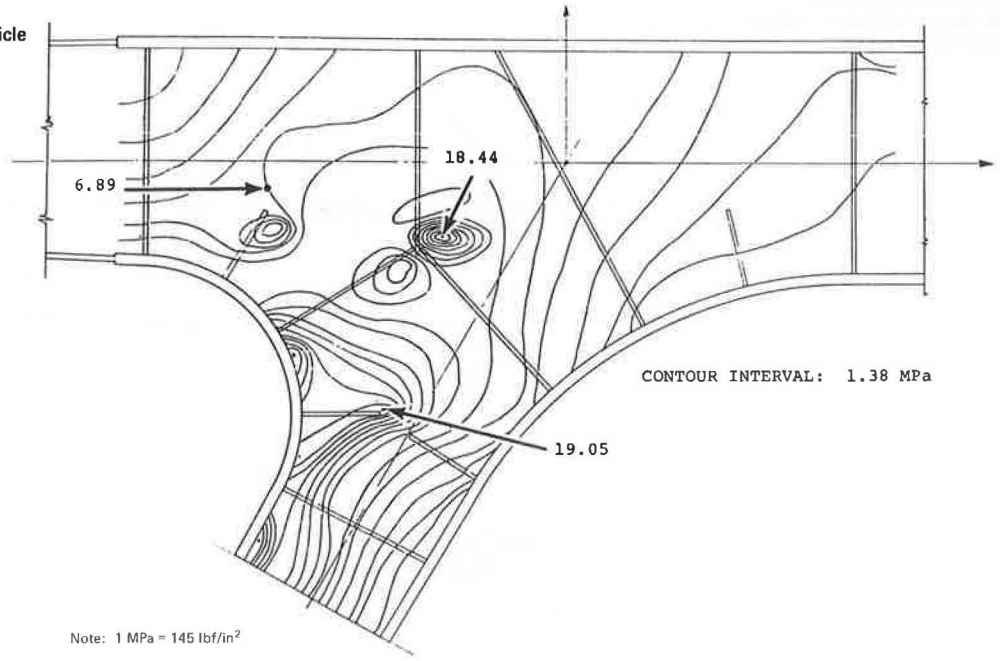

Figure 10. Stress contours in haunch that does not have stiffeners: vehicle at location 35 percent.

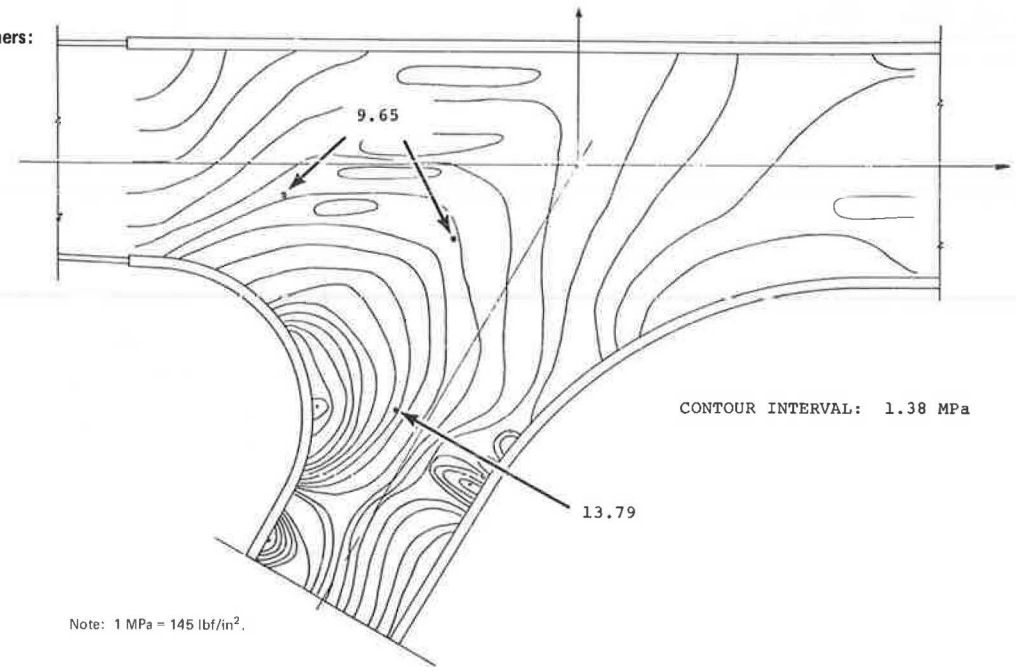

junctions of the stiffeners. These figures also indicate that the deletion of stiffeners altogether within the haunch appears to produce fewer areas of high stress concentration and smoother flow patterns of the stress contours. They also show that the absence of stiffeners does not necessarily increase the minimum compressive stress in all regions of the haunch web. If stiffeners are used, such areas of high stress concentration may be particularly susceptible to fatigue-type failures in the welds joining the stiffeners to the web. Thus, the use of stiffeners may have detrimental results in the web portion of the haunch and care should be exercised in the design of the haunch with regard to the use and placement of the stiffeners.

Effect of Web and Flange Thickness on Stress Levels

A number of analyses were made of the finite-element model of the haunch that had stiffeners for various web and flange thicknesses and the vehicle at location 28 percent. The flange thicknesses ranged from 2.54 to 50.8 cm (1.0 to 2.0 in), and the web thicknesses were varied from 0.95 to 1.27 cm (⅜ to ½ in). There appeared to be no recognizable pattern of stress magnitudes; the highest stresses occurred in different regions for the various web and flange thicknesses. Generally, for a constant flange thickness, the stresses in almost all regions of the haunch increased as the web became thinner—which is an expected result. A noteworthy observation was that, for a constant web thickness, the stress levels in all regions of the haunch did not necessarily increase as the flange thickness decreased. One possible explanation of this phenomenon could be the redistribution of stresses caused by the reduction in the thickness of the flange.

Stresses Caused by Dead Loads

The analysis of the haunch stresses caused by live loads indicated regions of stress concentration that might possibly be stressed beyond the allowable limit when the total dead load plus the live load was considered. Hence, a limited study was made to determine the approximate peak stresses in the haunch when the effect of dead loads was included.

For the haunch that had stiffeners, the minimum principal compressive stress caused by dead loads was 67.46 MPa (9784 lbf/in²) for the bridge on roller supports at the end abutments and, for the haunch that did not have stiffeners, the largest stress was 76.72 MPa (11 127 lbf/in²). Correspondingly, the largest live-load stresses were 21.70 MPa (3147 lbf/in²) and 24.24 MPa (3516 lbf/in²) for the haunch that did and the haunch that did not have stiffeners respectively. The worst possible combination of dead load plus live load for these two cases would be simply the sum of the two—i.e., approximately 89.64 MPa (13 000 lbf/in²) and 101.36 MPa (14 700 lbf/in²) in compression—which are well below the maximum allowable stress of 137.90 MPa (20 000 lbf/in²).

Another observation was that the dead-load stresses determined from computer runs based on the assumption of pin supports at the end abutments were all lower in magnitude than the results based on the assumption of roller supports. A possible explanation for this effect is that the internal forces about the haunch extremities are changed significantly whenever the horizontal movement of the bridge is restricted.

Table 1. Experimental and analytical live-load stresses in haunch web at gauge locations.

Rosette Gauge	Principal Stress	Vehicle at Location 28 Percent: Analytical Stress (MPa)		Vehicle at Location 35 Percent		
				Experimental Stress (MPa)	Analytical Stress (MPa)	
		Roller Support	Pinned Support		Roller Support	Pinned Support
R1 and R2	σ min	-6.78	-5.66	-2.99	-6.89	-3.08
	σ max	1.23	0.66	1.79	2.43	0.81
	τ max	4.01	3.16	2.39	4.66	1.94
R3	σ min	-14.65	-12.98	-7.55	-13.40	-7.51
	σ max	-1.21	-1.61	-3.15	0.48	-0.66
	τ max	6.72	5.68	2.20	6.94	3.43
R4	σ min	-10.37	-9.62	-10.02	-9.16	-6.17
	σ max	7.65	6.42	1.14	5.81	1.32
	τ max	9.01	8.02	5.58	7.48	3.75
R5	σ min	-13.83	-12.56	-9.78	-13.13	-8.48
	σ max	0.99	0.58	-0.85	0.01	-1.54
	τ max	7.41	6.56	4.47	6.56	3.47
R6	σ min	-7.36	-6.70	-7.87	-7.76	-4.67
	σ max	4.14	3.40	0.97	3.78	0.62
	τ max	5.76	5.05	4.42	5.76	2.65
R7	σ min	-2.08	-2.12	-4.82	-3.92	-3.66
	σ max	0.76	0.29	-1.64	1.39	-0.26
	τ max	1.42	1.21	1.59	2.65	1.70
R8	σ min	-2.83	-3.30	-6.16	-2.73	-3.53
	σ max	1.32	0.55	-3.03	2.30	-0.80
	τ max	2.08	1.92	1.57	2.52	1.37

Note: 1 MPa = 145 lbf/in².

DISCUSSION OF RESULTS

The determination of stresses in the haunch region caused by live and dead loads given above provides a basis for comparison with experimentally measured stresses.

In Table 1, the principal stresses in the web obtained in the experimental study are compared with those determined in the finite-element analysis. Both support conditions of the bridge at the end abutments were considered. Unfortunately, there were no experimental results available for the vehicle at location 28 percent.

As shown in Table 1, most of the analytical results compare favorably with the experimental results. The latter appear to be bounded by the former for pinned and roller supports at the end abutment. The experimental stresses do, however, appear to agree more closely with the analytical stresses for the pinned support, rather than for the roller support. For the live load considered, it appears that there may be some restriction of the horizontal movement of the bridge at the end abutments. This could be caused by either of two reasons: (a) frictional resistance of the girder against the bearing plate at the end abutments might restrict horizontal movement or (b) the relative magnitude of the live load might be so small, in comparison with the dead load, that most of the lateral movement of the bridge would be taken up by the rotation of the legs at the interior supports.

In Table 2, the stresses determined in the experimental and analytical studies are compared for the gauges on the upper and lower flanges and on the stiffeners. At locations 28 and 35 percent, the results of the analytical study compare satisfactorily with the experimental results for some gauges, but not favorably for the others. This discrepancy of the live-load stresses may be the result of a number of factors.

For example, the experimental results were measured manually from oscillograph tapes, and some discrepancies in the peak values of the stresses may have been introduced. Still, it is probable that these experimental values represent a good approximation to the actual values. Also, the stresses obtained at vehicle

Table 2. Experimental and analytical live-load stresses in haunch flanges at gauge locations.

Gauge	Vehicle at Location 28 Percent: Experimental Stress (MPa)	Vehicle at Location 28 Percent: Analytical Stress (MPa)		Vehicle at Location 35 Percent: Experimental Stress (MPa)	Vehicle at Location 35 Percent: Analytical Stress (MPa)	
		Roller Support	Pinned Support		Roller Support	Pinned Support
L2	0.52	-5.71	-5.37	-2.85	-4.40	-3.12
L3	-11.40	-7.36	-6.62	-7.07	-6.29	-3.63
L4	-15.97	-9.09	-7.83	-9.08	-8.72	-4.39
L5	-9.86	-4.19	-3.52	-6.18	-4.19	-1.90
L6	3.91	3.70	2.90	-2.94	3.08	0.34
L7	3.21	7.58	5.76	-3.44	5.98	-0.26
L8	-0.90	3.43	1.99	-4.54	2.76	-2.23
L9	-3.64	0.11	-1.09	-5.94	0.99	-2.91
L10	-3.94	-1.53	-2.76	-5.21	1.10	-2.82
L11	-3.97	-0.57	-3.67	-3.11	0.41	-0.68
U2	0.46	0.43	0.49	0	0.25	0.51
U3	-0.33	-0.36	-0.23	0	-0.90	-0.37
U4	-0.12	0.40	0.46	-0.34	1.24	1.51
U5	0	0.43	0.64	0	-0.38	0.39

Note: 1 MPa = 145 lbf/in^2.

locations 28 and 35 percent may be sensitive to the degree of restraint of the legs of the bridge. The bridge used for the analytical results models the legs as being pinned at their base, which appears to be a rational assumption, but the actual degree of restraint of the legs is not known.

Despite the variations between some of the experimental and analytical stresses, the agreement for the most part was surprisingly good. Factors that could not adequately be incorporated into the analytical model, such as residual stresses resulting from fabrication and induced loads transmitted through the diaphragms, may have caused some of the variations. Nevertheless, the calculated stresses were of the same order of magnitude as the experimental values, and when stresses were also calculated by using slightly different assumptions for the model, the analytical stresses frequently bounded the experimental values.

Thus, the haunch model developed in this study appears to provide an accurate representation of the actual structure and may be used with confidence for stress analyses of future similar structures.

CONCLUSIONS

The stresses determined in the analytical study compared reasonably well with corresponding stresses measured experimentally in both the web and the flanges of the haunch. Based on these results, it was concluded that the haunch model developed gives reliable stresses and can be used with confidence to study the effects of various parameters on haunch stresses.

The placement of stiffeners within the haunch region may induce areas of high stress concentration at the end and junctions of the stiffeners. This possibility could be a factor in designing against fatigue, and extreme care should be exercised in placing and locating stiffeners in the haunch region of a rigid-frame bridge. Variations in the thickness of the web had significant effects on the stress levels within the haunch, although variations in the thickness of the flange had relatively small effects. Decreasing the thickness of the web and keeping the thickness of the flange constant generally increased the stress levels in the web of the haunch. There was no recognizable pattern of stress distribution when the thickness of the flange was varied and the thickness of the web kept constant.

Although only one bridge configuration and haunch geometry were considered in the study, it is believed that the results can be readily extrapolated to other rigid-frame bridges and haunch configurations.

ACKNOWLEDGMENTS

The research reported here was conducted under the general supervision of Jack H. Dillard of the Virginia Highway and Transportation Research Council. W. T. McKeel, Jr., and H. L. Kinnier offered valuable suggestions during the analytical study and the preparation of the paper.

We acknowledge the assistance of the research council and the Federal Highway Administration in making available the experimental results from the field testing of the rigid-frame bridge modeled in the study. The assistance of personnel in the data section of the council and at the computer center of the University of Virginia is gratefully acknowledged. Finally, special appreciation is expressed to those many individuals who assisted in the preparation of the paper, in particular to Paul Hughes and Allen Baker for the graphics.

The opinions, findings, and conclusions are ours and not necessarily those of the sponsoring agencies.

REFERENCES

1. Standard Specifications for Highway Bridges. AASHO, 1965.
2. H. L. Kinnier and F. W. Barton. A Study of a Rigid-Frame Highway Bridge in Virginia. Virginia Highway and Transportation Research Council, Charlottesville, Rept. VHTRC 75-R47, April 1975.
3. W. D. Whetstone. SPAR Structural Analysis System Reference Manual. System Level 7, Lockheed Missiles and Space Company, Palo Alto, CA, June 1974.

Publication of this paper sponsored by Committee on Dynamics and Field Testing of Bridges.

Radar and Acoustic Emission Applied to Study of Bridge Decks, Suspension Cables, and Masonry Tunnel

Ted Cantor and Charles Kneeter, Port Authority of New York and New Jersey, Jersey City

Studies have been conducted that suggest that it is feasible to use acoustic-emission and radar techniques for the nondestructive testing of masonry and of bridge cables. The examination of the condition of a brick railroad tunnel was carried out by using both techniques. Radar was used to determine the conditions of several reinforced concrete roadways and bridge decks. Acoustic emission was used in a novel way involving the application of small stresses to bridge cables, and the resultant emission pattern was correlated with the condition of the cables. The equipment used is discussed in some detail, as are the uses of special techniques for obtaining and analyzing the data. Several means of loading the bridge cables to obtain the acoustic emission were used; the use of an air hammer is the most effective technique found thus far. Several photographic techniques were developed to correlate the mass of data obtained from radar studies of roadways. These photographic techniques and the advantages of each are discussed in some detail. It is concluded that radar and acoustic emission are potentially useful tools for nondestructive testing of masonry and bridge cables.

This paper describes progress in the state of the art of adapting acoustic-emission and radar techniques to the study of the condition of suspension-bridge cables, concrete bridge decks, and brick tunnels.

The research is motivated by the continuing need to maintain the structural integrity of our bridges and tunnels, which represent very substantial capital investments. This maintenance is complicated by complex construction features: for example, the main structural support of the George Washington Bridge is the four main cables, which are made up of 105 896 wires. At the New York and New Jersey landfalls, each cable splits into 61 strands, each of which is terminated at a turning shoe and anchored in a concrete block through an eye bar. Although these areas are inspected, a better, nondestructive technique of quantitatively evaluating the condition is desirable.

The George Washington Bridge, together with several other bridges, is part of a major arterial system through and around New York City. The decks of these bridges are constructed of reinforced concrete on steel beams. Although the designs vary, they generally consist of a 20-cm (8-in) thick structural portion and up to a 7.5-cm (3-in) asphalt riding surface.

Another part of our transportation net is an old brick railroad tunnel built before 1900. The walls are 0.76 m (2.5 ft) thick and consist of several courses of brick and mortar and a boiler-plate outer skin.

The research techniques that we are attempting to adapt to the study of these structures are acoustic emission and downward-looking radar. (In this paper, we are condensing two papers into one: In general, we have tried to discuss one technique and its use and then the other technique and its details.)

Acoustic emission is a technique that has been in use for about 10 years. It is generally defined as the class of phenomena whereby transient elastic waves are generated by the rapid release of energy from a localized source or sources within a material. In a popular sense, it could be described as listening to a stressed material talk (1).

Some applications of the use of acoustic emission are checking of pressure vessels for flaws or leaks, checking of welds for defects as the weld is fabricated, and detecting hidden active corrosion locations and created stress flaws. In all cases, the material is stressed, and the acoustic-emission counts are monitored (2).

Radar has been used for years, but this downward-looking high-precision technique has only recently evolved as a detector for nonmetallic mines. It has since been used experimentally to nondestructively check the condition of a concrete road and to check for voids under a concrete runway. The radar signal is directed into the material under test, and the patterns created by the reflected waves are observed. In the final interpretation, the results can be considered similar to those produced by an x-ray scan of the material.

We are attempting two unusual applications of acoustic emission. The first is to attempt to determine the condition of the George Washington Bridge cable without stressing it to the 10 percent overload generally associated with acoustic-emission testing (3). The second is an attempt, for the first time, to apply the acoustic-emission technique to the study of the condition of masonry—in this case, a brick railroad tunnel. Both applications seem promising, and we intend to continue developing these areas.

In addition to the use of acoustic emission in the tunnel, radar was also tested for this application. At this juncture, radar seems to be the more promising technique.

Our major experience with radar has been for bridge-deck evaluation. It has been used to nondestructively examine more than 45 km (28 miles) of riding surface, and the results are promising. Our latest data analysis suggests that we have developed a technique that has a reasonable confidence level for identifying good or deteriorating concrete.

EQUIPMENT DESCRIPTION

Radar

Ground-penetrating radar uses a single antenna for both transmitting and receiving (see Figure 1). Its special design allows high-frequency, short-pulse signals to be directed into the earth, concrete, masonry, or other nonmetallic materials. There is an initial return at the surface and additional returns at each interface or change in medium. It is these returns that provide the peaks in the observed signal and have allowed field detection of nonmetallic mines and apparently may allow evaluation of road and tunnel conditions.

The return signal or trace was viewed on a single-channel oscilloscope. For viewing in the laboratory, the radar signal was recorded on a three-channel tape recorder. The signal trace was recorded on one channel, the synch pulse on a second, and voice location annotations and comments on a third. The power was supplied

Figure 1. Horn and transmitting and receiving antenna with antenna hookup to rear of van.

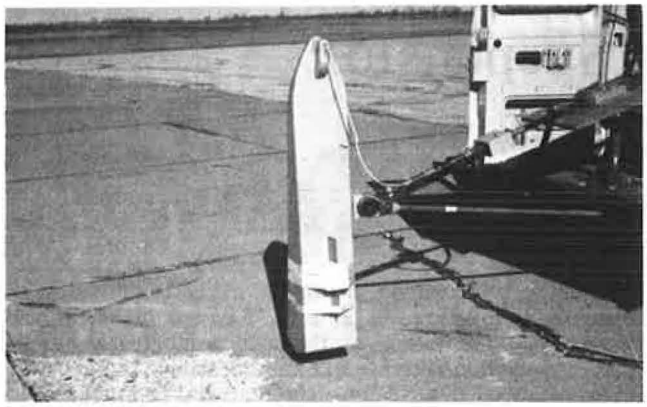

Figure 2. Typical topographic traces.

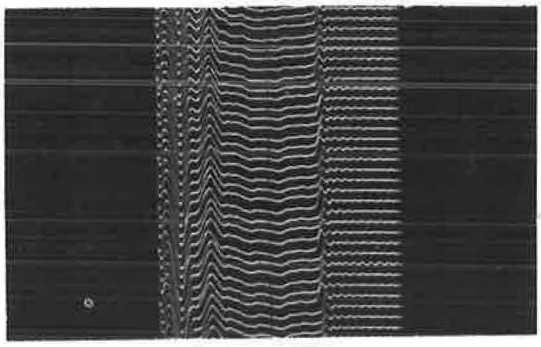

Stationary

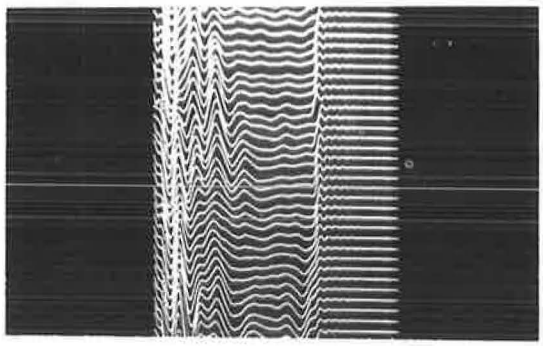

Normal Movement

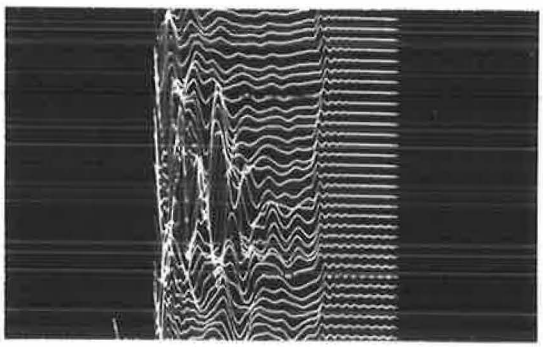

Disturbed Area

Figure 3. Comparison of core and radar trace.

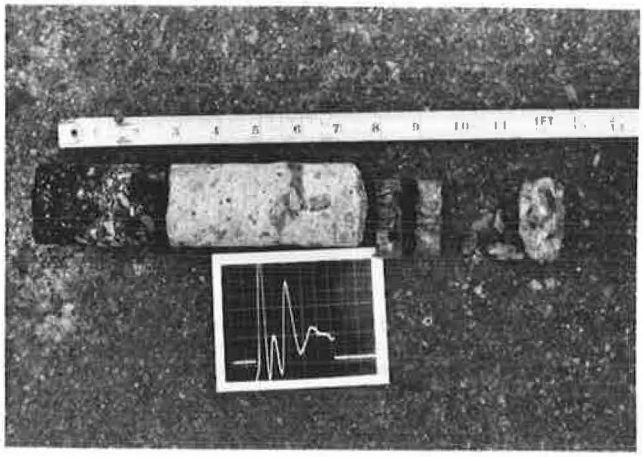

by two 12-V aircraft batteries for the radar and a 110-V gas-operated generator or a 110-V line for the auxiliaries. A high-speed streak (shutterless) camera was used to obtain a continuous 35-mm film reproduction of the oscilloscope traces. By adjusting the film speed, each trace can be displayed at a fixed distance from the preceding trace and, when the film is viewed, takes on a topographic appearance (Figure 2).

A polaroid scope camera was used to assist in analyzing the data and appears to be the most promising method of display for data interpretation developed thus far.

Acoustic Emission

Acoustic-emission counts are the number of times the acoustic-emission amplitude exceeds a preset threshold during any selected portion of a test (4). The equipment used provided a running digital display of the counts and a voltage output that was also displayed on a recorder. To induce local stress, either a variable-force, variable-frequency vibrator was used to provide stress by vibration or an air hammer was used to provide stress by hammer blows.

PROCEDURE

Radar: Bridges

A van was outfitted with the radar equipment, an oscilloscope, a 110-V gasoline-driven generator, and a tape recorder. The radar and its support equipment were operated on three bridges—Outerbridge Crossing, Bayonne Bridge, and George Washington Bridge.

The van was driven across the bridge in traffic at about 8-12 km/h (5-7 mph). The transmitter pulse-repetition rate was such that at this speed every 7.5 cm (3 in) of roadway was documented as a trace. The radar pulse was directed into the concrete roadway, and the reflections were observed on the cathode ray tube. An example of a trace is shown in Figure 3. At the Outerbridge Crossing, measurements were made in the right wheel track, the left wheel track, and between the tracks in each of the four lanes. On the Bayonne Bridge, measurements were recorded only in the wheel tracks and, on the George Washington Bridge, measurements were made only of the right wheel track of one lane. The Bayonne Bridge is more than 1.6 km (1 mile) long and was surveyed in a single afternoon. This was equivalent to more than 13 km (8 miles) of reading and approximately equivalent to taking a reading every 7.6 cm.

Viewing the taped data displayed on the oscilloscope indicated that a consecutive view of the traces in hard copy might be the best way to show changes taking place. Therefore, all of the tapes were photographed onto 61 m (200-ft) rolls of 35-mm film that show a topographic-like indication of the road as seen by radar. This film can be read on a modified motor-operated light table combined with a microfilm reader, which provides the observer both macro and micro viewing capabilities.

The latest and most promising technique has been to photograph (superimpose) approximately 5 s of continuous run (150 individual traces) onto one polaroid film. This has the effects of creating an envelope of traces and of showing deviations, if any, from the normal.

Radar: Tunnel

The dismounted radar equipment was used to examine the 0.76-m thick brick tunnel wall. The cross-sectional curvature of the elliptical tunnel walls seemed to affect the signal to a small extent, in that it changed as the radar horn was rotated angularly. This seemed to be true also for the distance the horn was held from the wall, which was restricted to 2.5 cm (1 in). Neither the angularity or the distance seemed a problem on the roadways and bridge decks. Not all of the tunnel radar data were tape recorded. Those that were not were filmed on polaroid from the oscilloscope display.

For both the bridge and the tunnel studies, the radar unit was standardized by measuring a shift in the position of the trace when the radar was reflected from a flat metal target at various distances from it in free air.

Acoustic Emission: Tunnel

The first laboratory-feasibility evaluation of masonry conditions by using acoustic emission was made on a string of bricks mortared end to end and established that there was signal transmission through brick. Subsequently, several bricks were mortared together and stressed in a compression test machine. The acoustic emissions were monitored by a transducer on the brick surface from a few counts as the load was applied to an avalanche of counts as failure approached.

Based on these results, acoustic-emission testing was next undertaken in the brick tunnel. After an initial series of tests to determine the field parameters (signal speed, distance, and depth of penetration) to be expected, a simple jacking-screw loading device was designed. Because large stresses in the wall were considered undesirable, the loads that were applied were extremely small.

Acoustic-emission signals were measured at several test points in the tunnel. The load was applied in 45.4-kg (100-lb) increments. Readings were made on the following day in some locations to check for relaxation effects.

Acoustic Emission: Bridge Cables

At the George Washington Bridge, the acoustic-emission technique was used on some of the strands of the 61 that make up a main cable. Tests were made on two of the main cables and were conducted in both the New York and the New Jersey anchorages. Because direct stressing is not desirable, very light stresses were applied by hammer blows and the acoustic emissions were recorded.

The first series of tests were those in the New York anchorage; a hand-held plastic-head mallet was used for hammering on the strands. The results were generally repeatable, but the mallet was difficult to use under the existing conditions. Next, a manually operated drop hammer was used to stimulate the cables with a controlled force. However, this technique was also inadequate for satisfactory results. A vibrator was then obtained, which vibrated the cable sufficiently to obtain acoustic emission but, again, the results were erratic. The use of a variable-speed, variable-force vibrator also gave erratic results.

Finally, an air hammer was obtained: This was used with a metal striking plate held between the hammer and the cable to protect the strands (see Figure 4), and gave the most repeatable and encouraging results.

Generally, a series of 8 to 10 blows were recorded and averaged to determine the rank order of the strands tested.

DISCUSSION OF DATA

Radar: Data Reduction

Generation of a trace every 7.5 cm for approximately 45 km creates a volume of data that is almost unmanageable. Reconstituting the data on an oscilloscope showed many variations that could not be coped with visually. The 35-mm shutterless streak camera seemed an appropriate technique with which to manage the visual information.

This technique gave a strip of film that was topographic in nature and appeared to indicate structural changes (see Figure 2). A more recent photographic technique being developed makes use of a time exposure that superimposes many traces, one upon another, which outlines the normally encountered envelope of variability

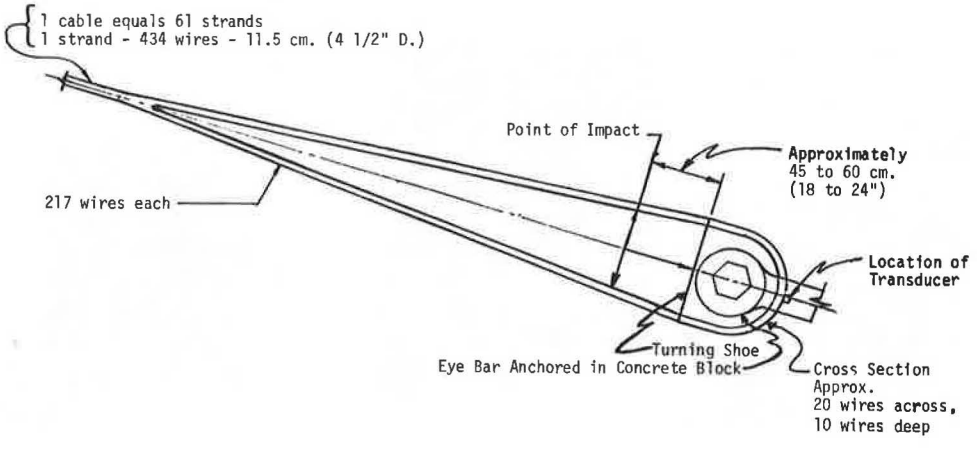

Figure 4. Arrangement for acoustic-emission test of George Washington Bridge strands.

Figure 5. Time exposure of envelope of radar traces.

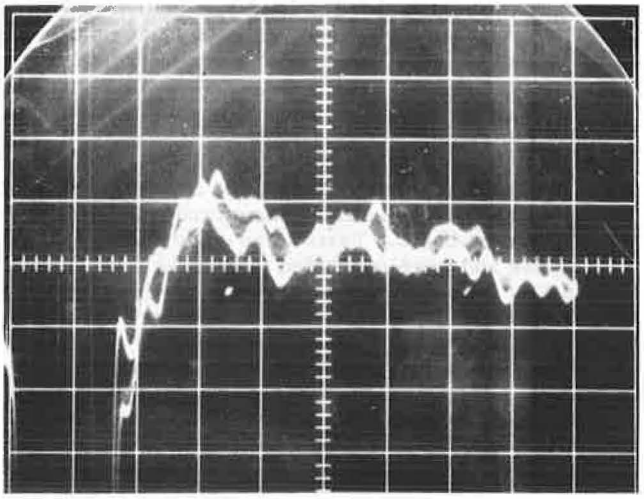

(see Figure 5). Major structural variations seem to be more readily identifiable with this technique.

Although this may be a workable system, we are also investigating computerized mathematical procedures that could approach real-time analysis.

Radar: Tunnel

At the present time, the radar data can be evaluated in only qualitative terms. The entire trace for a location or a series of traces for an area must be considered to determine the condition of the structure being viewed. In general, with assumed sound structures, the traces fall into a family of traces that has few, if any, variations. As can be seen from Figures 2 and 5, the envelope of traces falls within a relatively close pattern. Unfortunately, because of the presence of large metal drainage pipe in this tunnel that interfered with the radar signal at the location where acoustic-emission data had been taken, it was not possible to precisely compare the acoustic-emission and the radar data.

Radar: Roadway

By far our most voluminous set of data is that for the bridge roadways, 4800 m (15 750 ft) of tape that have been reduced to 1700 m (5800 ft) of 35-mm film (see Figure 2 for typical examples of this film). All that has been said about the radar data taken in the tunnel is applicable to the roadway data with two additional comments: first, the ratio between disturbed and quiet areas seems to be what might normally be expected in the field and, second, visible structures such as joints are clearly discernible in the data. Figure 3 shows a core and its previously taken radar signature. The first left-hand peak represents the interface between asphalt and concrete and the third peak shows the deterioration of the bottom of the core.

The latest procedure consists of superimposing a series of approximately 120 individual consecutive radar traces in about a 5-s period on a single polaroid picture. When the picture has all the traces superimposed on each other, they give the appearance of a single trace and cores taken from the area represented by the picture are sound. On the other hand, when many separate traces are visible or the picture has a ragged appearance, cores taken from the area represented by the data may be of poor quality (see Figures 6 and 7).

Acoustic Emission: Tunnel

The acoustic-emission data are shown in Figure 8. In addition, monitoring positions A5 to A9 when there were trains in an adjacent tunnel showed good agreement between counts observed under stress and counts observed when trains were passing.

Monitoring Position	Train	Highest Index
A5	371	300
A6	163	150
A7	1212	2000
A8	98	150
A9	1065	700

The data would seem to be consistent within themselves and may show the normal limits of variation in the structure. It was also interesting that the area giving the highest index (A7) was one that had a noticeable hollow sound when tapped. The Kaiser effect (5) (the absence of detectable acoustic emissions until previously applied stress levels are exceeded) is clear in some cases (such as A2, A4, A6, and A8), but in others, the second loading cycle produced early emissions.

Figure 6. Nonsuperimposed trace characteristic of deteriorated concrete.

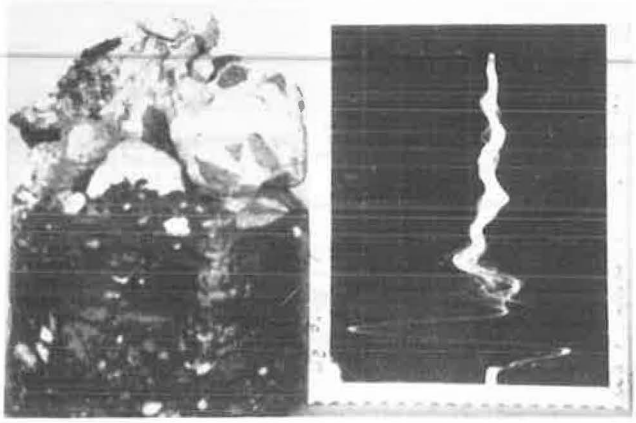

Figure 7. Tight envelope of traces indicating sound concrete.

Figure 8. Acoustic-emission reading from brick tunnel.

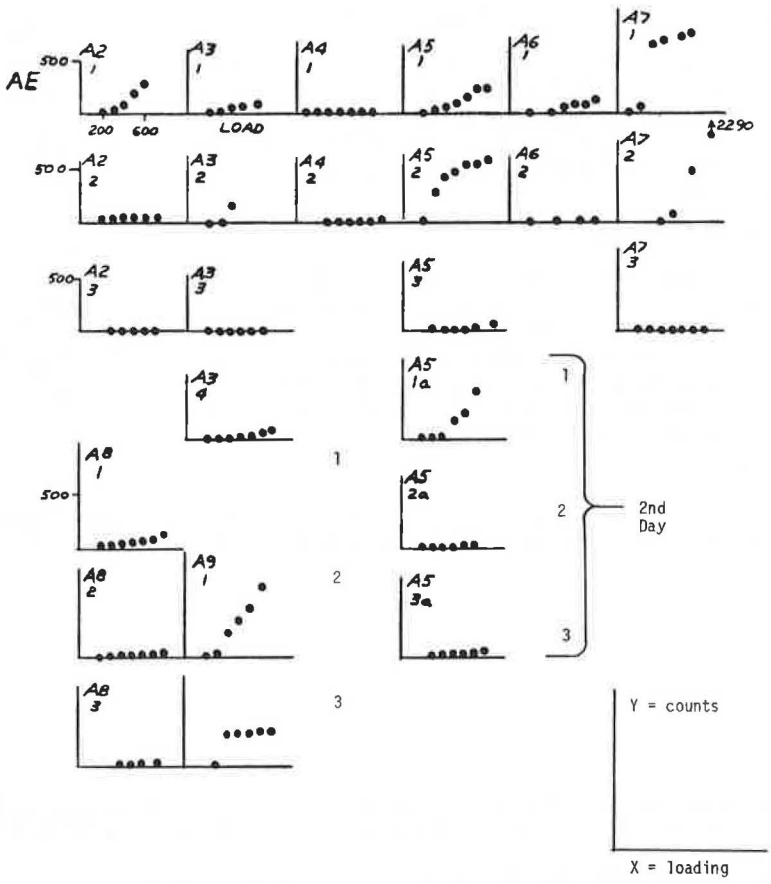

Acoustic Emission: Bridge Cables

Of the thirty strands examined (see Table 1), the strand condition indicated by the acoustic-emission index seemed to be reasonably consistent with the conditions indicated by other inspection procedures. For reasons that are not understood at present, the emission from the upper strands was greater than that from the lower strands. Blows on the shoe provided greatest index of acoustic emission, which may be attributable to the transmission medium, solid steel.

CONCLUSIONS

Based on our experiences in the state of the art of radar and acoustic-emission techniques, we feel that both have considerable potential for rapidly, economically, accurately, and nondestructively evaluating bridge decks, roadways, runways, masonry, and steel suspender cables. Both should be pursued and developed further.

This conclusion is based on the successful identification of both good and disturbed concrete by using superimposed polaroid trace images for radar and on the prospect of rapid data reduction and evaluation via some algorithm or computer procedure that would result in a digital display.

Acoustic emission detected different levels of emission in the tunnel and perhaps some differentiation in emission in the bridge-cable strands.

Furthermore, acoustic emission appears to have potential for determining the condition of inaccessible wires of a multiwire cable or strand. One of the difficulties that still exists is that of developing the best technique for introducing the minimum acceptable level of stress to the strands. Acoustic emission is probably a feasible method of nondestructively determining masonry condition. There are, however, two major disadvantages: (a) It is cumbersome to use in a tunnel and (b) it requires that the area be stressed. We have,

Table 1. Main cable index numbers.

Strand No.	Lower Strand	Upper Strand	Shoe
43	1	12	38
41	3	12	72
37	3	21	54
56	5	17	49
60	5	16	69
61	5	20	53
39	6	5	36
12	6	46	60
45	7	12	75
42	8	16	95
46	8	21	152
20	8	23	66
49	8	26	55
16	9	12	65
55	9	30	40
47	10	12	80
53	10	30	51
50	11	18	98
48	11	22	79
36	11	22	101
40	18	22	113
89	18	41	54
44	24	24	81
54	24	50	101
8	25	14	189
58	28	21	130
51	29	29	138
57	29	35	86
4	32	44	73
52	35	41	171
Max	35	50	189
Min	1	5	36

therefore, decided to temporarily defer its use in tunnels in favor of radar.

In our opinion, radar shows qualitative distinctions in the conditions of the brick tunnel. However, because the brick tunnel is a more complex system than the roadway in terms of the data, we have decided to direct our present efforts to the interpretation of the bridge-deck and roadway data.

ACKNOWLEDGMENTS

We wish to express our thanks to Anthony Alongi of Penetradar and to William Hartman, consultant to Trodyne, for their invaluable consultations and assistance in planning and developing the project. We also wish to thank Daniel Jacobs for his assistance in several phases of the work and various Port Authority staff members for their help in the field work.

REFERENCES

1. H. L. Dunegan and A. T. Green. Factors Affecting Acoustic Emission Response From Materials. Materials Research and Standards, ASTM, Vol. 2, No. 3, 1971.
2. R. G. Liptai and D. O. Harris. Acoustic Emission. Materials Research and Standards, ASTM, Vol. 2, No. 3, 1971.
3. D. O. Harris and H. L. Dunegan. Acoustic Emission Testing of Wire Rope. Dunegan/Endevco, Livermore, CA, Technical Rept. DE-72-3A, Oct. 1972.
4. A. A. Pollock. Acoustic Emission: A Review of Recent Progress and Technical Aspects. In Non-Destructive Testing, IPC Science and Technology Press, Surrey, England, Oct. 1973.
5. H. L. Dunegan. Using Acoustic Emission Technology to Predict Structural Failure. Metals Engineering Quarterly, Rheinhold Publishing Corp., Stamford, CT, Feb. 1975.

Publication of this paper sponsored by Committee on Dynamics and Field Testing of Bridges.

Abridgment

Dynamic Properties of Skewed Beam-Slab Highway Bridges

Celal N. Kostem, Department of Civil Engineering, Lehigh University

The dynamic response and vibrational characteristics of railroad and highway bridges are of concern to bridge designers. This is due to the fact that, through the prediction of the dynamic response, the amplification of the static live-load stresses and deformations can be estimated and this, in turn, may require the redimensioning of the superstructure. It has been shown that the amplification of the static response through the use of an impact factor can lead to erroneous results (1, 2). The vibrational characteristics (more specifically, the periods of vibration) of the bridges are usually used in conjunction with the definition of sensitivity to earthquake forces and the human perception of the vibration of the superstructure.

The natural periods of vibration of highway bridges can be used in the discrimination of the dynamic characteristics. The development of simple empirical formulas that can predict the natural periods of vibration would be the optimal solution. Analytical studies have resulted in sufficient information on the natural periods of vibration of simple-span beam-slab highway bridges that have reinforced concrete decks and prestressed concrete I-beams and may or may not have skew (1, 3, 4, 5, 6). This paper summarizes the results of research carried out to predict the natural periods of vibration of these types of bridges that have skew.

DESIGN AND ANALYSIS OF BRIDGES

The paper focuses attention on simple-span beam-slab bridges that have prestressed concrete I-beams. To be representative of the variety of bridges encountered in the field, 33 right bridges were designed by using current engineering practices (7). Their span lengths, curb-to-curb widths, and beam spacings varied from 12.20 to 27.44 m (40 to 90 ft), 7.32 to 18.30 m (24 to 60 ft), and 1.46 to 2.61 m (4 ft 9 in to 8 ft 7 in) respectively: A detailed description of the bridges is available elsewhere (3, 5). The configurations considered cover a wide range of variation in the design parameters.

In the definition of the dynamic characteristics of the bridges, the superstructures were simulated by using the finite-element method. The deck slab was modeled via plate-bending elements and the beams as beam-bending elements. The analysis was performed by using the computer program SAP IV (8). The first three fundamental periods of vibration of the superstructures, both those that had and those that did not have skew, are available elsewhere (3, 5). The empirical formulas for the prediction of the periods of vibration of right bridges that have not already been computed are also available (5). The analysis assumed that no vehicle is on the bridge. The differences between these unloaded and loaded periods have been presented previously (1).

SKEWED BRIDGES

In the parametric study, the design parameters of the 33 right bridges were retained intact, but the geometries of the bridges were changed for skew angles of 60° and 45° (90° skew being the right bridge). The inclusion of the new bridges has resulted in the consideration of a total of 99 bridges. Through the application of the finite-

Table 1. Nondimensionalized natural periods of vibration.

Bridge No.	t_1^{60}	t_1^{45}	t_2^{60}	t_2^{45}	t_3^{60}	t_3^{45}
1	0.96	0.90	0.94	0.85	0.88	0.73
2	0.96	0.91	0.94	0.86	0.88	0.72
3	0.93	0.85	0.93	0.83	0.87	0.70
4	0.95	0.88	0.94	0.86	0.92	0.81
5	0.95	0.89	0.95	0.87	0.91	0.78
6	0.93	0.84	0.92	0.82	0.90	0.77
7	0.89	0.83	0.92	0.87	0.94	0.84
8	0.95	0.89	0.95	0.89	0.93	0.83
9	0.93	0.85	0.92	0.82	0.91	0.77
10	0.96	0.91	0.94	0.85	0.87	0.70
11	0.96	0.90	0.95	0.84	0.91	0.75
12	0.96	0.91	0.96	0.90	0.93	0.84
13	0.97	0.92	0.94	0.84	0.87	0.70
14	0.97	0.93	0.95	0.87	0.87	0.70
15	0.96	0.91	0.94	0.86	0.87	0.70
16	0.97	0.92	0.95	0.87	0.91	0.78
17	0.96	0.92	0.96	0.90	0.91	0.79
18	0.96	0.90	0.95	0.87	0.91	0.79
19	0.96	0.92	0.95	0.89	0.93	0.82
20	0.96	0.92	0.96	0.91	0.94	0.84
21	0.95	0.90	0.94	0.88	0.94	0.85
22	0.97	0.93	0.97	0.93	0.96	0.92
23	0.96	0.92	0.96	0.93	0.96	0.92
24	0.96	0.92	0.96	0.93	0.96	0.92
25	0.98	0.94	0.94	0.86	0.86	0.68
26	0.98	0.95	0.95	0.88	0.87	0.70
27	0.97	0.93	0.95	0.87	0.85	0.68
28	0.97	0.94	0.96	0.90	0.91	0.79
29	0.97	0.94	0.97	0.91	0.92	0.80
30	0.97	0.92	0.96	0.90	0.91	0.79
31	0.97	0.93	0.97	0.91	0.94	0.84
32	0.97	0.94	0.97	0.92	0.94	0.86
33	0.96	0.92	0.96	0.90	0.94	0.85

Note: Subscripts indicate period of vibration, and superscripts indicate skew angle.

element simulation of the superstructure and the use of the SAP IV program, as had been done for the right bridges, the natural periods of vibration of skewed bridges were computed. Table 1 gives the nondimensionalized values of the periods of vibration (i.e., the period of vibration of the skewed bridge is divided by the corresponding period of the right bridge). This table shows that, for a given skew angle and nondimensionalized period, the values tend to be similar (i.e., within each column, the values are similar). The results of the statistical analysis of these values for bridges that have 60° skew are given below.

Value	Mean	SD	Standard Error of Mean
t_1	0.958	0.017	0.003
t_2	0.949	0.014	0.002
t_3	0.910	0.032	0.005

In the computation of these values, it is assumed that the corresponding nondimensionalized periods of vibration for right bridges are equal to 1.000.

The results of the statistical analysis of the periods of vibration of bridges that have 45° skew are given below.

Value	Mean	SD	Standard Error of Mean
t_1	0.908	0.030	0.005
t_2	0.878	0.031	0.005
t_3	0.787	0.071	0.012

The relatively small magnitudes of the SD and the standard error of the mean indicate the consistency of the mean values given here. Therefore, if the natural period of vibration of a right bridge is known, then the period of vibration of a skewed bridge can easily be approximated through the use of the appropriate value given in this paper. Another observation that can be made is in regard to the relatively small changes in the mean periods of vibration for different skew angles. For example, the first period of vibration has values of 1.000, 0.958, and 0.908 for skew angles of 90°, 60°, and 45°. This close proximity permits interpolation for the prediction of the natural periods of bridges that have skew angles between 90° and 45°. However, any extrapolation beyond 45° may lead to erroneous results because the variation of the periods beyond 45° has not been determined.

CONCLUSIONS

The dynamic and vibrational characteristics of bridge superstructures can be predicted through the use of predominant natural periods. It has been shown that the natural periods of vibration of skewed simple-span beam-slab bridge superstructures can be computed through the use of the appropriate multipliers given here, when the periods of vibration of the equivalent right bridge are known. The natural periods of vibration of bridges that have skew angles up to 45° have been computed. On the average, the reduction in the first fundamental period is at the most 10 percent and, for the second and third periods, this reduction can be up to 21 percent.

REFERENCES

1. C. N. Kostem. Dynamic Properties of Beam-Slab Highway Bridges. TRB, Transportation Research Record 645, 1977, pp. 23-24.
2. W. S. Peterson and C. N. Kostem. Dynamic Analysis of Highway Bridges Using the Finite-Element Method. Fritz Engineering Laboratory, Lehigh Univ., Bethlehem, PA, Rept. 400.7, May 1972.
3. C. N. Kostem. Dynamic Properties of Skewed Beam-Slab Highway Bridges. Fritz Engineering Laboratory, Lehigh Univ., Bethlehem, PA, Rept. 432.4, Dec. 1977.
4. C. N. Kostem. Identification of the Design Parameters Governing the Natural Periods of Vibration of Highway Bridges. Fritz Engineering Laboratory, Lehigh Univ., Bethlehem, PA, Rept. 378A.9, June 1977.
5. A. Thomson and C. N. Kostem. On the Prediction of the Natural Periods of Vibration of Highway Bridges. Fritz Engineering Laboratory, Lehigh Univ., Bethlehem, PA, Rept. 354.452, June 1977.
6. M. A. Zellin, C. N. Kostem, and D. A. VanHorn. Structural Behavior of Highway Bridges: A Summary of Completed Research and Bibliography. Fritz Engineering Laboratory, Lehigh Univ., Bethlehem, PA, Rept. 387.1, May 1973.
7. Standards for Bridge Design (Prestressed Concrete Structures). Bureau of Design, Pennsylvania Department of Transportation, Harrisburg, BD-201, 1973
8. K.-J. Bathe, E. L. Wilson, and F. E. Peterson. SAP IV—A Structural Analysis Program for Static and Dynamic Response of Linear Systems. Earthquake Engineering Research Center, Univ. of California, Berkeley, Rept. EERC 73-11, June 1973 (revised April 1974).

Publication of this paper sponsored by Committee on Dynamics and Field Testing of Bridges.

Repair of Cracked Structural Concrete by Epoxy Injection and Rebar Insertion

F. Wayne Stratton, Roger B. Alexander, and William J. Nolting, Kansas Department of Transportation

The objective of this project was the development of a technique for repairing cracked structural bridge concrete. The method developed consists of sealing the crack, drilling holes at 45° to the deck surface, crossing the crack plane with epoxy pumped under low pressure, and placing a rebar in the drilled hole in a position to span the crack. The epoxy bonds the bar to the walls of the hole, filling the crack plane and bonding the cracked concrete surfaces together in monolithic form, which thus reinforces the section. The epoxy injection equipment used was developed for hollow plane injection. A modified injection nozzle was built, and an enlarged vacuum swivel was designed, developed, and built. The hollow-stem carbide-tipped vacuum drill bits were 19.1 mm (0.75 in) in diameter and up to 2.44 m (8 ft) long. A mechanical-advantage motion detector was designed and built and used to detect fractional vertical and horizontal motions of 1.19 mm (3/64 in) and record them as 19.1-mm (0.75-in) motion. Drilling to a depth of 2.1 m (7 ft) required 22 min. Fifteen 0.914-m (36-in) long rebars were placed in repair zones. All crack injection attempted was successfully completed in 3 working d. Seventeen months after completion of the repair, no motion had been detected and the repair appeared to be permanent.

One of the major maintenance problems occasionally faced in Kansas is that of girder shear cracking in bridges that have continuously reinforced concrete deck girders. The basic cause of these cracks apparently relates to a structural design weakness—the specification of inadequate quantities of stirrup steel. Two methods have been developed for the repair of these cracked girders. The first, which we call simple rebonding, is exactly that. The procedure involves sealing the external area of the crack and then forcing bonding epoxy through tiny holes perforated in the sealant surface into the crack. The second procedure is more drastic and used only if an extreme crack is present in the girder. In this repair procedure, the cracked girder is fully supported with cribbing, the failed section is completely removed, additional reinforcement is added and, finally, the removed girder section is recast.

Obviously, simple rebonding adds little strength to the cracked structure; it bonds the cracked surfaces but does not reinforce against the original weakness, the lack of adequate reinforcing steel. However, the alternative used for failed structures is very expensive and time consuming. Thus, we have a real need for an efficient method that would rebond a cracked structure and simultaneously reinforce it in the crack zone.

PROJECT DEVELOPMENT

The concept that we proposed to investigate involved an extension of an earlier epoxy-injection study (1). In its fundamentals, the proposal called for drilling deep holes down to and intercepting the crack at an angle approximately normal to its surface. The holes were to extend beyond the crack about 0.5 m (1.5 ft). Then, an elastic sealant was to be used to confine the crack, and epoxy was to be pumped down through the bottommost hole and into the crack to fill it. During the process of filling the girder, rebars at least 0.914 m (3 ft) long were to be placed across the crack and bonded in place with the polymerized epoxy. After all the bars were in place, epoxy pumping was to be continued until the crack and drilled holes were completely filled.

Because the vacuum swivel we had developed earlier was a light-duty design, a new vacuum swivel was developed (1, 2). A larger unit was needed to cope with the almost doubled drilling load and an 80 percent increase in drill-dust evacuation. The increases in both the load and the evacuation were caused by the need for a minimum drill diameter of 19.1 mm (0.75 in), which is the absolute minimum that will allow clear access for installing a no. 4 or a no. 5 rebar, the size we believed would be required to provide adequate reinforcement.

The fabrication of the drills presented no problems because their geometrics were a direct extension of the earlier drills (1). One hundred drills were built in lengths of 0.3, 0.6, 1.2, 1.8, and 2.5 m (1, 2, 4, 6, and 8 ft). Each drill was to be used for its differential length and then changed, and so on until the hole was sufficiently deep.

The epoxy pump used was identical with that designed earlier except for a change in pump sprockets to give a resin-to-hardener ratio of 2:1. The probe nozzle was revised to allow injection sealing into the 19.1-mm diameter hole.

The next problem was that of determining whether the repair was satisfactory. Our solution to this was to determine whether there was any load-induced motion between the crack interfaces. If there was no motion, the crack was repaired. But if there was motion of any magnitude, we had failed. Consequently, motion detectors that are simple mechanical advantage multipliers (16:1) and operate in two planes, vertical and horizontal, were designed and built (3).

Two motion detectors were installed on the bridge selected that spanned two major cracks on opposite ends of the structure. This installation was made 60 d before the anticipated test. This time period should ensure probable maximum records of both vertical and horizontal motion. At the close of this time, we had recorded motions of 1.19 mm (3/64 in) in both planes (vertical and horizontal) at both cracks. No propagating failure of the crack could be detected in the vertical mode.

TEST

The work began by sealing the cracks. The crew was given basic instructions on mixing and applying the sealant (a translucent elastic epoxy gel). This work continued until a question arose: for instance, What do we do about adjacent but not connected cracks? Answer, If the crack is within the expected drill-penetration zone, it must be sealed even up into the deck.

After the sealing was finished, the hole positioning was begun. A simple geometric system was developed that located and laid out the system of holes to be drilled (3). In this procedure, the slab reinforcement was de-

Figure 1. Level of epoxy when rebar should be inserted in hole.

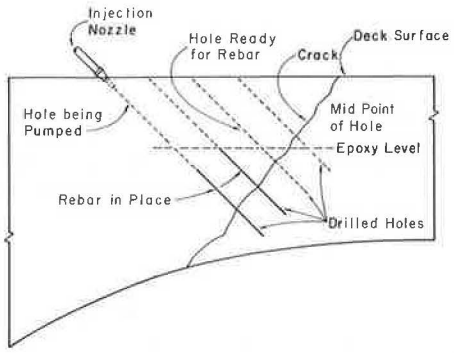

Figure 2. Typical repair sketch and description.

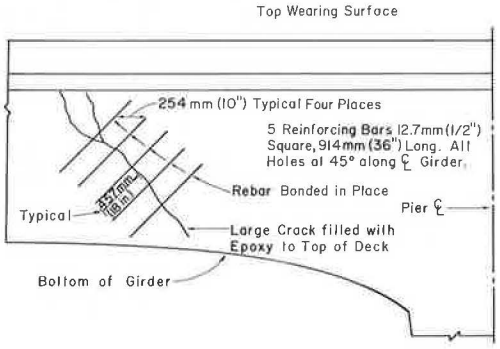

tected by using a pachometer and four holes were located to penetrate the crack.

But when the drilling began, so did the problems. First, drilling 19.1-mm diameter holes is obviously going to be pure hard work. Visually, it was very difficult to detect any penetration of the drill into the concrete. After 2 min, the drill was examined for dullness, but this was not the case. At this time, chalk marks were placed on the drill stems in 2.54-cm (1-in) increments; from these marks, a steady penetration could be noted. However, the effort needed to sink the drill was great, and it was noted that the carbide tips were chipping on the relief side of the bit (behind the cutting edge). Subsequent microscopic examination of the tips showed predrilling fractures that may have been induced during brazing or may have been present in the as-received tips.

In any case, the drilling continued. In spite of the difficulty and the chipping problems, 2.16 m (7 ft) of the concrete were penetrated in 22 min, which is a respectable rate of 102 mm/min (4 in/min).

As soon as the four holes were complete, epoxy pumping was begun. We pumped 11.3 L (3 gal) of high-modulus low-viscosity epoxy into this repair. All pumping was accomplished by using the drilled holes as access to the crack. Rebars were inserted into the drilled holes and spanned the crack 0.46 m (18 in) on either side (see Figure 1). Pumping continued until leaking occurred beyond the sealed zone.

In all, 11 major cracks were repaired. The repairs involved installation of 15 rebar sections, 9 of which were placed across the two largest cracks. We pumped 31.2 L (8.25 gal) of bonding epoxy and used 9.5 L (2.5 gal) of sealant epoxy. The total time for the repair was 192 working h (this included traffic control time but excluded research engineer time). Figure 2 shows a typical repair sketch.

PROJECT RESULTS

One of the most positive results of a program such as this is the discovery and resolution of a host of minor problems. No program can be considered successful if the problems it encompasses cannot be solved or averted.

One problem was crack sealing. We had hypothesized a need for an elastic sealant, based on the knowledge that crack interfaces can move in relation to each other. Furthermore, we wanted a quick-setting epoxy that was relatively transparent. That way, we could ascertain the position of the crack under the seal, which would improve our chances to repair leaks and to be sure that we have a good sealed margin beyond the edge of the crack. Our choice of epoxy had a minimum tensile elongation of 13 percent and, although not transparent, is not opaque in the film thicknesses used.

During the test, the epoxy itself performed as expected. Our problems were related mostly to the seal application and repairing of leaks. We believe that, when this technique becomes a commonly practiced one, the experience and workmanship factors will nearly eliminate leak problems. For those leaks that cannot be anticipated, we believe that an epoxy-putty plug could be used.

Our next problem was that of locating the drill entry points with reference to the deck rebar steel. The position of the deck steel directly affects the frequency and placement of the additional reinforcement. As a consequence, the spacing of the bars was adjusted as the deck reinforcement demanded. The angle of entry for the drill was not a major problem. A simple 45° template established the initial penetration angle and after approximately 15 cm (6 in), the drill was on its own.

Drill performance was fairly good but not without problems. As noted above, one of the first observations made was that a strong effort was needed to achieve penetration into the concrete. At the 1.22-m level, the crew began doubling and tripling up on the drill. It was at this point that the chipping damage to the carbide tip was first noted. Whether or not the carbide was cracked before or during brazing has not been determined but, after the crew stopped using two and three men on the drill, the chip damage was significantly reduced. The practical drill depth life before sharpening was about 30 cm (1 ft).

There is no visible evidence of this repair other than the sealant epoxy covering the extent of the cracks involved in the repair. This epoxy can be stripped away after the bond has cured, and the surface at the crack can be mopped with a mortar to cosmetically treat the surface.

To give us a reliable test of performance, we are monitoring the motion detectors that span the two major cracks in this bridge. At the time of this writing, 17 months after repair completion, no motion has been recorded on the detectors in either plane of either repair.

A second bridge has now also been repaired. This work involved four girders in three spans and encompassed about 10 cracks. Several newly developed pieces of equipment and procedures—a new mechanically powered drill stand, a new 50:1 motion detector, and a new locking self-supported injection probe—were used in this repair. Because of cold weather and motion problems, a silicone crack sealer was tested and used successfully.

SUMMARY AND CONCLUSIONS

It became obvious during the course of this test that cracked structures likely to be repaired by using this

technique should be evaluated by a design group, who could optimize the repair steel density and the pattern of installation. Minor cracking can probably be injected without referral to an engineering disposition.

It is also apparent from the drill-tip performance that some change is required. The suspicions remain that the as-received tips might have been cracked or that the tips might have cracked because of the brazing operation we performed. Our preliminary review in this area has led us to an alternative tip source and a different brazing alloy. Whatever avenue is taken, the correction must be cost and performance effective.

While on the subject of the drills, we must again mention the effort needed to drill one of these holes. No judgment is yet possible on the drill durability for concretes other than our sweetened mixed-aggregate (30 percent limestone and 70 percent sand gravel) concrete, but we anticipate more difficulty in western Kansas, where our aggregates are unsweetened river sands and gravels. As a consequence, we suggest that a powered drilling system might be a desirable refinement. Let us stress, on the other hand, that the difficulties notwithstanding, the evidence we have shows that the accomplished repair is very effective.

In closing, this report is positive in all areas investigated, and we have not begun to touch the many systems involved that could definitely be improved. We know from past activities that higher bit rotation speeds reduce load requirements and increase the penetration rate. We are also certain that the bit geometrics could be improved. We do not know with certainty that we have approached or understand the maximum structural capabilities offered so far as the steel placement, types of installations, and epoxy or other bonding systems available.

ACKNOWLEDGMENTS

This project was financed in part by a research and development study grant from the Federal Highway Administration through the Highway Planning and Research Program. The bridge crews from Kansas second and sixth districts, who made the actual repairs, deserve thanks for their diligent efforts.

REFERENCES

1. F. W. Stratton and B. F. McCollom. Repair of Hollow or Softened Areas in Bridge Decks by Rebonding With Injected Epoxy Resin or Other Polymers. State Highway Commission of Kansas; Federal Highway Administration, July 1974.
2. G. L. Morrison, Y. P. Virmani, K. Ramamurti, and W. J. Gilliland. Rapid In Situ Determination of Chloride Ion in Portland Cement Concrete Bridge Decks. Kansas Department of Transportation; Federal Highway Administration, Nov. 1976.
3. F. W. Stratton, R. B. Alexander, and W. J. Nolting. Cracked Structural Concrete Repair Through Epoxy Injection and Rebar Insertion. Kansas Department of Transportation; Federal Highway Administration, Interim Rept., July 1977.

Publication of this paper sponsored by Committee on Structures Maintenance.

Bridge-Deck Concrete-Cover Investigation in Michigan

P. W. O'Rourke and J. M. Ritchie, Testing and Research Division, Michigan Department of State Highways and Transportation

Ninety-seven concrete deck structures (282 spans) in Michigan were surveyed by using a pachometer to determine the average depth and variation of the concrete cover. Fifteen structures (36 spans) were surveyed by using the wet-depth method. It is believed that, if the clear-cover target value is increased to 7.62 cm (3.0 in) (and no attempt is made to control process variation), fewer than 3 percent of the structures will have less than 5.08 cm (2.0 in) of clear cover over more than 10 percent of their surface area. Increases in the cover specification have had no measurable effect on the mean span variation. For most structures, the distribution of measurements for individual spans is consistent with approximately 95 percent of the measurements within 1.9 cm (0.75 in) of the average value. Wet-depth measurements do not compare favorably with pachometer measurements and, in more than 50 percent of the spans, the mean difference between the two methods was greater than 0.64 cm (0.25 in). To adequately determine the depth of concrete cover, 100 measurements/span or one measurement for each 2.32 m^2 (25 ft^2), whichever is less, should be taken.

Bridge-deck deterioration from corrosion of the reinforcing steel is a serious problem in Michigan. Considerable national attention has also been directed toward determining its causes and cures. It is generally agreed that an inadequate depth of concrete cover over the steel reinforcement is a major factor. The Federal Highway Administration (FHWA) recognized the importance of this factor in 1972 and issued an instructional memorandum that directed the various state highway departments to require at least 5.08 cm (2 in) of clear concrete cover over the top mat deck reinforcement. At that time, the Michigan specification called for 5.08 ± 0.64 cm (2.00 ± 0.25 in) but, in response, that was changed to 6.35 ± 0.64 cm (2.50 ± 0.25 in). In 1975, a project was initiated to evaluate the variation in concrete cover over bridge-deck steel reinforcement and determine the level of compliance with the existing specifications for clear cover. The primary objectives of this investigation were

1. To determine the average depth and variation of concrete covers over bridge-deck steel reinforcements,
2. To determine the specification value that will ensure a prescribed minimum depth of clear concrete cover,

Table 1. Average clear cover and variation for all data according to design cover specification.

Clear-Cover Specification (cm)	No. of Structures Surveyed	No. of Spans Surveyed	Avg Clear Cover (point basis) (cm)	Avg SD (unweighted span basis) (mm)
5.08 ± 0.64	13	53	6.386	7.21
6.35 ± 0.64	78	211	6.612	6.93
7.62 ± 0.64	6	18	7.635	6.50

Note: 1 cm = 0.394 in.

3. To determine the number of measurements per span that are required to adequately determine the minimum depth of cover, and
4. To compare depth measurements made by using the pachometer (R-meter) and by using the wet-depth method and to determine whether the wet-depth method is adequate for construction control.

An interim report involving 10 structures released in December 1975 indicated that the level of compliance was still seriously deficient. As a result, the design clear-cover target was increased again—this time to 7.62 ± 0.64 cm (3.00 ± 0.25 in).

INSTRUMENTATION

Three R-meters were used to measure the concrete covers. The R-meter is an improved version of an earlier generation of pachometer. The essential modification is the introduction of a rechargeable battery pack. The R-meter is a portable, nondestructive testing device that can be used to locate and measure the depth of reinforcing steel of a known diameter. It measures the disturbance by an external magnetic source (the rebar) on a magnetic field generated at the probe. The magnitude of the disturbance is proportional to the distance from the probe and indicated at the instrument meter on a linear scale. The readings are converted to depths of clear cover through the use of a calibration curve.

ACCURACY

The R-meter used has an effective range of 0-10.8 cm (0-4 in). In general, instrument sensitivity is inversely related to depth of cover. With a modest amount of practice, measurements of depths less than 6.35 cm can be obtained with reasonable accuracy [± 0.32 cm (± 1/8 in)]. Measuring depths of cover greater than 8.89 cm (3.50 in) with consistent accuracy is difficult even for an experienced operator. A reasonable estimate of the overall accuracy in normal production conditions is approximately ± 0.64 cm. Two factors other than operator technique that affect the accuracy are the presence of magnetic aggregates and the variation in the magnetic properties of the reinforcing steel.

Magnetic Aggregate

The presence of magnetic material in the concrete affects the accuracy of the instrument. Even a small particle, if located near the surface, can cause considerable error. This is compounded by the fact that the magnetic effect varies from point to point. Although the amount of error is never known, the effect always occurs in the same direction. That is, those readings that are in error will always indicate less cover than actually exists. Therefore, results are conclusive if the data indicate that the cover is sufficient but, if the survey indicates less than minimum compliance, additional information is necessary to determine the actual amount of deficiency.

Grade and Manufacturing Process

The variation in material composition of different grades of steel has a significant effect on the magnetic properties of reinforcing bars. Also, variation within a specific grade of steel can affect calibration; differences on the order of 0.32 cm for no. 6 bars at 5.08 cm of cover are not unusual. This error increases rapidly at depths of cover greater than 7.62 cm because of the changing slope of the calibration curve. This potential source of error can be effectively eliminated, however, by calibrating the instruments against samples of the superstructure reinforcement.

DISCUSSION OF DATA

Determination of Average Depth and Variation in Concrete Cover Over Bridge-Deck Steel Reinforcement

From the summer of 1975 through the winter of 1976, 97 structures (282 spans) were surveyed by using the R-meter. The depth of the clear concrete cover was determined on a 1.52- × 1.52-m (5- × 5-ft) grid. For each span and structure, the mean or average depth of clear cover and the percentage of measurements (or area) less than a designated value were computed. These 97 structures represent three different specifications for clear concrete cover. The average depth of clear cover and the average variation (standard deviation) on a span basis were compiled according to specification (see Table 1). With the exception of those structures built to the 5.08 ± 0.64-cm specification, the results indicate excellent concurrence on an overall basis between observed average performance and design target.

As indicated by the average standard deviation, the overall variation has remained relatively constant and independent of the cover target. Despite the increased emphasis on concrete cover in the past 2 years no significant reduction in process variation has occurred.

A casual review of the data when they are grouped by span indicates good concurrence between the level of compliance and the observed range of cover depth. That is, those spans that have better than average cover also tend to have less variation. This trend emphasizes the importance of good construction control.

An inspection of the individual structure data shows considerable variation among spans, which emphasizes the need to examine each span separately. Table 2 shows that, when the span data are grouped by design clear-cover specification, 16.6 percent of the spans built to the 6.35-cm specification fail (i.e., more than 10 percent of the area has less than 5.08 cm of clear cover), whereas 22.7 percent of those built to the 5.08-cm specification fail. Thus far, only 18 spans have been surveyed that were built by using the current 7.62-cm specification; of these, none have failed. The passing and failing rates of the spans are summarized below (1 cm = 0.4 in).

Rate	Clear-Cover Specification		
	5.08 cm	6.35 cm	7.62 cm
Passing, %	77.3	83.4	100.0
Failing, %	22.7	16.6	0.0

Table 3 divides the data according to span length. There does not appear to be any significant trend. In Table 4, the data are grouped according to type of span (single or multispan, tail or midspan). Here the data show a much higher failure rate for midspans than for either single or tail spans for both the 5.08- and 6.25-cm specifications.

Determination of Necessary Specification Value to Ensure a Prescribed Minimum Depth of Cover at a Prescribed Confidence Level

An evaluation of the pachometer measurements on a span basis indicated that, regardless of the actual design cover specification, approximately 95 percent of the individual span data are within a range of 3.81 cm (1.50 in) or approximately ± 1.91 cm (±0.75 in) around the average or mean value for the span. The specific causes for this magnitude of variation are not known. However, it does represent the variation that can be expected from prevailing construction techniques and is comparable with that found in other states.

Since the study has been under way, the department has increased the cover specification from 6.25 ± 0.64 cm to 7.62 ± 0.64 cm. In addition, contractors are now required to physically tie both the top and the bottom mats to the structural steel. This was done to reduce the possibility that mat separation could be contributing to the overall variation. An evaluation of the effectiveness of this measure was made by comparing the distributions of the observed variation on a span basis for structures built before and after these changes. This comparison indicated that no significant reduction in the process variation has occurred, which suggests that either mat separation is not a problem or that the present requirements for mat tie down are not effective.

An evaluation of the effectiveness of increasing the design specification was made on the basis of the distributions of the 10th percentile cover. By using probability theory to analyze the data for the 211 spans constructed to the 6.35-cm specification, the chance of producing a deficient span was computed to be 18.7 percent. Because of the large amount of data available for spans constructed by using the 6.35-cm target, it is possible to check directly the accuracy of this estimate by comparing it with the observed failure rate. Of the 211 spans, 35 (16.6 percent) were deficient. Although

Table 2. Span areas that have less than 5.08 cm (2.0 in) of clear cover.

Percentage of Span Area That Has Less Than 5.08 cm of Clear Cover	Clear-Cover Specification					
	5.08 ± 0.64 cm		6.35 ± 0.64 cm		7.62 ± 0.64 cm	
	No.	Percent	No.	Percent	No.	Percent
0.0	26	49.0	127	60.2	17	94.4
0.1-5.0	12	22.6	40	18.8	1	5.6
5.1-10.0	3	5.7	9	4.3	0	0.0
10.1-25.0	7	13.2	20	9.5	0	0.0
25.1-50.0	3	5.7	8	3.8	0	0.0
>50.0	2	3.8	7	3.3	0	0.0
Total	53	100	211	100	18	100

Note: 1 cm = 0.394 in.

Table 3. Span areas that have less than 5.08 cm (2.0 in) of clear cover: summarized by span length and design cover specification.

Span Length (m)	No. of Spans: Percentage of Area That Has Less Than 5.08 cm of Clear Cover							Passing (%)
	0.0	0.1-5.0	5.1-10.0	10.1-25.0	25.1-50.0	>50.0	Total	
5.08-cm clear-cover specification								
<9.05								
9.45-15.2	9	2	1	1	1	0	14	85.7
15.5-21.3	4	4			1		9	88.9
21.7-27.4	3	2					5	100
27.8-33.5	10	1	1	4	1	1	18	66.7
33.8-39.4		2	1	1			4	75.0
>39.4		1		1		1	3	33.3
6.35-cm clear-cover specification								
<9.05	1						1	100
9.45-15.2	35	8		4	1	3	51	84.3
15.5-21.3	33	10	3	6	1		53	86.8
21.7-27.4	19	4	2	2	1	1	29	86.2
27.8-33.5	17	5	2	2	3	2	31	77.4
33.8-39.4	10	6	1	4	4	1	26	64.5
>39.4	12	7	1				20	100
7.62-cm clear-cover specification								
<9.05								
9.45-15.2	3						3	100
15.5-21.3	6						6	100
21.7-27.4								
27.8-33.5	2	1					3	100
33.8-39.4	4						4	100
>39.4	2						2	100

Note: 1 m = 3.28 ft.

Table 4. Span areas that have less than 5.08 cm (2.0 in) of clear cover: summarized by type of span and design cover specification.

Type of Span	Spans: Percentage of Area That Has Less Than 5.08 cm of Clear Cover: 0.0 No.	0.0 %	0.1-5.0 No.	0.1-5.0 %	5.1-10.0 No.	5.1-10.0 %	10.1-25.0 No.	10.1-25.0 %	25.1-50.0 No.	25.1-50.0 %	>50.0 No.	>50.0 %	Total No.	Passing (%)
5.08-cm clear-cover specification														
Single span	2	100	0	0	0	0	0	0	0	0	0	0	2	100
Multispan														
Tail	14	50	8	28.7	2	7.1	2	7.1	2	7.1	0	0	28	100
Midspan	10	43.5	4	17.4	1	4.3	5	21.8	1	4.3	2	8.7	23	65.2
6.35-cm clear-cover specification														
Single span	6	54.5	4	36.4	0	0.0	1	9.1	0	0.0	0	0.0	11	90.9
Multispan														
Tail	83	61.5	26	19.2	7	5.2	10	7.4	7	5.2	2	1.5	135	85.9
Midspan	37	56.9	11	16.9	2	3.1	9	13.9	1	1.5	5	7.7	65	76.9
7.62-cm clear-cover specification														
Single span													0	
Multispan														
Tail	11	100	0	0	0	0	0	0	0	0	0	0	11	100
Midspan	6	85.7		1	14.3	0	0	0	0	0	0	0	7	100

Note: 1 cm = 0.394 in.

slightly conservative, the predicted failure rate is in reasonable agreement with the observed frequency. Of the six structures (18 spans) thus far surveyed that were built by using the current specification (7.62 ± 0.64 cm), none were deficient. However, based on this limited experience and by using the same procedure as above, the probability of producing a deficient span can be computed to be 3.0 percent. In view of the demonstrated conservative nature of estimates computed in this manner, it is suggested that 3.0 percent is a reasonable estimate of the maximum limiting value.

If the total process variability inherent in the construction process itself continues to remain as constant as it has over the previous 2 years, then the current specification should provide adequate protection against insufficient cover.

General Comment on Process Variation

In evaluating the problem of achieving adequate clear cover, there are two basic approaches. One approach is to reduce and control the overall process variation. By using this approach, the smallest possible target value consistent with the minimum level of compliance could be determined. The alternative is to measure and accept the process variation at its existing level and adjust the target value as required to achieve the desired minimum compliance.

Although the first approach is technically possible, it would be extremely difficult. A detailed study to determine all of the parameters and their relative signficance would be required. A partial list of parameters that would have to be considered includes (a) the unpredictability of beam deflection under the dead-load effect of fresh concrete, (b) separation of the reinforcing mats, (c) concrete-placement procedure, (d) finishing techniques, and (e) limits of accuracy for level work on a surface subjected to constantly changing temperature and cloud cover.

A casual review of this list would discourage most workers. Even if a study of this magnitude were completely successful, there is no guarantee that the indicated changes would be feasible. For example, the costs of revising existing design procedures or of modifying established construction techniques would probably be prohibitive.

The second approach is clearly the preferred choice. There are three basic factors (all documented by this investigation) that recommend it over the alternative:

1. The process variability is basically constant and not likely to change.
2. The average performance is sensitive to changes in the specified target.
3. The variation is independent of the target value.

These three facts taken together suggest that the level of compliance can be effectively controlled by an appropriate adjustment of the design target.

This study has shown that, by increasing the clear-cover target value to 7.62 cm, but making no additional attempt to control the process variation, one can be reasonably confident that less than 3 percent of structures will be deficient. The economic impact of increasing the target value of 7.62 cm is minimal. The average cost of adding 1.27 cm (0.5 in) more concrete is less than 12 cents/m^2 (10 cents/yd^2) of deck area.

Determination of Number of Measurements per Span Required to Adequately Determine Minimum Depth of Cover

Another objective of this investigation was to determine an appropriate sampling frequency. All of the data were taken on a 1.52- × 1.52-m grid. This sampling frequency seemed excessive but, because of our inexperience in gathering this type of data, the decision to use it was based on an FHWA recommendation.

Sampling frequency is important. Sound judgment requires that the quantity of data be sufficient to justify the recommendation, but data collection is costly, and a reasonable balance between these two constraints is necessary. Thus, it was necessary to determine the appropriate number of measurements (N) per span such that the correct conclusion would be reached at some predetermined confidence level (the 0.05 confidence level was arbitrarily selected). Intuitively, to maintain this confidence level requires that the sample size increase as the percentage of the deck that has less than 5.08 cm of clear cover approaches the failure criterion (10 percent). Also, the minimum sampling requirement can be determined for spans that have been oversurveyed if

the number of available measurements is greater than approximately 2N. It follows that, if more than enough data have been collected, then random samples of considerably smaller size should consistently lead to the same conclusion regarding deficiency. With this in mind, 10 large spans ($N_T > 150$) were selected that had less than 5.08 cm of clear cover over 0 to 20 percent of their area. These spans were selected to cover the range between 0 and 20 percent as uniformly as possible. The first step was then to test each span to determine whether it was in fact overtested. To do this, 100 separate random samples (size $N_T/2$) were generated from the available data for each span. In turn, for each random sample, the percentage of area that had less than 5.08 cm of cover was calculated and checked against the failure criteria. If at least 95 percent of the smaller samples led to the same conclusion as was reached by using all of the data, that span was considered overtested.

The next step was to determine the minimum sample size consistent with the confidence level selected (0.05). This was accomplished by reiterating the above procedure. For each new set of 100 random samples, a smaller sample size was selected until the success rate for correctly predicting the deficiency status decreased to 95 percent. The minimum sampling frequency for each span was then plotted against the percentage of clear cover less than 5.08 cm (Figure 1). As expected, as the percentage of deck area that had less than 5.08 cm of clear cover approached 10, the sample size required increased exponentially. As shown, the point of diminishing returns occurs at approximately N = 100. This corresponds with a range of ±4 percent and indicates that, for any given span, the correct conclusion regarding deficiency made by using the 10 percent criterion is ensured at a confidence level of 0.05 or better if (a) at least 100 measurements were taken and (b) the observed percentage of area that has less than 5.08 cm of clear cover is either less than 6 or greater than 14. Because of the limited experience with the present specification (minimum of 7.62 cm of clear cover), an accurate estimate of the number of spans likely to fall within this range cannot be made at this time; however, a reasonable estimate would be approximately 3 percent. Based on this analysis, 100 measurements should be taken per span. This sampling size may be excessive for small decks; it is suggested that the 1.52- × 1.52-m grid size established by FHWA be used in those cases where the 100-size sample would result in more than 0.43 measurement/m^2 (1 measurement/25 ft^2) of deck area.

It is generally agreed that 5.08 cm of clear concrete cover is the minimum acceptable. However, the minimum acceptable level of compliance is somewhat arbitrary. In Michigan, it is at present based on the percentage of the total surface area that has less than 5.08 cm of clear cover. The department has established 10 percent as the critical value; this is the basis for the above analysis. However, FHWA has on occasion considered 40 percent to be the critical level of deficiency. For comparison, the above procedure was repeated by using the FHWA criteria (see Figure 2). As indicated, the results are similar with the following exception; the range for which the 0.05 confidence level cannot be supported increased from ±4 to ±6 percent.

Comparison of Depth Measurements Made by Using Pachometer and by Using Wet-Depth Method to Determine Whether Wet-Depth Method Is Adequate for Construction Control

A total of 15 structures (36 spans) for which both construction wet-depth measurements and pachometer readings were obtained were examined to determine how well the two methods compared. In the wet-depth method, a construction inspector pushes a calibrated rod into the freshly poured concrete immediately behind the finishing machine and records the depth to the top of the reinforcing steel. The comparison technique consisted of determining the distribution characteristics of the differences between the (a) averages for each span, (b) 40th percentile value taken from the cumulative frequency distribution of clear-cover depth for each individual span, and (c) the 10th percentile value. In all cases, the differences were determined by subtracting the pachometer readings from the wet-depth measurements. The results of this analysis are summarized in Table 5. They show that wet-depth measurements, on the average, show more depth of clear cover than do pachometer readings. Depending on the comparison criterion chosen, the mean of differences varied from 4.27 to 6.76 mm (0.168 to 0.266 in). The standard deviation for the three distributions varies from 8.58 to 9.25 mm (0.338 to 0.364 in), which indicates that, approximately 53 percent of the time, one can expect the mean difference between the two measurement methods to vary by more than ±6.4 mm

Figure 1. Relationship between percentage of deck area that has less than 5.08 cm (2.0 in) of clear concrete cover and required sampling frequency: 10 percent criterion.

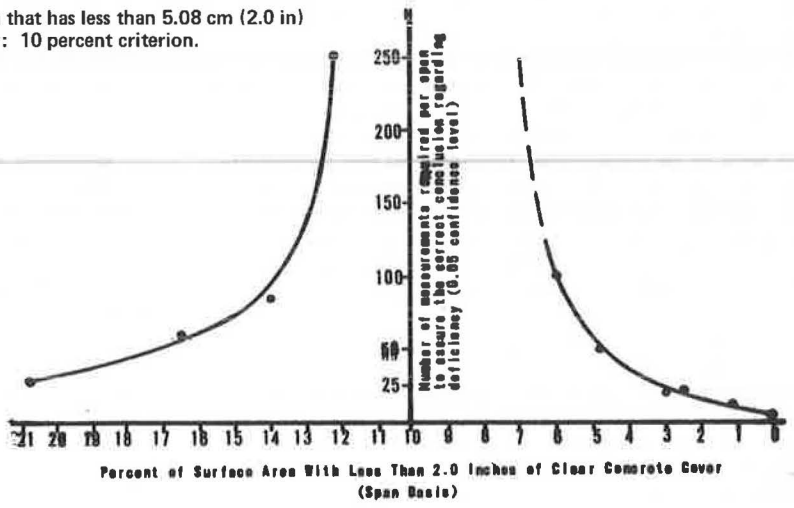

Figure 2. Relationship between percentage of deck area that has less than 5.08 cm (2.0 in) of clear concrete cover and required sampling frequency: 40 percent criterion.

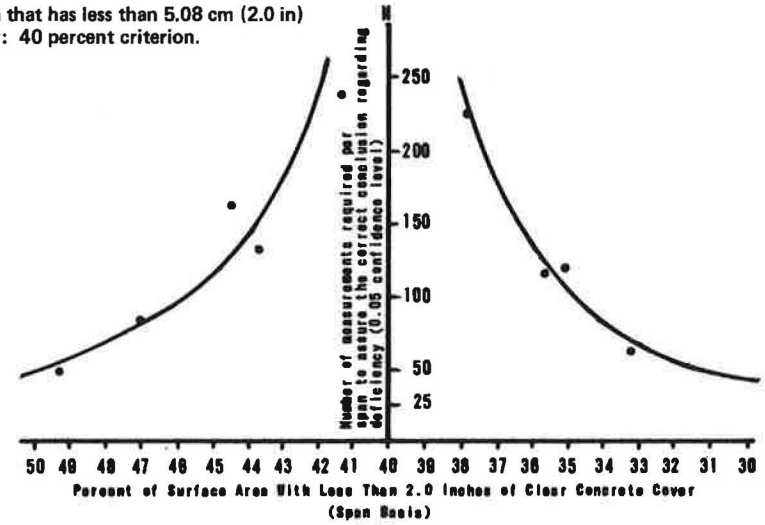

Table 5. Comparison of wet-depth measurements with pachometer readings.

Comparison Criterion	Total Number of Spans	Mean of Differences (mm)	SD of Differences (mm)	Coefficient of Variation	Range of Differences (mm)	No. of Spans Where Wet-Depth Measurements Were Greater	Remarks
Average value	36	5.51	8.84	1.60	-1.48-22.3	27	53 percent of the time, difference between methods will be greater than ±6.4 mm
40th percentile value of clear cover	36	4.27	8.58	2.01	-17.4-16.0	24	54 percent of the time, difference between methods will be greater than ±6.4 mm
10th percentile value of clear cover	38	6.76	9.25	1.37	-15.7-26.8	27	52 percent of the time, difference between methods will be greater than ±6.4 mm; 14 percent of the time, difference between methods will be greater than ±12.5 mm

Note: 1 mm = 0.0394 in.

(±0.25 in) and about 15 percent of the time to vary by more than ±12.5 mm (±0.50 in).

CONCLUSIONS

1. A specification value of 7.62 ±0.64 cm for clear concrete cover should provide adequate protection for at least 97 percent of all new construction.
2. For most structures, the distribution of measurements for individual spans is consistent with approximately 95 percent of the measurements being within a range of about 1.91 cm (±0.955 cm) of the average cover.
3. The two previous increases in the concrete-cover specification have had no measurable effect on the average variation, which has remained basically constant throughout this investigation.
4. The overall average depth of concrete cover for those structures built to either the 6.35- or the 7.62-cm cover specification agrees closely with the target value.
5. There is considerable variation among spans for the same structure, which emphasizes the need to examine spans individually. In some cases, individual spans were found to be seriously deficient, despite the fact that the data for the structure as a whole indicated substantial compliance.
6. Within a span, the distribution of cover generally appears to be random.
7. Wet-depth measurements do not compare favorably with R-meter measurements. This study indicated that, on the average, wet-depth measurements show more depth of clear cover than R-meter measurements and that more than 50 percent of the time, the mean difference will be greater than 0.64 cm.
8. At depths of clear cover of 5.1 to 7.6 cm, a properly calibrated R-meter has an accuracy of ±0.32 cm. Bar size, grade of steel, and presence of magnetic aggregates have a pronounced effect on measurements.
9. To adequately determine the depth of concrete cover, 100 measurements/span or 0.43 measurement/m^2 (whichever is less) should be taken.

Publication of this paper sponsored by Committee on Construction of Bridges and Structures.